

EXTREME WIND SPEEDS FOR THE SOUTH-WEST INDIAN OCEAN USING SYNTHETIC TROPICAL CYCLONE TRACKS

Giles Fearon

*Thesis presented in fulfilment of the requirements for the degree of
Master of Science in the Faculty of Civil Engineering at Stellenbosch
University*



Supervisor: Mr Geoffrey Toms
Department of Civil Engineering

December 2014

DECLARATION

By submitting this thesis electronically, I declare that the entirety of the work contained therein is my own, original work, that I am the sole author thereof (save to the extent explicitly otherwise stated), that reproduction and publication thereof by Stellenbosch University will not infringe any third party rights and that I have not previously in its entirety or in part submitted it for obtaining any qualification.

December 2014

Copyright © 2014 University of Stellenbosch

All rights reserved

ABSTRACT

Tropical cyclones are synoptic scale rotating storms capable of generating intense wind speeds and rainfall with potentially devastating social and economic consequences. In addition to abnormally high winds and rainfall, the associated storm surge and extreme waves can lead to severe coastal erosion, damage to coastal property and inundation. A good understanding of the risk exposure to these events is therefore of great importance to planners and designers of coastal infrastructure in vulnerable regions.

Probabilistic approaches have been routinely adopted for the calculation of extreme tropical cyclone induced wind speeds, with significant developments in these techniques over the last few decades. While the application of these approaches has become widely adopted in regions such as the North Atlantic, North Pacific and South Pacific Oceans, relatively little attention has been paid to the South-West Indian Ocean. This thesis focusses on the quantification of the risk exposure to tropical cyclones over the South-West Indian Ocean, using current state-of-the-art techniques. The primary results of the thesis are extreme wind speed maps at various return periods of interest for engineering design.

Best track data for the South-West Indian Ocean, as archived by the Joint Typhoon Warning Centre (JTWC), has been used as the primary dataset forming the basis of this study. These data provide estimates of the location and intensity of historical tropical cyclones at six hourly intervals. Location data are provided as estimates of longitude and latitude of the eye, while intensity data are provided as estimates of the maximum sustained surface (10 m elevation) wind speed and/or minimum central pressure.

The modelling of tropical cyclone wind fields has been carried out using both the Holland (1980) and the Willoughby et al. (2006) parametric wind field models. Using the limited information available in the best track data as input to the model, surface wind fields which reasonably resemble those of actual storms have been generated. Both considered parametric wind field models have been shown to yield reasonable wind speeds and directions when compared with measurements. Of the two considered models the Willoughby et al. (2006) model has been shown to provide the best fit to historical wind speed measurements.

Extreme value analyses of tropical cyclone induced wind speeds based on historical data alone have been shown to lead to potentially large errors, owing to the small sample size of the historical data. This highlights the need to augment the historical database through a probabilistic approach. Largely following the methods described in Powel et al. (2005) and Emanuel et al. (2006), a synthetic track model for the South-West Indian Ocean has been developed. The objective of the synthetic track

model is to simulate thousands of years of tropical cyclone tracks, thereby circumventing errors induced by small sample sizes in the available historical best track data. The synthetic track model developed as part of this study is a Markov chain model, capable of simulating track propagation and intensity evolution along the track, from track genesis through to termination. The model is purely statistical, based on properties derived from the historical best track data. Adjustments have however been made to account for physical limitations such as those imposed by the equator and the maximum potential intensity which an event can attain. The statistical characteristics of synthetic tracks have been shown to agree well with those of the historical population.

Applying the Willoughby et al. (2006) wind field model along synthetic tracks has enabled the simulation of 5 000 years of tropical cyclone induced wind speeds at any location of interest in the South-West Indian Ocean. Applying calculations on a 1 degree geographical grid, wind speed maps corresponding to return periods of 50, 100, 200 and 500 years have been generated for the South-West Indian Ocean. Extreme wind speeds along coastal regions provide valuable input for the design of coastal infrastructure in the region.

OPSOMMING

Tropiese siklone is sinoptiese orde roterende storms wat in staat is om aansienlike windspoed en reënval, tot gevolg te hê met potensiële vernietigende sosiale en ekonomiese gevolge. Benewens die abnormale sterk winde en hoë reënval kan die verwante stormdeinings en vloedgolwe lei tot ernstige kus-erosie, skade aan kusfront-eiendom en oorstromings. 'n Goeie begrip van die risiko-blootstelling aan hierdie gebeurtenisse is daarom van groot belang vir die beplanners en ontwerpers van kus-infrastruktuur in kwesbare gebiede.

As gevolg van die beduidende ontwikkeling van probabilistiese benadering tot die berekening van windspoed wat veroorsaak word deur ekstreme tropiese siklone, word hierdie tegnieke huidige op 'n roetine basis aangewend. Terwyl die toepassing van hierdie benaderings wyd aanvaar word in gebiede soos die Noord-Atlantiese, Noordelike- en Suidelike Stille Oseaan, word relatief min aandag gegee aan die Suid-Westelike Indiese Oseaan. Hierdie tesis fokus op die kwantifisering van die risiko-blootstelling aan tropiese siklone in die Suid-Westelike Indiese Oseaan met die gebruik van die huidige gevorderdste tegnieke. Die primêre resultaat van die tesis is uiterste wind spoed kaarte vir 'n verskeidenheid herhaal periodes wat van belang is vir ingenieursontwerp.

Beste roete-ata vir die Suid-Westelike Indiese Oseaan, soos voorsien deur die Gesamentlike Tifoon Waarskuwing Sentrum (JTWC), is gebruik as die primêre data stel wat die basis vorm van hierdie studie. Hierdie data gee die beste skattings van die ligging (lengte- en breedtegraad), en intensiteit (maksimum volgehoue oppervlak (10m hoogte) wind spoed en/of sentrale druk tekort) van historiese tropiese siklone teen ses-uurlikse intervale.

Die modelering van tropiese sikloon windvelde was uitgevoer met die gebruik van die Holland (1980) en die Willoughby et al. (2006) parametriese windveldmodelle. Met die gebruik van beperkte inligting wat beskikbaar is in die beste roete data as invoer vir die model, was oppervlak wind velde gegenereer wat 'n billike ooreenstemming het met die van werklike storms. Beide tegnieke se parametriese windveldmodelle is al bewys om redelike akkurate windspoed en windrigtings te lewer in vergelyking met waargenome waardes. Van die twee modelle het die Willoughby et al. (2006) model se resultate die beste ooreenstemming gewys met historiese wind spoed metings.

Dit is al uitgewys dat uiterste waarde-analises van tropiese sikloon veroorsaakte windspoed moontlik kan lei tot groot foute in die resultate as gevolg van die klein monster-grootte van die historiese data. Dit beklemtoon die noodsaaklikheid om die historiese databasis aan te vul met behulp van probabilistiese metodes. Die metodes soos beskryf deur Powel et al. (2005) en Emanuel et al. (2006) is hoofsaaklik gebruik om 'n sintetiese roete-model vir die Suid-Westelike Oseaan te ontwikkel. Die

doelwit van die sintetiese roete model is om duisende jare se tropiese sikloonroetes te produseer, en in effek foute te vermy as gevolg van die gebruik van klein monster groottes van die beskikbare historiese beste roete data. Die sintetiese roete model wat tydens hierdie studie ontwikkel is, is 'n Markov kettingmodel wat in staat is om die roete verspreiding asook die evolusie van intensiteit saam die roete te simuleer vanaf die ontstaan tot die beëindiging van die sikloon se roete. Die model is suiwer statisties en is gebaseer op die eienskappe soos afgelei vanaf die historiese beste roete data. Aanpassings is gemaak om rekening te hou van die fisiese beperkings soos die wat opgelê word deur die ewenaar en die maksimum potensiële intensiteit wat 'n sikloon kan bereik. Dit is voorgelê dat die statistiese eienskappe van die sintetiese roetes goed saamstem met die van die historiese populasie.

Die toepassing van die Willoughby et al. (2006) wind veld model langs die sintetiese roetes het dit moontlik gemaak om 5000 jaar se windspoed, wat veroorsaak is deur tropiese siklone, te genereer by enige ligging wat van belang is in die Suid-Westelike Indiese Oseaan. Met berekeninge wat op 'n 1 grade geografiese ruitnet gedoen is, is windspoedkaarte vir herhaal periodes van 50, 100, 200 en 500 jaar opgestel vir die Suid-Westelike Indiese Oseaan. Die uiterste wind spoed in kusgebiede gee waardevolle invoer vir die ontwerp van kus-infrastruktuur in die omgewing.

ACKNOWLEDGEMENTS

First and foremost I would like to thank my wife, Shelley, for her continued support, encouragement and understanding over the duration of this thesis.

Thank you to my employer, PRDW, for financing my studies and providing me with the opportunity to work on some interesting tropical cyclone related projects, where the first seeds of this thesis were sown. In particular, I would like to thank Stephen Luger for the considerable time and effort he has invested in my development as a coastal modeller.

Thank you to my supervisor, Geoff Toms, for providing valuable comments and feedback during the completion of this thesis.

The Danish Hydraulics Institute has kindly provided me with an academic license for this study. Thank you to Mr Andrew Pott for facilitating this.

Professor Kerry Emanuel of the Massachusetts Institute of Technology has provided maximum potential intensity data, while Mr Francois Bonnardot of Météo France has provided measured wind data for this study. Thank you for these valuable contributions.

EXTREME WIND SPEEDS FOR THE SOUTH-WEST INDIAN OCEAN USING SYNTHETIC TROPICAL CYCLONE TRACKS

TABLE OF CONTENTS

DECLARATION	i
ABSTRACT	ii
OPSOMMING	iv
ACKNOWLEDGEMENTS	vi
TABLE OF CONTENTS	vii
LIST OF FIGURES	x
LIST OF TABLES	xv
LIST OF SYMBOLS	xvi
1. INTRODUCTION	1
1.1 Background	1
1.2 Thesis Objective	3
1.3 Study Approach	3
1.4 Thesis Structure	3
2. LITERATURE REVIEW	4
2.1 Introduction	4
2.2 Characteristics of Tropical Cyclones	4
2.2.1 Definition.....	4
2.2.2 Genesis, Development and Structure	4
2.2.3 Wind-Pressure Relationship.....	7
2.2.4 Classification	8
2.3 Best Track Data	10
2.3.1 Description of Data	10
2.3.2 Historical Development of Analysis Techniques	11
2.3.3 Accuracy of Best Track Data.....	12
2.4 Wind Field Models	13
2.4.1 Radius to Maximum Wind Speed.....	14
2.4.2 Wind Profile Models	15
2.4.3 Planetary Boundary Layer Corrections	22
2.4.4 Asymmetry Corrections	25
2.4.5 Wind Inflow Angle Corrections	25
2.4.6 Correcting for Wind Speed Averaging Period	26
2.5 Site Specific Probabilistic Models	27
2.6 Synthetic Track Models	30
2.6.1 Genesis.....	31
2.6.2 Track Propagation	33
2.6.3 Intensity Evolution	36
2.6.4 Termination.....	37
2.7 Summary and Conclusions	37

3. STUDY APPROACH	39
3.1 Introduction.....	39
3.2 Overview	39
3.2.1 Best Track Data (Section 4)	40
3.2.2 Wind Field Model (Section 5).....	40
3.2.3 Synthetic Track Model (Section 6)	40
3.2.4 Extreme Wind Speed Maps (Section 7)	41
3.3 Summary and Conclusions.....	41
4. BEST TRACK DATA FOR THE SOUTH-WEST INDIAN OCEAN.....	42
4.1 Introduction.....	42
4.2 Description of Data	42
4.3 Processing Methodology	44
4.3.1 Identifying Relevant Data.....	44
4.3.2 Gap-Filling for Missing Estimates of V_{max}	44
4.3.3 Track Speed and Direction	45
4.4 Summary Statistics	46
4.4.1 Annual Occurrence.....	46
4.4.2 Seasonal Occurrence.....	47
4.4.3 Intensity Data	48
4.5 Summary and Conclusions.....	50
5. WIND FIELD MODEL.....	51
5.1 Introduction.....	51
5.2 Description of the Model.....	51
5.2.1 Radius to Maximum Wind Speed (R_{max}).....	51
5.2.2 Axisymmetric Flight Level Wind Speed Profiles	52
5.2.3 Asymmetric Surface Wind Fields	54
5.3 Validation of the Model.....	55
5.3.1 Description of Data	56
5.3.2 Methodology.....	59
5.3.3 Results.....	61
5.3.4 Discussion.....	69
5.4 Summary and Conclusions.....	71
6. SYNTHETIC TRACK MODEL	73
6.1 Introduction.....	73
6.2 Motivation for Synthetic Track Modelling	73
6.3 Description of the Model.....	76
6.3.1 Overview	76
6.3.2 Genesis.....	77
6.3.3 Track Propagation	81
6.3.4 Intensity Evolution	83
6.3.5 Termination.....	86
6.4 Validation of the Model.....	88
6.4.1 Spatial and Temporal Occurrence.....	88

6.4.2	Distributions of Track Speed, Direction and Intensity	91
6.5	Limitations to the Model	96
6.6	Summary and Conclusions	97
7.	EXTREME WIND SPEEDS FOR THE SOUTH-WEST INDIAN OCEAN	99
7.1	Introduction	99
7.2	Methodology	99
7.3	Results	100
7.3.1	Comparison with EVAs on Historical Data	100
7.3.2	Extreme Wind Speed Maps.....	101
7.4	Application to Coastal Engineering.....	104
7.4.1	Design Wind Speeds for the Southern African Coastline.....	104
7.4.2	Ocean Response Modelling.....	105
7.5	Uncertainty	107
7.6	Summary and Conclusions	107
8.	CONCLUSIONS AND RECOMMENDATIONS.....	109
8.1	Conclusions.....	109
8.2	Recommendations	110
9.	REFERENCES	112
APPENDIX A:	TIME-SERIES OF MODELLED AND MEASURED WIND SPEEDS	118
APPENDIX B:	NON-PARAMETRIC PROBABILITY DENSITY FUNCTIONS	128
APPENDIX C:	MAXIMUM POTENTIAL INTENSITY ESTIMATES	131

LIST OF FIGURES

	Page No
Figure 1-1: Satellite image of Tropical Cyclone Eline prior to landfall on 21 February 2000 (INGC, 2009).....	1
Figure 2-1: Monthly averaged wind velocities over the South-West Indian Ocean for the month of January, highlighting the band of low wind speeds characteristic of the ITCZ (adapted from Mavume et al. (2009)).	5
Figure 2-2: Schematic of the physical structure of a mature tropical cyclone (USGS, 2013).....	6
Figure 2-3: Observed relationship between V_{max} and ΔP from 15 years of aircraft reconnaissance measurements (Knaff & Zehr, 2007).....	7
Figure 2-4: “Basins” where tropical cyclones occur on a regular basis (NOAA, 2014).....	8
Figure 2-5: Global tropical cyclone tracks, colour coded by the number of organisations providing best track data for each storm. The stars denote the locations of the organisations monitoring tropical cyclone activity (Levinson et al., 2010).	11
Figure 2-6: Schematic example of a parametric wind field (Dima & Desflots, 2010). The winds are stronger to the right hand side of the forward motion in this example, as the example is of a northern hemisphere tropical cyclone.	14
Figure 2-7: The effect of varying the Holland B parameter on the pressure profile (Holland, 1980).....	17
Figure 2-8: The effect of varying the Holland B parameter on the gradient level wind speed profile (Holland, 1980).....	19
Figure 2-9: Schematic illustration of a sectionally continuous wind speed profile. A ramp function is used to create a smooth transition between the inner (V_i) and outer (V_o) profiles (Willoughby et al., 2006).	21
Figure 2-10: Mean measured wind speed profiles for the eyewall and outer vortex regions of tropical cyclones. The normalised wind speed represents the factor to convert from 700 mb (3 km) flight level wind speed to the level of interest (Franklin et al., 2003).	24
Figure 2-11: Overview of simulation approach for site specific probabilistic models (Vickery et al., 2009b).	28

Figure 2-12: Sixty random tracks from a synthetic track model (a) and a historical dataset (b) over the North Atlantic Ocean (Emanuel et al., 2006). 31

Figure 2-13: Example of calculated genesis density (in red) from historical genesis locations (in blue) over the North-West Pacific Ocean (Yin et al., 2009). 33

Figure 2-14: Example of calculated PDFs for change in direction ($\Delta\theta$) for eight directional bins at a given geographical location and season (Powell et al., 2005). 35

Figure 3-1: Flow diagram summarising the tropical cyclone risk model developed as part of this study. 39

Figure 4-1: JTWC best track data for the South-West Indian Ocean for the year 2012. Scale corresponds to the Saffir-Simpson scale. 43

Figure 4-2: Wind-pressure relationship determined from JTWC best track data. 45

Figure 4-3: Best track data for the South-West Indian Ocean (1952 to 2012). 46

Figure 4-4: Average occurrence rate of tropical cyclone tracks over the South-West Indian Ocean (1952 to 2012). Contours represent the number of tracks passing within 2 geographical degrees (approximately 200 km) per year on average. 47

Figure 4-5: Average occurrence rates of tropical cyclones by month for the South-West Indian Ocean (SWIO) and the Mozambique Channel (MC) (1952 to 2012). 48

Figure 4-6: Best track data for the South-West Indian Ocean for which wind speed data are available (1980 to 2012). Scale corresponds to the Saffir-Simpson scale. 49

Figure 4-7: Average occurrence rates of tropical cyclones by Saffir-Simpson scale category for the South-West Indian Ocean (SWIO) and the Mozambique Channel (MC) (1980 to 2012). 49

Figure 5-1: Comparison of Holland (1980) and Willoughby et al. (2006) wind speed profiles for a range of intensities (V_{Fmax}). 53

Figure 5-2: Example of a parametric wind field, including the effect of forward motion asymmetry. 55

Figure 5-3: Locations of wind speed measurement stations. 56

Figure 5-4: Plan view of Tromelin Island, indicating the size of the island and the location of the measurement station (Penn State, 2014). 58

Figure 5-5:	Time-series of 10-min average wind speed measured at Tromelin Island. See Figure 5-3 for the location of the measurement station.....	59
Figure 5-6:	Historical tropical cyclone tracks used to compare modelled vs measured wind speeds at Tromelin.	60
Figure 5-7:	Example of the extraction of modelled wind speeds at Tromelin for Tropical Cyclone Geralda (1994). The time-series indicates the measured wind speeds at Tromelin over the same period of time.	61
Figure 5-8:	Time-series of modelled vs measured 10-min average wind speeds at Tromelin. The name of each corresponding tropical cyclone is provided for reference. Figure 5-6 shows the best track data used as input to the parametric wind field models.	62
Figure 5-9:	Scatter plots of modelled vs measured peak 10-min average wind speeds at Tromelin using both the Willoughby et al. (2006) and Holland (1980) parametric wind field models.	64
Figure 5-10:	Scatter plots of modelled vs measured peak 10-min average wind speeds for all measurement stations, excluding those on Réunion Island, using both the Willoughby et al. (2006) and Holland (1980) parametric wind field models.	65
Figure 5-11:	Scatter plots of modelled vs measured peak 10-min average wind speeds at all measurement stations using both the Willoughby et al. (2006) and Holland (1980) parametric wind field models.	66
Figure 5-12:	Time-series of modelled vs measured wind directions at Tromelin. The name of each corresponding tropical cyclone is provided for reference. Figure 5-6 shows the best track data used as input to the parametric wind field models.	68
Figure 6-1:	Historical tracks for which intensity data are available (1980 – 2012) in the vicinity of two hypothetical locations on the Mozambique coastline.....	74
Figure 6-2:	Extreme value analysis of modelled wind speeds at two hypothetical locations on the Mozambique coastline (see Figure 6-1 for model output locations).....	75
Figure 6-3:	Flow diagram of synthetic track model.....	76
Figure 6-4:	Bar charts of the number of historical events occurring in the South-West Indian Ocean for the months of January and February from 1952 to 2012. The plots include the theoretical Poisson distribution (in blue) for the respective months.	78

Figure 6-5:	Binned kernel density estimate of genesis locations. Historical genesis locations from which the density is derived are shown as black points.	79
Figure 6-6:	Non-parametric probability density functions (PDFs) for initial conditions of track speed (c), track direction (θ) and intensity (V_{max}). Three locations are compared.....	81
Figure 6-7:	Non-parametric probability density functions for change in track direction ($\Delta\theta$) for various track directional bins. Two locations are compared.	82
Figure 6-8:	Non-parametric probability density functions for change in track speed (Δc) for various track speed bins. Two locations are compared.....	83
Figure 6-9:	Non-parametric probability density functions for change in track intensity (ΔV_{max}) for various intensity bins. Two locations are compared.....	84
Figure 6-10:	Land-filling model. Left window shows the best fit to the historical landfall events, while the right window shows the residuals from the best fit model.....	86
Figure 6-11:	Probability of track termination for $V_{max} < 20$ m/s and track duration between 160 hours and 240 hours.....	87
Figure 6-12:	Comparison of 33 years of historical tracks (1980 to 2012) with 33 years of randomly selected synthetic tracks. The scale corresponds to the Saffir-Simpson scale.	89
Figure 6-13:	Comparison of average occurrence rates of tropical cyclones from 61 years (1952 to 2012) of historical tracks and 5 000 years of synthetic tracks. Contours represent the number of tracks passing within 2 geographical degrees (approximately 200 km) per year on average. Numbered points refer to control points for the comparison of track parameters.	90
Figure 6-14:	Comparison of historical and synthetic distributions of track direction (θ) occurring within 2 geographical degrees (approximately 200 km) of selected control points. Locations of control points are shown in Figure 6-13.....	93
Figure 6-15:	Comparison of historical and synthetic distributions of track speed (c) occurring within 2 geographical degrees (approximately 200 km) of selected control points. Locations of control points are shown in Figure 6-13.	94
Figure 6-16:	Comparison of historical and synthetic distributions of track intensity (V_{max}) occurring within 2 geographical degrees (approximately 200 km) of selected control points. Locations of control points are shown in Figure 6-13.....	95

Figure 7-1: Comparison of extreme wind speeds calculated from historical data and synthetic data at two hypothetical locations on the Mozambique coastline..... 101

Figure 7-2: 50 year return period 1-min average wind speeds due to tropical cyclones for the South-West Indian Ocean. 102

Figure 7-3: 100 year return period 1-min average wind speeds due to tropical cyclones for the South-West Indian Ocean. 102

Figure 7-4: 200 year return period 1-min average wind speeds due to tropical cyclones for the South-West Indian Ocean. 103

Figure 7-5: 500 year return period 1-min average wind speeds due to tropical cyclones for the South-West Indian Ocean. 103

Figure 7-6: 50, 100, 200 and 500 year return period 1-min average wind speeds due to tropical cyclones as a function of latitude along the south-east African coastline..... 104

LIST OF TABLES

	Page No
Table 2-1: Saffir-Simpson scale	9
Table 2-2: Météo France La Réunion classification scale.....	9
Table 2-3: Recommended factors to convert between 1-min average to 10-min average wind speeds provided in best track data (Harper et al., 2008).....	26
Table 2-4: Results of Monte Carlo simulations done on 2.5° latitude increments for the Southern African East Coast (Rossouw, 1999).....	30
Table 4-1: Extract from raw JTWC best track data (IBTrACS, 2014).....	43
Table 5-1: Details of wind measurement stations	57
Table 6-1: Coordinates of control points used to compare distributions of synthetic and historical track parameters.	92
Table 7-1: Example of 100 year return period design storm parameters off the coastline of Maputo Bay. 106	

LIST OF SYMBOLS**ACRONYMS**

DHI	:	Danish Hydraulics Institute
ENSO	:	El Niño–Southern Oscillation
JTWC	:	Joint Typhoon Warning Centre
MFR	:	Météo France La Réunion
MJO	:	Madden-Julian Oscillation
MPI	:	Maximum Potential Intensity
NHC	:	National Hurricane Centre
RSMC	:	Regional Specialised Meteorological Centre
RI	:	Relative Intensity
TCWC	:	Tropical Cyclone Warning Centre
UTM	:	Universal Transverse Mercator
PDF	:	Probability Density Function
SST	:	Sea Surface Temperature
WMO	:	World Meteorological Organisation
WPR	:	Wind Pressure Relationship

ROMAN SYMBOLS

a, b	:	Generically used to indicate empirically derived constants
A	:	Vickery & Wadhera (2008) dimensionless parameter for calculating B
B	:	Holland (1980) shape parameter
B_s	:	Holland (2008) shape parameter

c	:	Translation speed of a tropical cyclone
C	:	Parameter in Willoughby et al. (2006) parametric wind field model
f	:	Coriolis parameter
n	:	Number of events
P	:	Atmospheric pressure
P_0	:	Ambient atmospheric pressure on the outskirts of a tropical cyclone
P_c	:	Minimum atmospheric pressure in the centre of a tropical cyclone
Pr	:	Probability
ΔP	:	Central pressure deficit ($P_0 - P_c$)
r^2	:	Coefficient of determination
R	:	Radial distance from tropical cyclone eye
R_{max}	:	Radial distance from tropical cyclone eye to location of maximum wind speed
R_d	:	Gas constant for dry air
RP	:	Return period
S	:	Size parameter
t	:	Time
V	:	Surface (10 m elevation) wind speed
V_G	:	Gradient level wind speed
V_F	:	Flight level wind speed
V_{max}	:	Maximum sustained surface (10 m elevation) wind speed anywhere in a tropical cyclone wind field
V_{RP}	:	Surface (10 m elevation) wind speed with a recurrence interval of RP years
x	:	Parameter in modified rankine vortex parametric wind field model

- $X_{1,2}$: Parameters in Willoughby et al. (2006) parametric wind field model
- γ : Parameter in Willoughby et al. (2006) parametric wind field model

GREEK SYMBOLS

- β : Wind inflow angle
- ε : Residual term (measured – predicted)
- Δ : Difference or change in a parameter
- φ : Latitude
- ψ : Longitude
- θ : Direction
- θ_{max} : Angle to maximum wind speed, measured relative to angle of forward motion of storm
- ρ_A : Density of air
- δ : Fraction of track speed (c) added to or subtracted from axisymmetric parametric wind field
- λ : Mean occurrence rate per unit time t
- ω : Angular frequency of the earth's rotation.

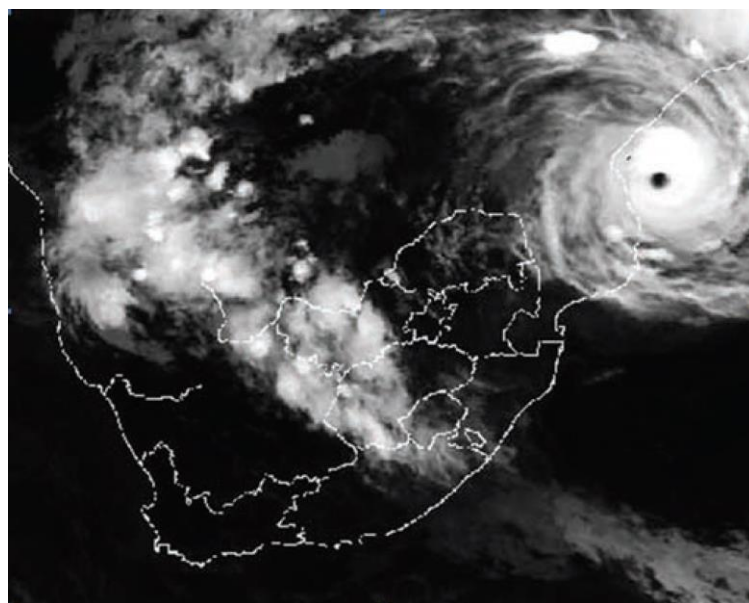
1. INTRODUCTION

1.1 Background

Tropical cyclones are among the most catastrophic natural phenomena known to man. These synoptic scale rotating storms are formed over warm waters of the tropical oceans, and have the potential to produce intense rain and abnormally high winds. The strong winds of tropical cyclones in turn drive ocean response in the form of extreme waves, storm surge and currents; which can lead to coastal erosion, damage to infrastructure, coastal inundation, and loss of life.

The South-West Indian Ocean experiences about 14 tropical cyclone events per year on average. The social and economic impacts of historical events in this region have been significant, an example being Tropical Cyclone Eline, which occurred during February 2000. That system, just prior to landfall over central Mozambique, is shown in Figure 1-1. As a Category 4 event (Saffir-Simpson scale), Tropical Cyclone Eline is the most intense storm to have made landfall on the coastline of Mozambique in recorded history. Although the storm surge associated with the event was not measured, it is estimated likely to have been in excess of 4 m (INGC, 2009). The overall impact of the event led to the displacement of approximately 2 million people, and the loss of about 600 lives. The total estimated economic impact stood at more than US \$ 167 million (INGC, 2009).

Figure 1-1: Satellite image of Tropical Cyclone Eline prior to landfall on 21 February 2000 (INGC, 2009).



The potentially devastating social and economic impact of tropical cyclones underlines the need for a thorough understanding of the frequency and intensity of these events in the South-West Indian Ocean. The risk exposure to tropical cyclones at a given location can be quantified through the estimation of wind speeds at return periods of interest (the n year return period wind speed is the wind speed which is expected to occur once every n years on average). Estimates of wind speeds at return periods of interest for engineering design are of interest to both governments and private sectors, particularly for the development of infrastructure in vulnerable coastal areas.

Considerable uncertainty in the characteristics of tropical cyclones makes the estimation of extreme wind speeds a complicated task. Tropical cyclones occur relatively infrequently and the extent of maximum impact is relatively small (damaging winds are generally confined to within 100 km of the eye). The frequency of storms at a given site is therefore typically significantly less than 1 storm per year (Resio et al., 2007), which leads to small sample sizes, and consequently large errors in the extrapolation of the historical records to return periods of interest.

The inability of the historical records alone to provide a robust basis for the quantification of extreme tropical cyclone wind speed estimates has led to much research into the development of probabilistic tropical cyclone risk models. Such models use a Monte Carlo type approach to generate a database of tropical cyclones which is statistically consistent with the historical events, but is sufficiently long to avoid sampling errors. There is a large variety of such tropical cyclone risk models, although the state-of-the-art approach involves the simulation of thousands of years of synthetic tropical cyclone tracks. In this approach, the development of each synthetic track is modelled from genesis through to termination. Coupling a wind field model to the synthetic track model allows for the generation of thousands of years of extreme wind speeds at any location of interest, thus circumventing problems associated with small sample sizes associated with the historical data.

Research in the field of tropical cyclone risk modelling has typically focussed on economically developed regions such as the North Atlantic (Powell et al., 2005; Emanuel et al., 2006; Hall & Jewson, 2007; Lee & Rosowsky, 2007), North-West Pacific (Rumpf et al., 2007; Yin et al., 2009; Graf & Nishijima, 2009) and South Pacific (James & Mason, 2005) Oceans. There has been relatively little research into the quantification of extreme wind speeds for the South-West Indian Ocean, underlining the need for the present research.

1.2 Thesis Objective

The objective of this thesis is to quantify risk exposure to tropical cyclones over the South-West Indian Ocean through the generation of extreme wind speed maps for the region.

1.3 Study Approach

The thesis objective has been achieved through the development of a tropical cyclone risk model, consisting of a wind field model and a synthetic track model. Tropical cyclone wind fields have been modelled using the Willoughby et al. (2006) wind profile model. Synthetic tracks have been simulated using a statistical model based on historical best track data, largely following the methods proposed by Powel et al. (2005) and Emanuel et al. (2006). The extreme wind speed maps due to tropical cyclones produced as part of this thesis are intended to provide much needed guidance for the planning and design of port and coastal infrastructure in the region.

1.4 Thesis Structure

Section 2 provides the supporting literature upon which this study is based, while Section 3 provides an overview of the approach used to achieve the thesis objective. Section 4 presents the best track data forming the basis of the study, and provides an overview of the climatology of tropical cyclones in the South-West Indian Ocean. Sections 5 and 6 present the two components of the tropical cyclone risk model developed as part of this study; namely the parametric wind field model and the synthetic track model respectively. Section 7 presents the results of the tropical cyclone risk model in the form of extreme wind speed maps for the region. Conclusions and recommendations are discussed in Section 8.

2. LITERATURE REVIEW

2.1 Introduction

Owing largely to the great threat which they pose to infrastructure and human life around the world, there has been an enormous amount of research carried out to better understand tropical cyclones. This section focusses on the literature which specifically addresses the objective of this thesis, as described in Section 1.2. As such, the topic of tropical cyclone risk modelling, for the calculation of extreme wind speeds, forms the main focus of the literature review.

This section begins with a description of the general characteristics of tropical cyclones and discusses best track data, which forms the basis to all tropical cyclone risk models. Tropical cyclone risk models are then described in terms of their two main components; namely wind field models and synthetic track models.

2.2 Characteristics of Tropical Cyclones

2.2.1 Definition

Tropical cyclones are defined as any warm-core, non-frontal, low pressure synoptic scale system that develops over tropical or subtropical waters, and has a definite organised surface circulation (Neumann et al., 1999).

These systems are locally referred to as 'hurricanes' when they occur in the North Atlantic and North-East Pacific Oceans, and 'typhoons' when they occur in the North-West Pacific and North Indian Oceans. Nomenclature can be further complicated as systems are sometimes only classified as 'tropical cyclones' when their intensity exceeds a defined threshold (see Section 2.2.4).

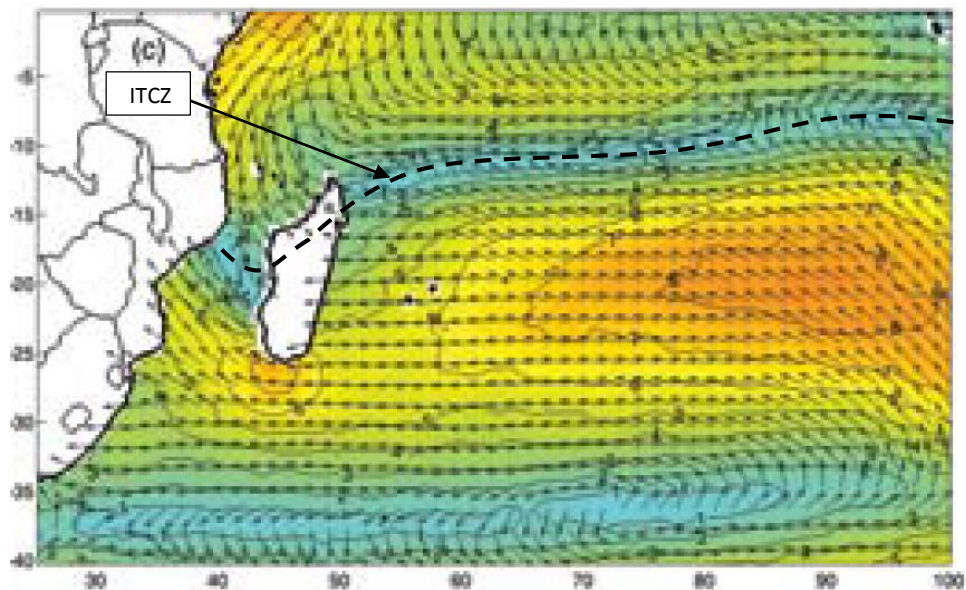
The generic term 'tropical cyclone' is used throughout this study to describe any system satisfying the technical description provided above.

2.2.2 Genesis, Development and Structure

The initial formation of a tropical cyclone is referred to as tropical cyclone genesis. In the South-West Indian Ocean, tropical cyclone genesis typically occurs over the Inter-Tropical Convergence Zone (ITCZ) or monsoon trough (Rhome & Raman, 2006). This is a zonal band of low atmospheric pressure and cloud clusters caused by converging trade winds, rising air and intense thermal heating near the equator. Figure 2-1 shows the monthly averaged wind

velocities over the South-West Indian Ocean for the month of January (the peak of the tropical cyclone season for the region), highlighting the band of low wind speeds characteristic of the ITCZ.

Figure 2-1: Monthly averaged wind velocities over the South-West Indian Ocean for the month of January, highlighting the band of low wind speeds characteristic of the ITCZ (adapted from Mavume et al. (2009)).



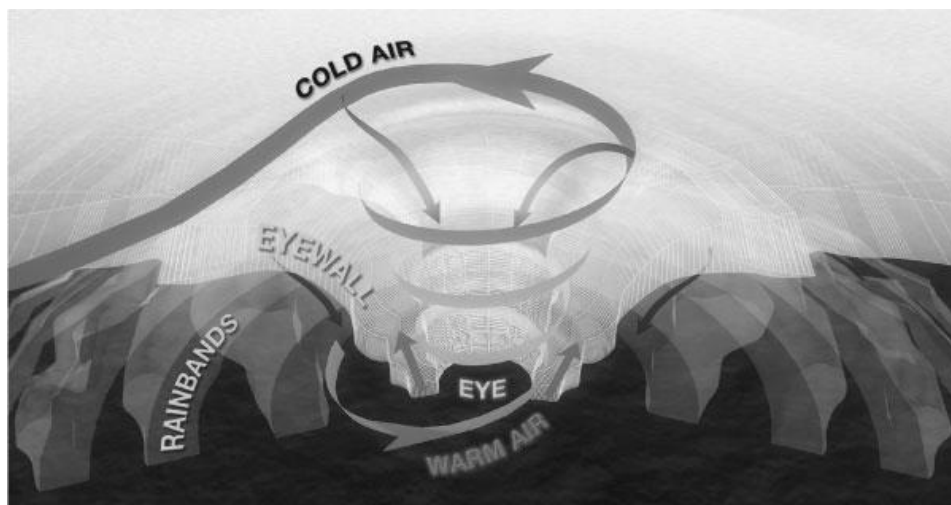
Although the environmental conditions necessary for the genesis of tropical cyclones are notoriously difficult to predict, various authors have identified some general requirements which are summarised as follows (Harper et al., 2001; Gray et al., 1994):

- Sufficiently warm sea surface temperature (SST) (above 26-27°C). Warm water is the primary source of energy which fuels tropical cyclones. Warm water temperature to a sufficient depth (about 60 m) is also a requirement so that surface mixing due to strong winds does not significantly reduce the SST.
- An atmosphere which cools fast enough with height to result in moist instability between the surface and the 500 hPa level (approximately 5600 m above sea level).
- High values of relative humidity in the lower to middle layers of the troposphere. Dry middle layers are not conducive to continual development of thunderstorm activity.
- Exceedance of a threshold of the Coriolis force (corresponding to latitudes greater than about 500 km away from the equator). Without the Coriolis force the low pressure of the disturbance cannot be maintained.

- Low values of vertical wind shear between the surface and upper troposphere. Vertical wind shear is the magnitude of change in wind speed with height.
- A pre-existing disturbance which results in a weakly organized system with sizable spin and low level inflow.

If conditions for tropical cyclone genesis are met, weak but organised winds may begin to rotate about a small pressure deficit (Gray, 1998). Deflection due to the Coriolis force causes winds to rotate in a clockwise direction in the southern hemisphere, and in an anticlockwise direction in the northern hemisphere. The development of a weakly organised disturbance to a mature tropical cyclone is not discussed in any detail here, but it is a function of the prevailing oceanic and atmospheric conditions, land influences, and the dynamics of the inner core of the system. A review on this subject is provided by Rhone & Raman (2006). The main structural features of a mature tropical cyclone at the earth's surface are the eye, the eyewall and the spiral rain bands (Harper et al., 2001). These features are depicted in Figure 2-2.

Figure 2-2: Schematic of the physical structure of a mature tropical cyclone (USGS, 2013).



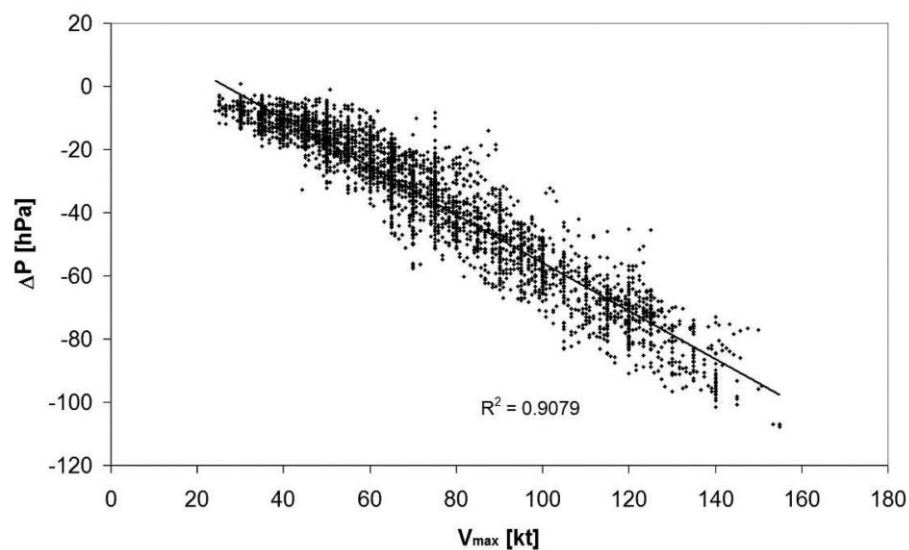
The eye is typically 20 to 50 km in diameter and is located at the centre of the system, where the surface pressure is the smallest. Within the eye, skies are clear and winds are light, providing a convenient visual structure which can be tracked with the aid of satellite, radar or aircraft observations. The eyewall is an area of cumulonimbus cloud, which swirls around the eye. The eyewall is in the order of 50 to 100 km wide and is typically the region associated with the heaviest rainfall and strongest winds. The rain bands spiral inwards towards the eye and can extend over 1000 km or more from the eye (Harper et al., 2001).

Owing largely to the forward motion of the system, tropical cyclone wind speeds are very rarely axisymmetric (radially symmetric about the eye). The translational speed of the storm either adds to wind speeds in the same direction as the motion, or reduces those in the opposite direction. Due to the clockwise rotation of wind speeds in the southern hemisphere, wind speeds are consequently higher to the left of the forward motion of these tropical cyclones.

2.2.3 Wind-Pressure Relationship

Tropical cyclone intensity at a given moment in time is defined either by the maximum sustained surface (10 m elevation) wind speed anywhere in the storm (V_{max}) or the difference between the atmospheric pressure at the centre of the system (P_c) and the ambient pressure (P_0). Figure 2-3 presents the observed relationship between V_{max} and the central pressure deficit ($\Delta P = P_0 - P_c$) from 15 years of aircraft reconnaissance measurements, mostly over the North Atlantic Ocean (Knaff & Zehr, 2007).

Figure 2-3: Observed relationship between V_{max} and ΔP from 15 years of aircraft reconnaissance measurements (Knaff & Zehr, 2007).



The strong relationship between V_{max} and ΔP is often approximated through a one-to-one relationship of the following form:

$$V_{max} = a(\Delta P)^b$$

Equation 2-1

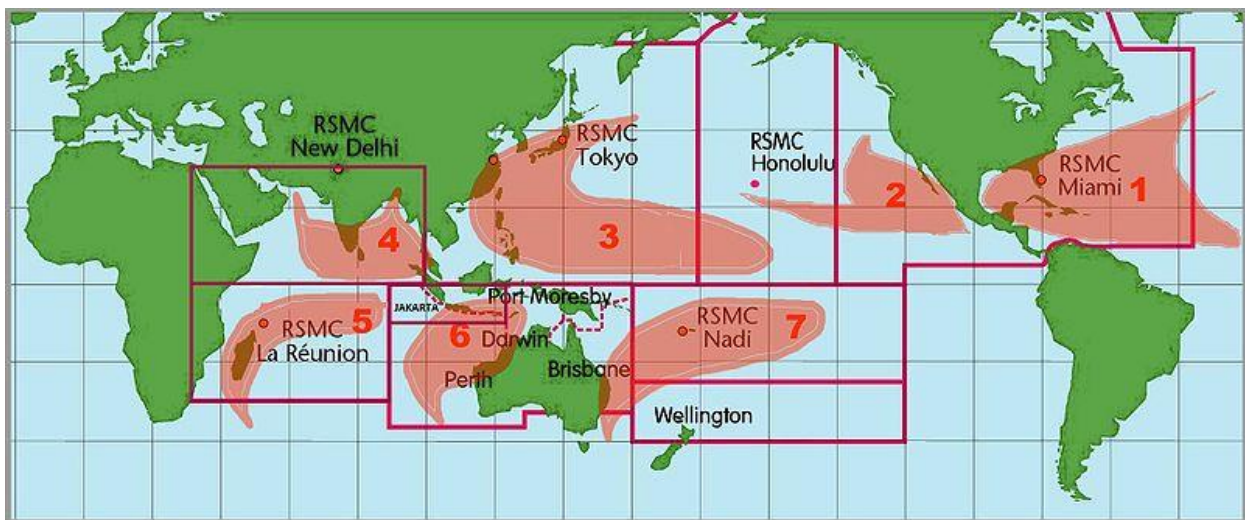
where a and b are empirically derived constants. Many such wind-pressure relationships (WPR's) can be found in the literature. Notably, the Atkinson & Holliday (1977) relationship (a

= 6.7, $b = 0.644$), and modifications thereof, have been extensively adopted by various meteorological centres. More recently proposed WPR's have been adapted to include the dependence on the forward motion of system, the latitude and the size of the system (Knaff & Zehr, 2007; Holland, 2008).

2.2.4 Classification

There are seven defined "basins" around the globe where tropical cyclones occur on a regular basis, as shown in Figure 2-4. The South-West Indian Ocean is defined as the region of the Indian Ocean lying south of the equator and west of 90° E (basin 5 in Figure 2-4).

Figure 2-4: "Basins" where tropical cyclones occur on a regular basis (NOAA, 2014).



Tropical cyclone activity within each basin is monitored by various Tropical Cyclone Warning Centres (TCWC's) and Regional Specialised Meteorological Centres (RSMC's). The primary function of these organisations is to provide real-time analysis and forecasting of tropical cyclones so that public warnings can be issued accordingly. The classification of tropical cyclones into predefined categories provides a useful tool for the issuing of public warnings as well as for the analysis and comparison of historical events.

Although a number of classification systems are in use, the one most widely referenced is the Saffir-Simpson scale which uses the 1-min average V_{max} as the determining parameter. The Saffir-Simpson scale is shown in Table 2-1, while more exhaustive descriptions of the expected damage due to each category are provided in NWS (2012).

Table 2-1: Saffir-Simpson scale

Category	1-min average V_{max} (m/s)	Expected Damage
Tropical Depression	< 17	None or minimal
Tropical Storm	17 – 33	Minimal
1	34 – 42	Minimal
2	43 – 49	Moderate
3	50 – 58	Extensive
4	59 – 69	Extreme
5	> 69	Catastrophic

The RSMC responsible for issuing warnings throughout the South-West Indian Ocean is Météo France La Réunion (MFR). Official World Meteorological Organisation (WMO) sanctioned warnings for the region are issued on the Météo France web site (MFR, 2013). MFR uses the estimated 10-min average V_{max} to classify tropical cyclone intensity, and the categories adopted by this organisation are shown in Table 2-2.

Table 2-2: Météo France La Réunion classification scale

Category	10-min average V_{max} (m/s)
Tropical Disturbance	< 14
Tropical Depression	15 – 17
Moderate Tropical Storm	18 – 24
Severe Tropical Storm	25 – 32
Tropical Cyclone	33 – 46
Intense Tropical Cyclone	47 – 59
Very Intense Tropical Cyclone	> 59

The distinction between 1-min (Table 2-1) and 10-min (Table 2-2) average wind speeds is an important one as lower averaging times will lead to higher wind speed estimates, due to the gustiness of strong winds. Converting between wind speed averaging periods is discussed in more detail in Section 2.4.6.

2.3 Best Track Data

2.3.1 Description of Data

A by-product of the operational activities of the various Tropical Cyclone Warning Centres (TCWC's) and Regional Specialised Meteorological Centres (RSMC's) is the maintenance of historical records of tropical cyclones, termed "best track" data. These best track data provide the longest available historical records of tropical cyclone activity and form the basis of tropical cyclone risk assessments.

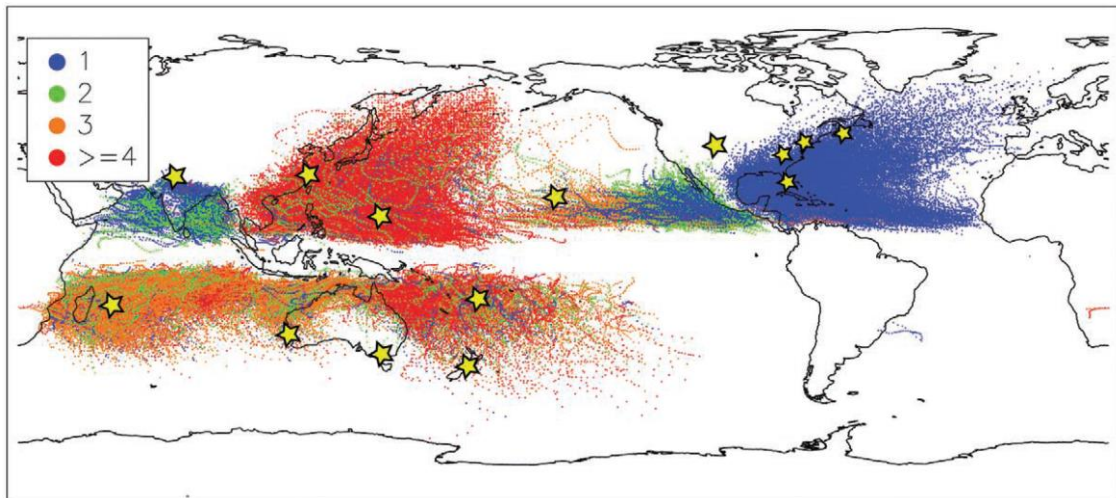
Global best track data from various meteorological organisations tracking cyclone activity are freely available online from the International Best Track Archive for Climate Stewardship (IBTrACS). The IBTrACS project was specifically set up to address issues with the accessibility and comparison of the numerous available international best track datasets being archived by the various meteorological organisations (Levinson et al., 2010). As such, the IBTrACS database provides independent estimates of best track parameters for all historical tropical cyclones on record, as supplied by the various meteorological organisations tracking global cyclone activity. Although different organisations provide varying levels of detail for each tropical cyclone event, the following data are commonly available at 6 hourly intervals:

- Location of the eye in geographical coordinates of longitude (ψ) and latitude (φ),
- Minimum central pressure (P_c),
- Maximum sustained 1-min or 10-min average surface (10 m elevation) wind speed anywhere in the storm (V_{max}).

Figure 2-5 presents the global IBTrACS database and indicates the number of organisations archiving best track data for each storm. The figure indicates that three independent best track estimates are available for most historical tropical cyclones over the South-West Indian Ocean. These datasets are available from the following sources (Levinson et al., 2010):

- The US Navy/Air Force Joint Typhoon Warning Centre (JTWC),
- Météo France La Réunion (MFR),
- C. Neumann's southern hemisphere data (Neumann et al., 1999).

Figure 2-5: Global tropical cyclone tracks, colour coded by the number of organisations providing best track data for each storm. The stars denote the locations of the organisations monitoring tropical cyclone activity (Levinson et al., 2010).



2.3.2 Historical Development of Analysis Techniques

Global best track data archives extend as far back as the mid-19th century. Without the availability of any remote sensing techniques, the tracks of storms before the 1940s have been estimated entirely from vessels and land-based observations where storms happened to pass sufficiently nearby to be detected. Large errors are therefore to be expected in both the number of events, and the location estimates over this period of time.

The development of radar during World War II led to an increase in detection of tropical cyclones, while the advent of satellite imagery in the 1960s provided the ability to easily monitor the movement of storm tracks. Satellite imagery also provided the first means by which the intensity of storms could be estimated remotely.

Developed since the start of the satellite era, the Dvorak technique (Dvorak, 1984) remains the most widely used tool for estimating tropical cyclone intensity to this day (Knaff et al., 2010). The details of the Dvorak technique are beyond the scope of this study, but it involves the evaluation of cloud patterns and infrared cloud-top temperatures to define an estimate of the current intensity index (CI). The maximum sustained surface (10 m elevation) wind speed and/or central pressure is then read off from a predefined table, varying between basins and organisations. A detailed description of the application and historical development of the technique is provided by Velden et al. (2006).

The accuracy of storm location and intensity estimates are significantly improved when aircraft reconnaissance data are available. These data are measured by instruments fitted to aircraft which fly into storms at elevations sufficiently high to avoid dangerous wind speeds and turbulence (usually about 3 km altitude (Franklin et al., 2003)). Surface wind speeds are inferred from flight level wind speeds via numerical boundary layer models, or determined directly from dropsonde data. Dropsondes are instruments released from the aircraft which measure the vertical wind speed profile as they fall toward the sea surface. Correcting from flight level to surface wind speeds is important for the numerical modelling of tropical cyclone wind fields and is discussed in Section 2.4.3.

2.3.3 Accuracy of Best Track Data

While aircraft reconnaissance data are routinely collected over the North Atlantic Ocean, this is not the case over the South-west Indian Ocean, where the Dvorak technique remains the primary method for estimating intensity (Knaff & Harper, 2010). The accuracy of the best track data for the South-west Indian Ocean is therefore largely limited by the accuracy of the Dvorak technique.

The Dvorak technique lends itself to errors associated with natural variability in the cloud pattern/cyclone intensity relationship, as well as errors associated with the subjective nature of the technique (Velden et al., 2006). In an analysis of 20 years (1989 - 2008) of data for the North Atlantic basin, the performance of the Dvorak technique was measured against tropical cyclones for which aircraft reconnaissance data were available (Knaff et al., 2010). The bias in the technique was found to be primarily a function of storm intensity, and to a lesser extent the latitude, storm translational speed, and storm size. The overall root mean square error in the method was found to be 11 kt (5.7 m/s), with the method tending to under-predict the intensity of more intense storms. This error is not insignificant (in the order of half a Saffir-Simpson scale category), and should be born in mind when interpreting the data. Knaff et al. (2010) do however note that errors and biases may vary between different best track datasets, given the varying climatology between basins and the application of the method by different organisations.

The error in track location associated with best track data has been quantified through an analysis of the “position accurate within” value, as archived by National Hurricane Centre (NHC) forecast advisories for both Atlantic and Eastern Pacific tropical cyclones from the year 2000 to 2009 (Torn & Snyder, 2012). These estimates are subjectively determined by NHC

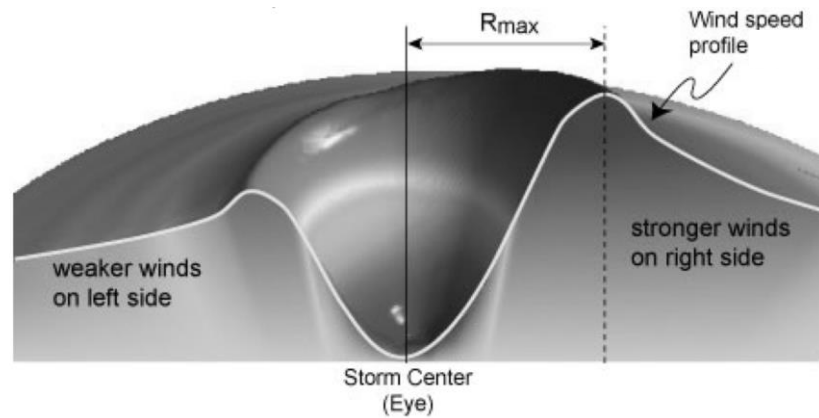
forecasters, based on the difficulty in estimating the location of the centre of the system. Generally, the uncertainty in track location is inversely proportional to increasing storm intensity, since more intense storms tend to have a more clearly defined eye. Torn & Snyder (2012) found the root mean square uncertainty to decrease almost linearly from 43 n mi (80 km) for tropical depressions to 16 n mi (30 km) for category 4 and 5 tropical cyclones (Saffir-Simpson scale).

2.4 Wind Field Models

Best track data provide estimates of the location of the eye and the intensity of a given tropical cyclone, but rarely provides any information on the spatial arrangement of wind speeds around the eye. The generation of tropical cyclone wind fields from the limited available data therefore forms a vital component of any risk assessment model. This task is either carried out using a dynamic numerical model, or (more commonly) using a simplistic parametric model. Dynamic numerical models use the underlying atmospheric physics as the basis to generate surface wind fields, but are computationally expensive, as they rely on very fine grids. The relative uniformity of the intense vortex of a tropical cyclone lends itself to a simplistic parametric representation, with the performance of parametric models being comparable to more complicated dynamic models (Dima & Desflots, 2010; Holland et al., 2010). Only the parametric representation of the wind field is considered in this study.

The basis for all parametric models is the calculation of a wind speed profile. The calculated profile is applied radially around the eye of the storm to generate a two dimensional axisymmetric (radially averaged) wind field. Adjustments to the wind field are then applied to allow for planetary boundary layer corrections, forward motion asymmetry, wind inflow angle and correcting for the wind speed averaging period (these adjustments are defined and discussed individually in Sections 2.4.3 to 2.4.6). A typical schematic example of the output of a parametric wind field model is provided in Figure 2-6.

Figure 2-6: Schematic example of a parametric wind field (Dima & Desflots, 2010). The winds are stronger to the right hand side of the forward motion in this example, as the example is of a northern hemisphere tropical cyclone.



2.4.1 Radius to Maximum Wind Speed

A good estimate of the radius to maximum wind speed (R_{max} , shown in Figure 2-6) is a key parameter for accurately reproducing tropical cyclone wind fields. This parameter is however difficult to estimate remotely (e.g. through satellite imagery alone), and is not routinely provided in best track data. Researchers have therefore developed empirical formulae which provide estimates for R_{max} as a function of more readily available parameters.

Generally, it has been found that the magnitude of R_{max} is negatively correlated with storm intensity, in that more intense storms tend to have smaller radii to maximum wind speed. This can be likened to a figure skater drawing in her arms and spinning faster. R_{max} has also been found to be correlated with latitude (φ), with storms tending to increase in size as they move further away from the equator. Deterministic relationships for R_{max} show low correlation coefficients (r^2 in the order of 0.2 to 0.3) when compared with measurements. They are therefore useful in providing statistically non-biased estimates of storm size, but may yield large errors for individual storms. Some commonly used relationships are provided below.

Willoughby & Rahn (2004) used aircraft reconnaissance data measured over the Atlantic and Pacific Oceans from 1977 to 2000 to determine the following empirical relationship for R_{max} (in km):

$$R_{max} = 46.29e^{-0.0153V_{Fmax}+0.0166\varphi}$$

Equation 2-2

where V_{Fmax} is the flight level (i.e. at several kilometres altitude) wind speed (in m/s). It is important to note that Equation 2-2 was derived from radially averaged measured wind speed profiles (i.e. average profiles from a number of traverses over the vortex), including vector subtraction of the storm's forward motion.

Vickery & Wadhera (2008) considered the same aircraft reconnaissance data as Willoughby & Rahn (2004), but used the central pressure deficit (in hPa) as the measure of the storm intensity:

$$\ln(R_{max}) = 3.559 - 7.229 \times 10^{-5} \Delta P^2 + 5.296 \times 10^{-4} \varphi^2$$

Equation 2-3

Knaff et al. (2007) used wind radii estimates made by the National Hurricane Centre (NHC) and the Joint Typhoon Warning centre (JTWC) between 1988 and 2003 to determine the following operational predictor of R_{max} for the North Atlantic basin:

$$R_{max} = 66.86 - 0.0469V_{max} + 1.063(\varphi - 25)$$

Equation 2-4

The V_{max} referred to in Equation 2-4 is the maximum sustained 1-min average surface (10 m elevation) speed anywhere in the tropical cyclone (as directly provided in the best track data). The coefficients have been adjusted from those presented in Knaff et al. (2007) to convert the units of R_{max} and V_{max} to km and m/s respectively, to allow for direct comparison with the other presented relationships.

2.4.2 Wind Profile Models

2.4.2.1 Modified Rankine Vortex

The simplest form of a parametric wind profile model is that of a modified rankine vortex, initially proposed by Depperman (1947). In this model, the stationary wind field is approximated according the following relationship:

$$V(R) = V_{max} \left(\frac{R_{max}}{R} \right)^x \text{ for } R \geq R_{max}$$

$$V(R) = V_{max} \left(\frac{R}{R_{max}} \right) \text{ for } R < R_{max}$$

Equation 2-5

where x is an empirically determined scaling parameter. Typical values for x have been found to be in the range of 0.4 to 0.6 (Hughes, 1952). Most recently, the following relationship for the parameter x was found for Atlantic basin tropical cyclones (Knaff et al., 2007):

$$x = 0.1147 + 0.0026V_{max} - 0.001(\varphi - 25)$$

Equation 2-6

where V_{max} is the 1-min sustained surface wind speed. Equation 2-6 has been adjusted from that presented in Knaff et al. (2007) to convert the units of V_{max} from knots to m/s. The positive correlation of x with V_{max} implies that more intense storms tend to have a more rapid decrease in wind speed away from the eyewall (i.e. a steeper profile).

The monotonic decrease in wind speed away from the eyewall described by the Rankine vortex model tends to be a poor representation of measured wind speed profiles, making it not particularly widely used (Harper et al., 2001). It has however been presented here for completeness.

2.4.2.2 Holland (1980) Model

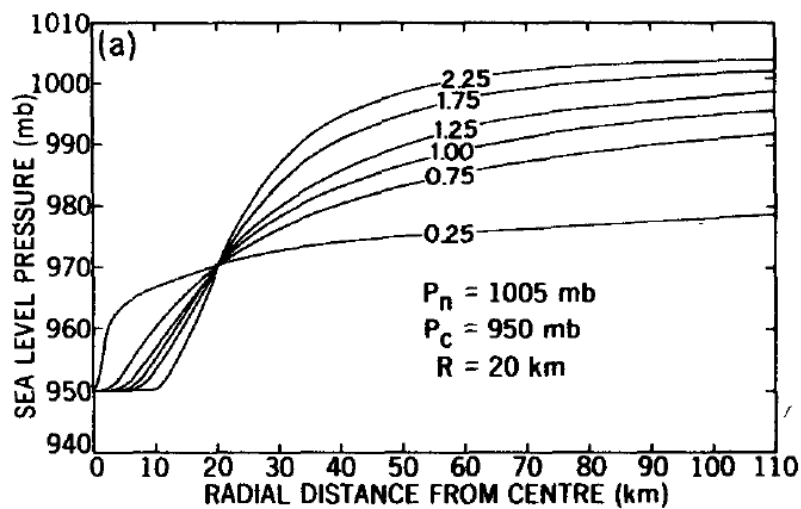
An alternative approach to generating a realistic wind speed profile is to determine a reliable sea-level pressure profile from which wind speeds can be analytically inferred (using the theoretical relationship between V_{max} and ΔP). Schloemer (1954) compared a number of analytical pressure profile models against sea-level pressure measurements of historical tropical cyclones, and found a rectangular hyperbola model to provide the best fit to the data. Extending the work of Schloemer, Holland (1980) showed that the analytical profile model could be improved through the inclusion of a shape or 'peakedness' parameter B . The Schloemer (1954) pressure profile equation, with the inclusion of the Holland (1980) B parameter, is expressed as follows:

$$P(R) = P_c + \Delta P e^{-\left(\frac{R_{max}}{R}\right)^B}$$

Equation 2-7

Physically, B determines the shape, or gradient of the pressure profile, as depicted in Figure 2-7.

Figure 2-7: The effect of varying the Holland B parameter on the pressure profile (Holland, 1980).



The analytical pressure profile is used to calculate the gradient level wind speed under the assumption that the centripetal and coriolis forces exactly balance the atmospheric pressure gradient (cyclotrophic balance). The gradient level wind is defined as the “wind blowing under conditions of circular motion, parallel to the isobars, in which the centripetal and coriolis accelerations together exactly balance the horizontal pressure-gradient force per unit mass” (NOAA-NWS, 1979). Physically, the gradient level is the level most representative of the air flow in the lower atmosphere, immediately above the layer affected by surface friction of the earth (the planetary boundary layer). The gradient level is at an elevation of about 1000 m in the outer vortex region, and decreases to about 500 m near the region of maximum winds (Franklin, et al., 2003; Powell, et al., 2003; Vickery, et al., 2009a). The force balance gradient level wind speed equation is as follows:

$$\frac{V_G^2}{2} + fV_G = \frac{1}{\rho_A} \frac{dP}{dR}$$

Equation 2-8

where:

V_G = Gradient level wind speed,

ρ_A = Density of air,

f = Coriolis parameter = $2\omega \sin\phi$, where ω is the angular frequency of the earth’s rotation.

Differentiating Equation 2-7 and substituting into Equation 2-8 yields the gradient wind speed at any radius (R) from the centre of the eye:

$$V_G(R) = \left[\frac{B\Delta P}{\rho_A} \left(\frac{R_{max}}{R} \right)^B e^{-\left(\frac{R_{max}}{R} \right)^B} + \frac{R^2 f^2}{4} \right]^{\frac{1}{2}} - \frac{fR}{2}$$

Equation 2-9

Holland (1980) demonstrated that at the maximum wind speed (when $R = R_{max}$) the contribution of the Coriolis parameter to the gradient wind speed is negligible, therefore:

$$V_{Gmax} = \sqrt{\frac{B\Delta P}{e\rho_A}}$$

Equation 2-10

and Equation 2-9 can be recast as:

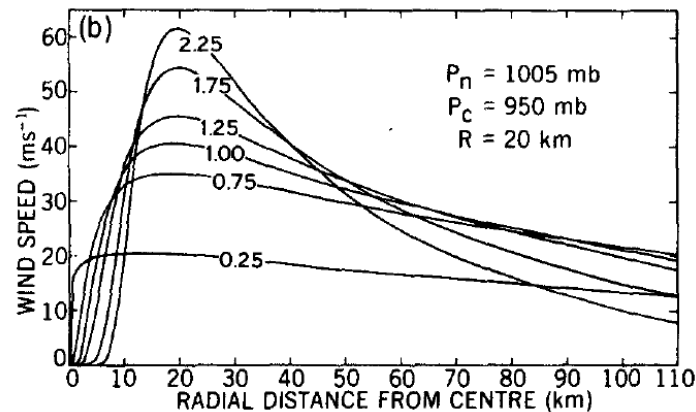
$$V_G(R) = V_{Gmax} \left[\left(\frac{R_{max}}{R} \right)^B e^{(1-R_{max}/R)^B} \right]^{\frac{1}{2}}$$

Equation 2-11

Given a central pressure deficit (ΔP) and an estimated radius to maximum wind speed (R_{max}), the wind speed at any distance from the centre of the eye (R) can be computed through Equation 2-10 and Equation 2-11. Alternatively, if V_{Gmax} is known, for example through aircraft reconnaissance measurements, then the wind speed profile can be computed directly through Equation 2-11. The Holland (1980) parametric model represented by these equations remains one of the most popular parametric models used to describe tropical cyclone wind fields (Willoughby & Rahn, 2004).

The application of the Holland model requires the estimation of the shape parameter B . Higher values of B result in more peaked profiles, as illustrated in Figure 2-8. B represents the calibration parameter for the model, therefore much research has been carried out to quantify this variable. Only a few of the recently proposed methods for its estimation are discussed below.

Figure 2-8: The effect of varying the Holland B parameter on the gradient level wind speed profile (Holland, 1980).



Willoughby & Rahn (2004) developed an algorithm to select the shape parameter B which provided the best fit to measured wind speed profiles from aircraft reconnaissance data. Relationships for B were determined when R_{max} is both included and excluded as a dependent variable. As this parameter is not routinely known, only the relationship excluding dependence on R_{max} is presented here:

$$B = 0.866 + 0.0177V_{Fmax} - 0.0094\phi$$

Equation 2-12

As per Equation 2-2, V_{Fmax} is the flight level (i.e. at several kilometres altitude), azimuthally averaged (i.e. radially averaged about the cyclone eye) wind speed. If V_{Fmax} is known, then the flight level wind speed profile can be computed from Equation 2-12, and then substituting V_{Fmax} for V_{Gmax} in Equation 2-11.

Vickery & Wadhwa (2008) found the Holland B parameter to be a function of a dimensionless parameter A :

$$A = \frac{R_{max}f}{\sqrt{2R_dSST \ln\left(1 + \frac{\Delta P}{P_c e}\right)}}$$

Equation 2-13

where:

R_d = Gas constant for dry air,

SST = Sea surface temperature.

The relationship between the parameters B and A was found to be as follows:

$$B = -2.237\sqrt{A} + 1.732$$

Equation 2-14

Holland (2008) presented an alternative calculation of the shape parameter specifically designed for the direct calculation of maximum surface wind speeds (rather than axisymmetric gradient level wind speeds):

$$B_s = -4.4 \times 10^{-5} \Delta P^2 + 0.01 \Delta P + 0.03 \frac{dP_c}{dt} - 0.014 \varphi + 0.15 c^{0.6} \left(1 - \frac{\Delta P}{215}\right) + 1.0$$

Equation 2-15

where:

B_s = shape parameter (subscript 's' denotes surface),

$\frac{dP_c}{dt}$ = change in intensity in hPa/h,

c = storm translation speed in m/s.

In this revised approach, information readily available in best track data can be used to calculate B_s , which can be substituted for B in Equation 2-10 and Equation 2-11 to generate the surface (10 m elevation) sustained wind speed profile through the region of maximum wind speed (taking asymmetry due to forward motion into account).

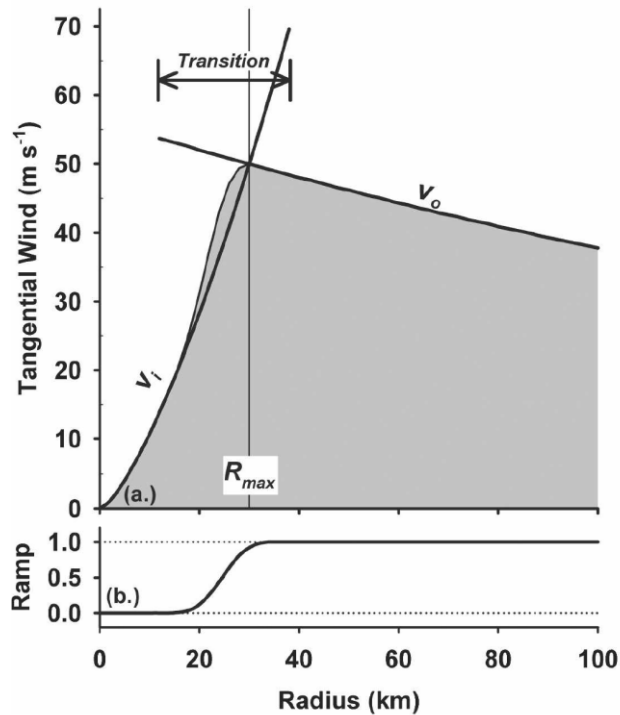
2.4.2.3 Willoughby et. al (2006) Model

In an evaluation of the Holland (1980) model against aircraft reconnaissance wind profile measurements, Willoughby and Rahn (2004) found the model to yield systematic errors. The observed bias was an over-estimation of wind speeds in the vicinity of the maximum wind, while the wind speeds further away from the eyewall were found to drop off too rapidly.

In further research, using the same measured wind speed profiles as those analysed by Willoughby and Rahn (2004), Willoughby et al. (2006) proposed an alternative family of profiles, comprising piece-wise continuous analytical segments patched smoothly together. The proposed model consists of an inner profile (V_i) and an outer profile (V_o). A polynomial ramp function is used to combine the inner and outer profiles within the transition zone (from R_1 to R_2), spanning the peak of the wind speed profile. The model is entirely empirical,

providing the best fit to nearly 500 flight level axisymmetric (radially averaged) wind speed profiles measured over the Atlantic and East Pacific Oceans during the years 1977 to 2000. Figure 2-9 presents a schematic illustration of the proposed model.

Figure 2-9: Schematic illustration of a sectionally continuous wind speed profile. A ramp function is used to create a smooth transition between the inner (V_i) and outer (V_o) profiles (Willoughby et al., 2006).



Willoughby et al. (2006) present both single and dual exponential profile models for the outer profile (V_o). The dual exponential model for V_o was however found to yield a better fit to the data, particularly for more intense storms. Considering the dual exponential model for the outer profile, the flight level axisymmetric wind speed profile at any distance R from the eye can be computed as follows:

$$V_F(R) = V_i = V_{Fmax} \left(\frac{R}{R_{max}} \right)^y \text{ for } 0 \leq R \leq R_1$$

$$V_F(R) = V_i(1 - w) + V_o w \text{ for } R_1 \leq R \leq R_2$$

$$V_F(R) = V_o = V_{Fmax} \left[(1 - C)e^{\left(-\frac{R-R_{max}}{X_1} \right)} + Ce^{\left(-\frac{R-R_{max}}{X_2} \right)} \right] \text{ for } R_2 \leq R$$

Equation 2-16

where w is the polynomial ramp function, required to ramp up from 0 to 1 as R ranges from R_1 to R_2 (see Figure 2-9). w is expressed in terms of a dimensionless parameter $\xi = (R - R_1) / (R_2 - R_1)$:

$$w(\xi) = 126\xi^5 - 420\xi^6 + 540\xi^7 - 315\xi^8 + 70\xi^9$$

Equation 2-17

Recognising that $V'(R_{max}) = 0$, and that $V_i(R_{max}) = V_o(R_{max}) = V_{max}$, the polynomial ramp function at R_{max} becomes:

$$w\left(\frac{R_{max} - R_1}{R_2 - R_1}\right) = \frac{yX_1}{yX_1 + R_{max}}$$

Equation 2-18

The width of the transition zone ($R_2 - R_1$) is specified a priori at a value between 10 and 25 km. R_1 can then be solved for, through the numerical inversion of Equation 2-17. The remaining constants required for the generation of the wind speed profile have been determined through fitting the model to the aircraft reconnaissance measurements, as a function of storm intensity and latitude. The following empirical relationships result:

$$X_1 = 317.1 - 2.026V_{Fmax} + 1.915\varphi$$

Equation 2-19

$$X_2 = 25$$

Equation 2-20

$$y = 0.4067 + 0.0144V_{Fmax} - 0.0038\varphi$$

Equation 2-21

$$C = 0.0696 + 0.0049V_{Fmax} - 0.0064\varphi, (C \geq 0)$$

Equation 2-22

2.4.3 Planetary Boundary Layer Corrections

The estimated wind speeds provided in the best track data are at a standard reference level of 10 m above the surface. This is also the level required for ocean response modelling i.e. for the prediction of waves and storm surge. The parametric wind field models discussed above are however often based on the derivation of gradient level (Holland, 1980), or measured flight level (Willoughby et al., 2006) wind speeds. Correcting to and from surface, gradient level and flight level wind speeds is therefore an important aspect of many parametric wind field models.

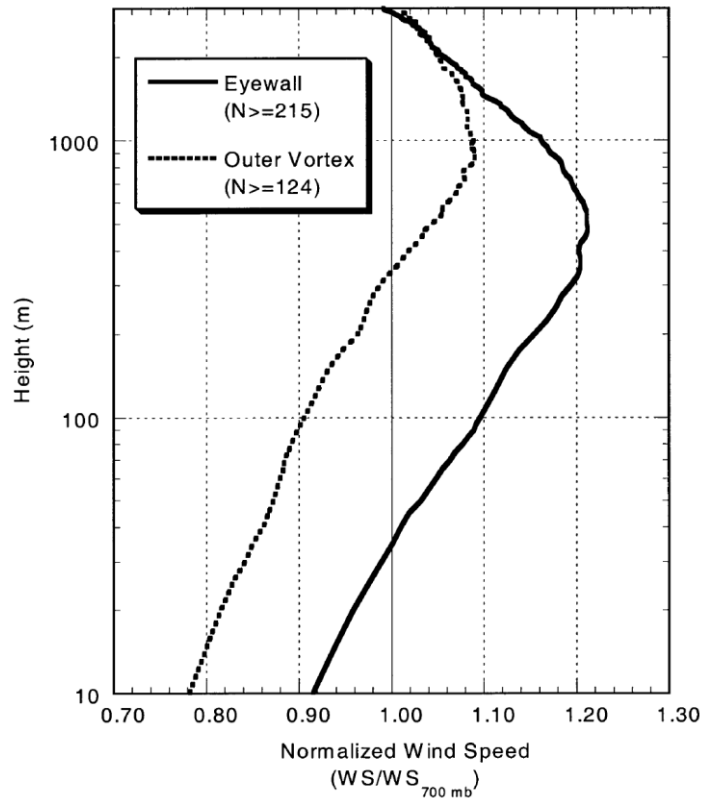
The conversion of flight level or gradient level wind speeds to surface wind speeds was initially carried out through comparisons of flight level measurements with oceanic platform or land based measurements (e.g. Powell & Black, 1990), or through two-dimensional numerical atmospheric boundary layer models (e.g. Thompson & Cardone, 1996; Vickery et al., 2000a). The analysis of dropsonde data from the late 1990s to present has however greatly improved the understanding of the vertical profile of tropical cyclone winds, particularly in the region of the eyewall.

Figure 2-10 compares the mean measured vertical wind speed profiles calculated from dropsonde data collected near the eyewall with those collected in the outer vortex region (Franklin et al., 2003). The definitions of the eyewall and outer vortex regions were however somewhat subjective in the analysis by Franklin et al. (2003). In a practical application of these results, Knaff et al. (2011) assumed the eyewall and outer vortex regions to be < 100 km and > 700 km from the centre of the eye respectively.

Figure 2-10 shows that the increase in wind speed with height above the surface of the ocean is approximately logarithmic over the first few hundred metres (note that the y-axis is logarithmic), before reaching a maximum (representing the upper level of the atmospheric boundary layer or gradient level), and decreasing at higher elevations until the flight level is reached. The gradient level is at an elevation of about 1000 m in the outer vortex region and decreases to about 500 m near the region of maximum winds (Franklin et al., 2003; Powell et al., 2003; Vickery et al., 2009a).

Based on the results of the dropsonde data, Franklin et al. (2003) proposed adjustment factors of 0.9 and 0.8 for eyewall and outer vortex regions respectively to convert from 700hPa (3 km) flight level wind speeds to 10 m surface wind speeds. The 10 m surface wind speeds were found on average to be about 0.75 times as strong as the peak, or gradient level, wind speeds.

Figure 2-10: Mean measured wind speed profiles for the eyewall and outer vortex regions of tropical cyclones. The normalised wind speed represents the factor to convert from 700 mb (3 km) flight level wind speed to the level of interest (Franklin et al., 2003).



Powell et al. (2003) analysed the dropsonde data as a function of the mean boundary layer (MBL) wind speed, defined as the vertically averaged wind speed below 500 m elevation. The 10 m surface wind speed was found to be about 0.78 times the MBL wind speed.

Vickery et al. (2009a) developed an empirical model for the boundary layer which was fitted to measured vertical wind speed profiles obtained from the dropsonde data. The ratio of the gradient level wind speed to the 10 m surface wind speed was found to vary between 0.67 and 0.74 as a function of intensity and storm size, with a mean of about 0.71.

It is noted that the factors discussed above are applicable to open-ocean conditions only. Generally, the increased roughness introduced in coastal regions and overland will tend to reduce the surface wind speeds. In the absence of overland dropsonde data, this reduction has been quantified through empirical boundary layer models. In a review of various methods adopted in the literature, Vickery et al. (2009b) quotes reduction factors of 15% to 20% for coastal regions, with further reduction (up to 30%) expected a few kilometres inland.

2.4.4 Asymmetry Corrections

The output of the parametric wind field models discussed above is a wind speed profile which is applied in an axisymmetric fashion around the centre of the eye. Tropical cyclones are however rarely axisymmetric, owing largely to the forward motion of the system. The forward motion will add to wind speed components in the same direction as the forward motion and will decrease components in the opposite direction to the forward motion of the system. As tropical cyclones rotate clockwise in the southern hemisphere, a system travelling in a westerly direction in the South-West Indian Ocean will tend to have stronger wind speeds to the south of the cyclone eye than to the north. The general adjustment for the wind field asymmetry takes the following form (Harper et al., 2001):

$$V(R, \theta) = V(R) + \delta c \cos(\theta_{max} - \theta)$$

Equation 2-23

where:

δ = the fraction of the forward motion added to or subtracted from the axisymmetric wind speed. Typical values of δ are 0.5 to 1, with higher values of δ leading to more asymmetric wind fields.

c = the translation speed of the system.

θ_{max} = the angle to the maximum wind speed, measured from the direction in which the cyclone is moving (typically 65° to 115°). θ_{max} is measured clockwise in the northern hemisphere and counter-clockwise southern hemisphere owing to the opposite side of the location of maximum winds.

It is important to note that the asymmetry correction presented in Equation 2-23 is intended to be applied to a radially averaged wind profile model, leading to a higher maximum wind speed than in the derived input wind profile. If, for instance, the best track data estimate of V_{max} is used as a basis to generate the two-dimensional wind field, then the methodology should be adjusted so that peak wind speed in the asymmetric wind field is equal to that in the best track data (e.g. Mattocks & Forbes, 2008).

2.4.5 Wind Inflow Angle Corrections

The parametric wind field models described above assume a circular wind flow pattern i.e. wind vectors tangential to the pressure isobars. In reality, frictional effects cause winds to be

deflected towards the centre of the storm. The magnitude of the inward deflection is known as the wind inflow angle (β). Over open-ocean conditions, β is typically in the order of 20° (Knaff et al, 2011), although it has been suggested that the angle decreases towards the storm centre (Harper et al., 2001):

$$\beta = 10 \frac{R}{R_{max}} \text{ for } R \leq R_{max}$$

$$\beta = 10 + 75 \left(\frac{R}{R_{max}} - 1 \right) \text{ for } R_{max} < R < 1.2R_{max}$$

$$\beta = 25 \text{ for } R \geq 1.2R_{max}$$

Equation 2-24

2.4.6 Correcting for Wind Speed Averaging Period

It has already been introduced that estimates of both the 1-min average and 10-min average V_{max} are provided in best track archives, depending on the meteorological organisation providing the data. This discrepancy complicates the direct comparison of these datasets and has led to recommendations for the conversion between these two commonly used wind averaging periods. A commonly used correction factor to convert from 1-min average to 10-min average wind speed is 0.88 (WMO, 1993). It has however recently been suggested that this 'traditional' correction factor should be updated according to the location and direction of the considered winds with respect to land, as indicated in Table 2-3 (Harper et al., 2008).

Table 2-3: Recommended factors to convert between 1-min average to 10-min average wind speeds provided in best track data (Harper et al., 2008).

(10-min V_{max}) = K (1-min V_{max})	At-Sea	Off-Sea	Off-Land	In-Land
K	0.93	0.90	0.87	0.84

where:

Off-Land = any land-based near-coastal exposure with offshore wind,

Off-Sea = any land-based near-coastal exposure with onshore wind,

At-Sea = nominally > 20 km offshore.

Tropical cyclone wind speed estimates are often used as input to ocean response models so that the associated waves, storm surge and currents can be estimated. The formulations of

these models have however been based on the ‘mean’ wind speed, i.e. once wind gusts have been averaged out. An averaging interval of 30 – 60 min is generally considered sufficient to filter turbulence from boundary layer winds (Thompson & Cardone, 1996). It is therefore necessary to convert the wind speed estimates provided in the best track data to ‘mean’ wind speeds if they are to be used to force ocean response models. The following provides a useful relationship to convert from an averaging period of t seconds (V_t) to hourly averaged (V_{3600}) wind speeds (USACE, 2008):

$$\frac{V_t}{V_{3600}} = 1.277 + 0.296 \tanh \left[0.9 \log_{10} \left(\frac{45}{t} \right) \right]$$

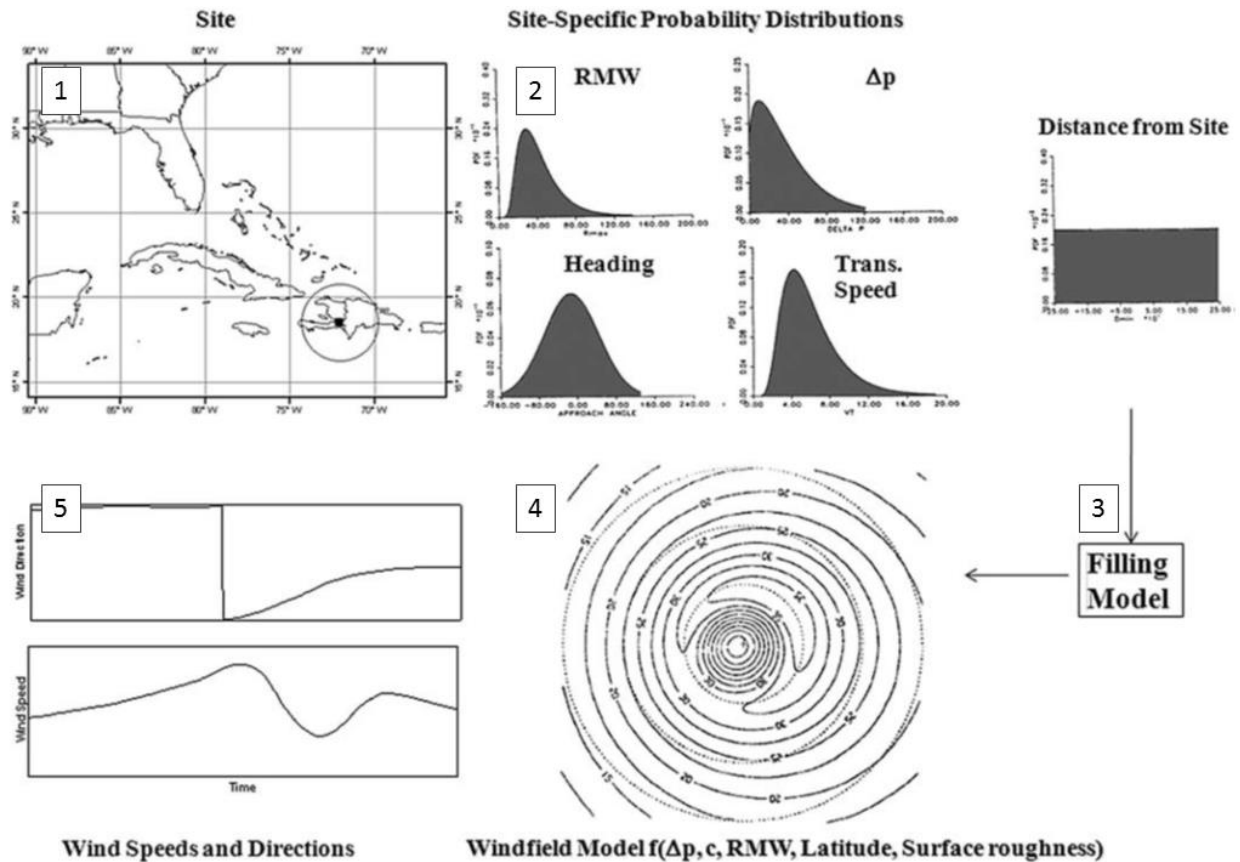
Equation 2-25

2.5 Site Specific Probabilistic Models

Through the application of wind field models (Section 2.4) - along historical tropical cyclone tracks (Section 2.3) - it is possible to model the time-series of wind speed and direction at any location of interest. It is then theoretically possible to carry out an extreme value analysis (EVA) on the modelled peak wind speeds of these historical storms for the quantification of extreme wind speeds at that location. This approach is however severely hampered by the small sample sizes available from historical data, which has the potential to lead to large errors in extreme wind speed estimates. Historical records are therefore considered insufficiently long for the determination of extreme tropical cyclone induced wind speeds required for engineering design (Resio, et al., 2007).

The lack of historical data has led to the development of a variety of probabilistic approaches for the estimation of extreme tropical cyclone induced wind speeds. Such models have been introduced since the 1970s (Russel, 1971) and have been in a state of continual development and improvement. Initial probabilistic models used historical data occurring with a threshold distance of a given site as their basis and are consequently referred to as site specific probabilistic models. An overview of the simulation approach for these models is given in Figure 2-11 (Vickery et al., 2009b).

Figure 2-11: Overview of simulation approach for site specific probabilistic models (Vickery et al., 2009b).



The various components of site specific probabilistic models (labels 1 to 5 in Figure 2-11) are described individually below:

1. The approach begins by identifying historical best track data occurring within a defined threshold distance of a given site of interest. It is assumed that the statistical distributions of the considered parameters can be thought of as homogenous in space within the defined threshold distance of a given site.
2. Probability distributions of key track parameters of interest are derived from the site specific historical best track data. In the shown example, ΔP is used as the intensity parameter, however this can be substituted for V_{max} . The probability distributions of the track parameters are repeatedly sampled in a Monte Carlo simulation, generating thousands of years of combinations of track parameters.

3. For each combination of track parameters generated by the Monte Carlo simulation, a straight line track satisfying the sampled track parameters is generated. The intensity of the track is kept constant until the track makes landfall. The intensity of the track is subsequently reduced as a function of time over land, according to a land filling model.
4. A wind field model (Section 2.4) is applied along each track generated by step 3, yielding two-dimensional wind fields along the track.
5. The modelled parameters of wind speed and direction, as generated by the wind field model, are recorded at the site of interest.

From the described approach, it is possible to generate thousands of years of tropical cyclone induced wind speeds at any site of interest, from which extreme wind speeds at return periods of interest can be derived.

Rossouw (1999) employed a site-specific probabilistic model to determine the occurrence rate of tropical cyclone tracks and their associated intensities at a number of locations along the southern African east coast. Statistical distributions were fitted to historical best track data within 400 km of various sites, in 2.5° latitude increments along the southern African coastline, between 2.5° S and 32.5° S. A limitation to the approach adopted by Rossouw (1999) is that no wind field models were applied to the generated parameters at each site of interest, the conservative assumption being that the site would experience the maximum intensity of a tropical cyclone passing within 400 km of the site. The results of the study are summarised in Table 2-4, as these are particularly relevant to this study.

Table 2-4: Results of Monte Carlo simulations done on 2.5° latitude increments for the Southern African East Coast (Rossouw, 1999).

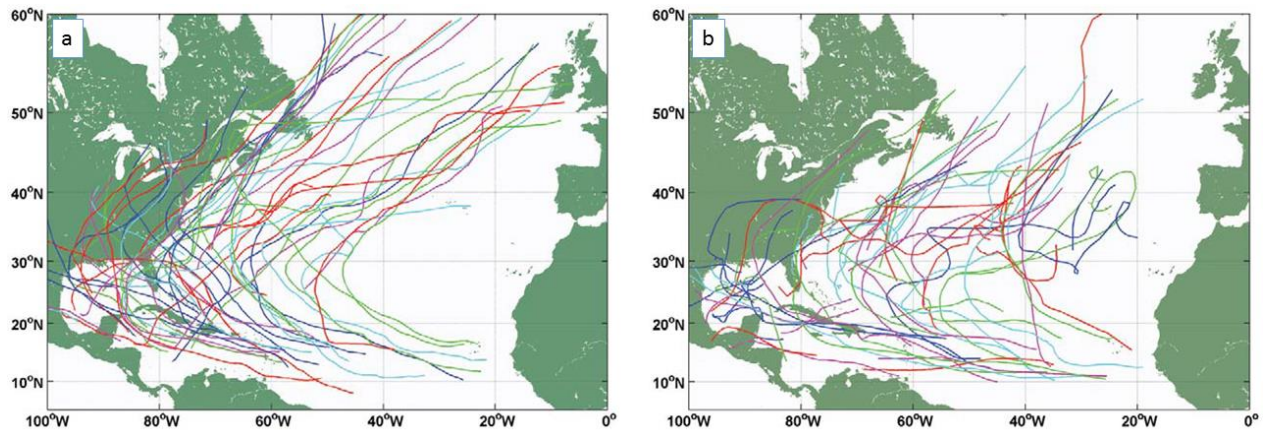
Latitude (degrees South)	Average no. of tropical cyclones in 100 years (no.)	Average maximum intensity (V_{max}) in 100 years (m/s)
2.5	2.2	13
5	4.9	28
7.5	11.4	42
10	28.4	51
12.5	72.5	75
15	157.2	64
17.5	118.5	74
20	70.9	61
22.5	80.2	70
25	34.3	53
27.5	11.5	41
30	1.5	34
32.5	0.0	-

One of the main limitations to site-specific models is the fact that the time history of tropical cyclones is not considered. This becomes particularly important if extreme wave heights are a required output of the analysis as the development of the storm intensity far away from the site will have a significant influence on the generated waves at the site (Resio, et al., 2007). Further, the method is particularly hampered in regions which experience very low activity (Hall & Jewson, 2008) as the distributions derived from the historical tracks may be poor representations of the actual underlying distributions.

2.6 Synthetic Track Models

In a pioneering study, Vickery et al. (2000b) extended the techniques used in site specific probabilistic models through the development of a basin-wide synthetic track model. Rather than generating track parameters at a given site, entire tracks are synthesised over large areas (often over entire basins), from their genesis through to termination. This process effectively produces synthetic best track data in the same format as historical best track data (Section 2.3), but over a duration of thousands of years. Figure 2-12 presents an example of the output of a synthetic track model in comparison to historical best track data for the North Atlantic Ocean (Emanuel et al., 2006).

Figure 2-12: Sixty random tracks from a synthetic track model (a) and a historical dataset (b) over the North Atlantic Ocean (Emanuel et al., 2006).



Through the application of a wind field model along each synthetic track (as per steps 4 and 5 of Figure 2-11) it is possible to generate thousands of years of modelled wind speeds at any location of interest over the model domain. By applying calculations on a regular grid over the domain it is possible to generate extreme wind speed maps over large areas. The use of synthetic tracks in this way remains the current state-of-the-art technique for the quantification of extreme tropical cyclone induced wind speeds (Vickery et al., 2009b; Zhang & Nishijima, 2012).

A wide variety of models have been proposed in the literature for the generation of synthetic tracks. The main components common to all synthetic track models can however be summarised as follows:

- Genesis.
- Track propagation.
- Intensity evolution.
- Termination.

Some of the approaches adopted in the literature for each of these components are discussed below.

2.6.1 Genesis

Tropical cyclone genesis refers to the initial formation of a tropical cyclone. Historical genesis events are identified in the best track archives as the first data entry for a given event.

2.6.1.1 Temporal Occurrence

The temporal occurrence of tropical cyclone genesis in a given basin can be modelled in a number of ways, the simplest being the random sampling of the number of events in a year in the historical data (Hall & Jewson, 2007). Alternatively, genesis can be modelled as a Poisson process (Yin et al., 2009; Chu & Wang, 1998), or using a negative binomial distribution (Vickery et al., 2000b; Powell et al., 2005). Both Poisson and negative binomial models have been used successfully, the difference between them having been shown to be negligible (Xu & Brown, 2008). Only the Poisson distribution is described below.

A Poisson process is one which satisfies the following criteria:

- The event can have only dichotomous outcomes: occurrence or non-occurrence.
- Individual events are independent.
- Events occur randomly but at an approximately constant average rate.
- Events should be rare enough so that the probability of two or more occurring simultaneously is very small.

The probability that there will be n number of tropical cyclones within a time interval t is expressed as follows:

$$Pr(n) = \frac{e^{-\lambda} \lambda^n}{n!} \quad n = 0, 1, 2, \dots$$

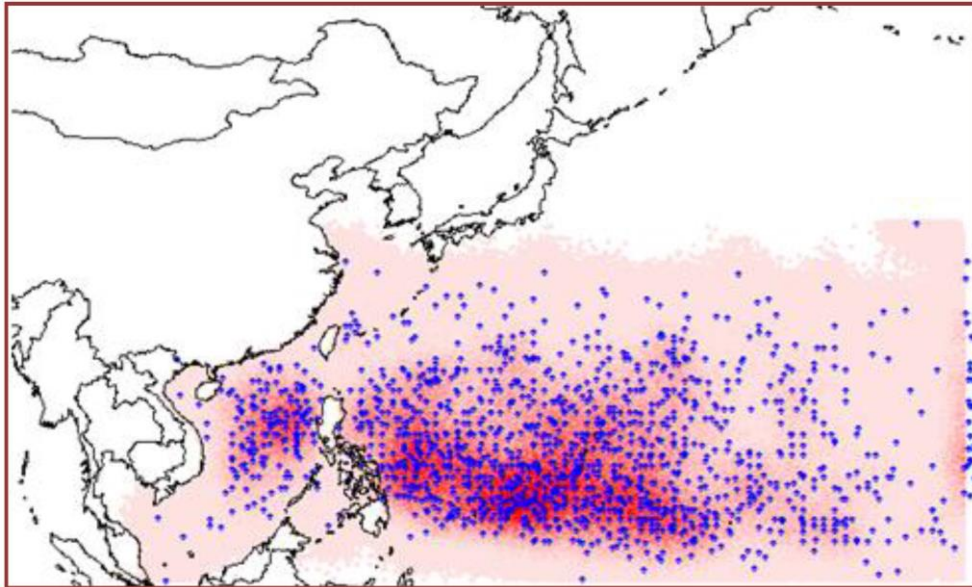
Equation 2-26

where λ is the underlying mean recurrence rate per time interval t , determined from the historical best track data.

2.6.1.2 Spatial Occurrence

Given a defined temporal occurrence of track genesis within a basin, the spatial variation can be modelled by simply sampling from historical genesis points in the best track database (Vickery et al., 2000b; Graf & Nishijima, 2009). A more sophisticated methodology is to sample from space varying probability density estimates, derived from historical genesis locations, using two dimensional kernels with optimized bandwidths (Hall & Jewson, 2009; Powell et al., 2005; Yin et al., 2009). An example of calculated genesis density from historical genesis locations over the North-West Pacific Ocean is shown in Figure 2-13 (Yin et al., 2009).

Figure 2-13: Example of calculated genesis density (in red) from historical genesis locations (in blue) over the North-West Pacific Ocean (Yin et al., 2009).



Emanuel et al. (2006) modelled the space and time dependence of storm genesis by sampling from a time and space dependent probability density function determined from binning the historical data and smoothing using a three dimensional kernel.

2.6.2 Track Propagation

Given the initial storm position, heading and translation speed (determined from the storm genesis), the track propagation model estimates the position, heading and translation speed in the subsequent time-steps. 6 hour time-steps are usually used to propagate the tracks as this is the temporal resolution of the best track data forming the basis for the model. A number of various track propagation models have been adopted in the literature and can be generally categorised as either autoregressive or Markov chain models.

2.6.2.1 Autoregressive Models

In autoregressive models subsequent changes in track speed and heading are determined through empirically fitted equations determined from the best track data. The number of dependent variables as well as the order of the model (number of considered previous time-steps) varies across the literature. Various forms of possible autoregressive models are discussed in Zhang & Nishijima (2012). An example of an autoregressive model for track propagation is that proposed by Vickery et al. (2000b):

$$\Delta \ln(c_{i+1}) = a_1 + a_2\varphi + a_3\psi + a_4\ln(c_i) + a_5\theta_i + \varepsilon_{c,i}$$

Equation 2-27

$$\Delta\theta_{i+1} = b_1 + b_2\varphi + b_3\psi + b_4c_i + b_5\theta_i + b_6\theta_{i-1} + \varepsilon_{\theta,i}$$

Equation 2-28

where c_i and θ_i are the track translation speed and direction respectively at time-step i . φ and ψ are latitude and longitude, while $a_1 - a_5$ and $b_1 - b_6$, are constants derived from a linear regression analysis on the observed relationships in the best track data. The error terms $\varepsilon_{c,i}$ and $\varepsilon_{\theta,i}$ model the observed scatter in the best track data about the fitted model, accounting for the observed randomness in the historical tracks. The error term for each time-step is determined through the sampling of a statistical distribution, which is ultimately drawn from the model residuals. The residual terms have been modelled using both normal (Yin et al., 2009) and non-normal (Hall & Jewson, 2007; Zhang & Nishijima, 2012) empirical distributions.

The obvious spatial variability in observed track propagation is taken into account by generating new sets of coefficients for different areas within the basin. The basin can be divided into subjectively chosen regions (Rumpf et al., 2007), or rather subdivided onto a regular grid, typically with dimensions $5^\circ \times 5^\circ$ (Vickery et al., 2000b; Graf & Nishijima, 2009; Yin et al., 2009). The choice of coefficients in the track propagation model for time-step i therefore depends on the geographical location of the synthetic track at that time-step.

Track propagation models are often based on annual statistics alone (Vickery et al., 2000b), however it has been suggested that the influence of the season on track propagation is an important component and should be included in the track propagation model, for example through the generation of new coefficients for different months (Zhang & Nishijima, 2012; Graf & Nishijima, 2009).

2.6.2.2 Markov Chain Models

A Markov process is a series of states, discrete or continuous, in which the transition from one state to the next is defined by a transition probability conditioned only upon the immediately preceding state (called the first prior), independently of the path by which the preceding state was reached (Lange, 2003). A Markov process in which states are discrete is called a Markov chain. Track propagation using Markov chains is carried out through the direct sampling of conditional probability density functions (PDFs) of instantaneous rates of change of track speed and angle given prior speeds and angles (Powell et al., 2005; Emanuel et al., 2006). It is

assumed that there is no interrelation between track speed and direction, therefore it is required to compute the following independent PDFs at each time-step:

$$Pr(\Delta c_{i+1} | c_i, \psi, \varphi, t)$$

Equation 2-29

$$Pr(\Delta \theta_{i+1} | \theta_i, \psi, \varphi, t)$$

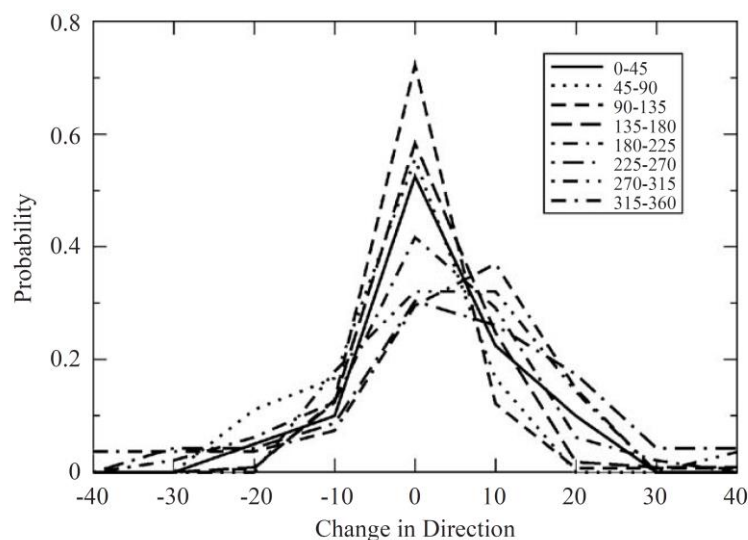
Equation 2-30

where ψ , φ and t are longitude, latitude and time (i.e. the season) respectively. The PDFs are defined on a regular geographical grid and are derived from variably sized regions around the grid point of interest. Kernel smoothing techniques are used to generate the non-parametric PDFs. Kernel smoothing techniques are described in Wand & Jones (1995).

The size of the region used to construct each PDF is dependent on the density of the best track data in the vicinity of the grid point and is chosen to be that which gives a robust PDF for the quantities of interest. The track speed and directions (c_i and θ_i) are binned in discrete intervals, again chosen such that there is sufficient data in each bin to generate robust PDFs.

An example of PDFs for change in direction ($\Delta\theta$) for eight directional bins at a given geographical location and season is shown in Figure 2-14 (Powell et al., 2005). This example from the North Atlantic basin shows that tracks at this particular location and season have a high probability of maintaining their heading with more westerly directions tending to turn clockwise.

Figure 2-14: Example of calculated PDFs for change in direction ($\Delta\theta$) for eight directional bins at a given geographical location and season (Powell et al., 2005).



2.6.3 Intensity Evolution

The evolution of intensity along each track is generally modelled as a statistical process along the same lines as the track propagation models discussed above (the exception being the dynamic deterministic model proposed by Emanuel et al. (2006), not discussed further herein). As with the track propagation models, purely statistical intensity evolution models can either be described as autoregressive or Markov chain models.

2.6.3.1 Autoregressive Models

The autoregressive intensity model proposed by Vickery et al. (2000b) is as follows:

$$\ln(I_{i+1}) = c_0 + c_1 \ln(I_i) + c_2 \ln(I_{i-1}) + c_3 \ln(I_{i-2}) + c_4 TSS_i + c_5 (TSS_{i+1} - TSS_i) + \varepsilon_{I,i}$$

Equation 2-31

where I_i and TSS_i are the intensity and sea-surface temperature at time-step i . $c_1 - c_5$ and the error term $\varepsilon_{I,i}$ are defined in an analogous fashion as described above for the autoregressive model for track propagation.

2.6.3.2 Markov Chain Models

A Markov chain intensity model is one in which the instantaneous change in intensity is modelled through the direct sampling of conditional probability density functions (PDFs) given a prior intensity (Powell et al., 2005):

$$Pr(\Delta I_{i+1} | I_i, \psi, \varphi, t)$$

Equation 2-32

2.6.3.3 Maximum Potential Intensity

Tropical cyclones derive their energy from the thermodynamic disequilibrium that exists between the tropical oceans and the overlying atmosphere (Holland & Emanuel, 2011). This implies that for a given sea surface temperature and the stratospheric temperatures overhead, it is theoretically possible to calculate the maximum potential intensity (MPI) that a given tropical cyclone can attain. A theoretical calculation procedure for the calculation of MPI is provided in Emanuel (1988, 1995), the details of which are not reproduced here. Intensity propagation models often use the theoretical MPI as an upper limit which the modelled intensity can attain (James & Mason, 2005). Alternatively, intensity evolution is modelled using changes in relative intensity (RI), rather than absolute intensity (Darling,

1991). Relative intensity is calculated as the estimated intensity divided by the monthly averaged MPI at the considered geographical location.

2.6.3.4 Land Filling Models

When tropical cyclones move over land they tend to weaken as the central pressure increases or 'fills'. Land filling intensity models for central pressure generally take the following form (Vickery et al., 2009b):

$$\Delta P(t) = \Delta P_0 e^{-at}$$

Equation 2-33

where $\Delta P(t)$ is the central pressure deficit after elapsed time t since making landfall, ΔP_0 is the central pressure deficit at landfall, and a is an empirically derived decay constant.

2.6.4 Termination

The termination of a synthetic tropical cyclone track can be modelled in a number of ways that are linked to both the simulated intensity and geographical location of the track. These methods are analogous to the techniques used to model track genesis.

2.7 Summary and Conclusions

A review of the existing literature on the topic of tropical cyclone risk modelling has been carried out. In this review, the techniques currently used for the estimation of extreme wind speeds due to tropical cyclones have been detailed.

Best track data, which forms the basis of all tropical cyclone risk models, has been introduced and described. Best track data provide six hourly estimates of the geographical coordinates of the track eye (ψ , φ) as well as estimates of the intensity of the storm (V_{max} and/or ΔP). The historical development of tropical cyclone data collection, and the accuracy typically associated with best track data estimates, has been discussed.

Parametric wind field models, commonly used in probabilistic tropical cyclone risk models, have been described. Given the limited information provided in best track data, together with an estimate of the radius to maximum wind speed (R_{max}), these models provide estimates of two-dimensional wind fields which reasonably represent those of actual events. Three families of parametric models have been described; namely the modified Rankine vortex, the Holland (1980) model and the Willoughby et al. (2006) model. These models are all subject to

adjustments in the form of planetary boundary layer corrections, asymmetry corrections, wind inflow angle corrections and wind speed averaging period corrections.

Small sample sizes of historical tropical cyclone events have led to the development of probabilistic approaches for the quantification of tropical cyclone risk exposure. The current state-of-the-art methodologies involve the simulation of synthetic tropical cyclone tracks, thus augmenting the historical best track database to thousands of years. A number of approaches to synthetic track modelling have been described. The components common to all synthetic track models are tropical cyclone genesis, track propagation, intensity evolution and track termination.

The presented literature has largely focussed on economically developed regions such as the North Atlantic (Powell et al., 2005; Emanuel et al., 2006; Hall & Jewson, 2007; Lee & Rosowsky, 2007), North-West Pacific (Rumpf et al., 2007; Yin et al., 2009; Graf & Nishijima, 2009) and South Pacific (James & Mason, 2005) oceans. Tropical cyclone risk exposure has therefore been well documented over these regions, however relatively little attention has been paid to the South-West Indian Ocean. There is therefore a need to quantify risk exposure to tropical cyclones in this region through the application of the current best practise techniques.

3. STUDY APPROACH

3.1 Introduction

The objective of this thesis, as introduced in Section 1.2, is the quantification of risk exposure to tropical cyclones over the South-West Indian Ocean through the generation of extreme wind speed maps for the region. This section provides an overview of how the current best practise techniques, as described in the Section 2, have been used to develop a tropical cyclone risk model to meet this objective.

3.2 Overview

Figure 3-1 provides a flow diagram summarising the tropical cyclone risk model developed as part of this study.

Figure 3-1: Flow diagram summarising the tropical cyclone risk model developed as part of this study.

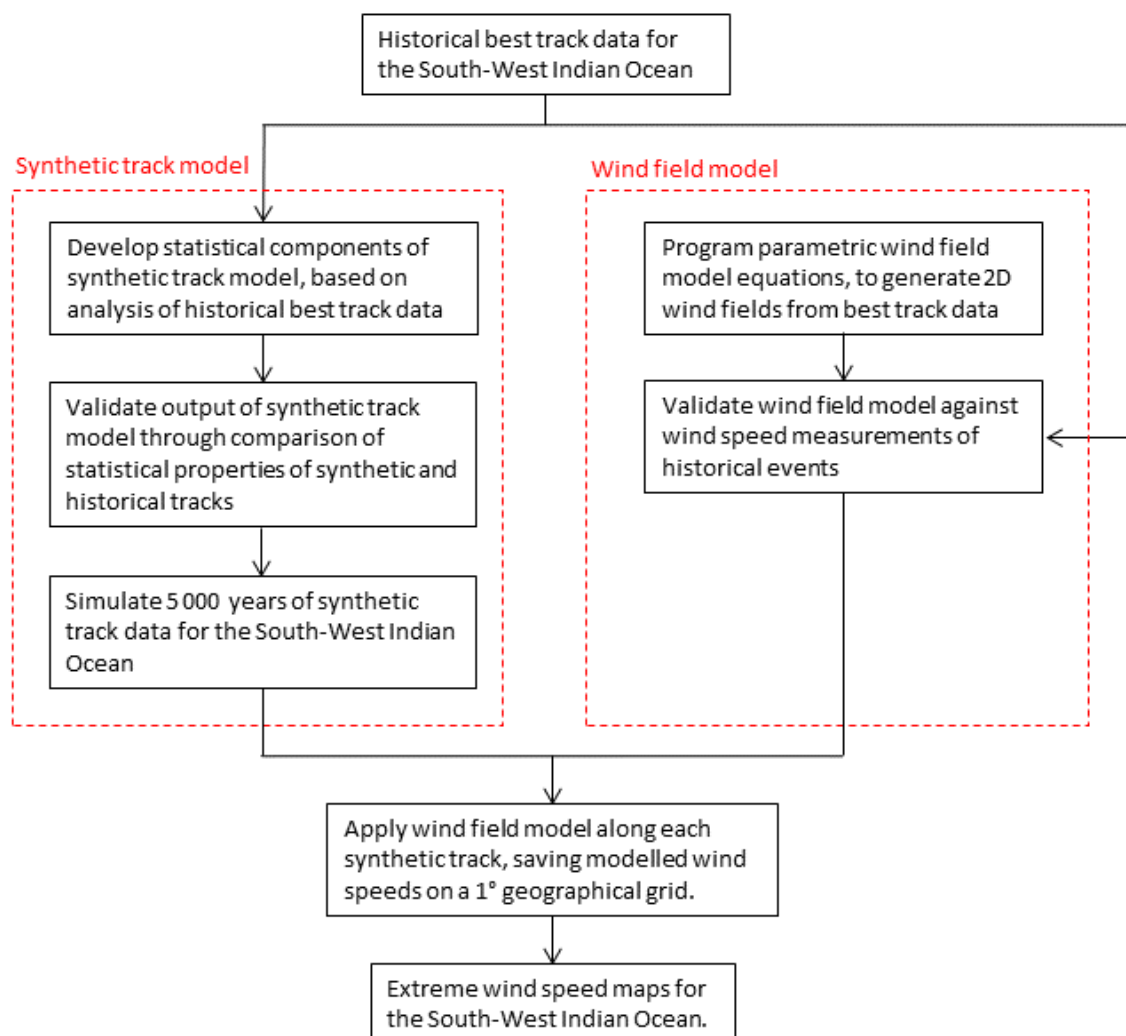


Figure 3-1 indicates that the overall study approach can be subdivided into the following components:

- Best track data (Section 4).
- Wind field model (Section 5).
- Synthetic track model (Section 6).
- Generation of extreme wind speed maps (Section 7).

A brief description of each component, detailing the context within the overall study approach, is provided below.

3.2.1 Best Track Data (Section 4)

Best track data from the Joint Typhoon Warning Centre (JTWC), downloaded from IBTrACS (2014), provides the basis for this study. The parameters of particular interest for this study are the following (provided at 6 hourly intervals):

- Location of the eye in geographical coordinates of longitude (ψ) and latitude (φ).
- Maximum sustained 1-min average surface (10 m elevation) wind speed anywhere in the storm (V_{max}).

3.2.2 Wind Field Model (Section 5)

The Willoughby et al. (2006) parametric wind profile model has been used as part of this study. The parametric equations, as presented in Section 2.4.2, have been programmed using the C# programming language. Input to the parametric wind field models takes the form of best track data (either historical or synthetic), while the model output is a two dimensional surface (10 m elevation) wind field at 6 hour time-steps.

The wind field model has been validated through a comparison of modelled and measured wind speeds at a number of islands throughout the South-West Indian Ocean, thus confirming the validity and sound application of the model.

3.2.3 Synthetic Track Model (Section 6)

The synthetic track model developed as part of this study largely follows the methods described in Powel et al. (2005) and Emanuel et al. (2006) (Section 2.6). The statistical components of the synthetic track model are based on historical best track data for the region and have been developed using the R programming language (R Core Team, 2013). Output of

the synthetic track model is 5 000 years of synthetic track data, in the same format as the historical best track data.

The validation of the model has taken the form of a formal comparison of synthetic track properties with those of historical tracks, thus ensuring that the statistical properties of the historical tracks are adequately reproduced by the model.

3.2.4 Extreme Wind Speed Maps (Section 7)

The Willoughby et al. (2006) parametric wind field model has been applied along each of the 5 000 years of tracks generated by the synthetic track model. The modelled wind speeds for each track have been recorded on a 1° geographical grid over the South-West Indian Ocean. Following the methods described in Vickery et al., (2000b), the model results have been used to calculate extreme wind speeds at return periods of interest at each grid point, allowing for the generation of extreme wind speed maps for the South-West Indian Ocean at various return periods.

3.3 Summary and Conclusions

An overview of the study approach used to generate extreme wind speed maps for the South-West Indian Ocean has been presented. A brief description of each component has been provided, while full details of these components are provided in the following sections.

4. BEST TRACK DATA FOR THE SOUTH-WEST INDIAN OCEAN

4.1 Introduction

Best track data, described in Section 2.3, provide the most complete historical record of tropical cyclone activity throughout the world. These data consequently form the most appropriate basis for the quantification of tropical cyclone risk exposure.

This section presents the historical best track data available for the South-West Indian Ocean. The data have been processed and presented in a manner which provides a general overview of the tropical cyclone climatology for the region. The best track data presented in this section forms the basis for the tropical cyclone risk model developed as part of this study.

4.2 Description of Data

Best track data for this study was downloaded from the International Best Track Archive for Climate Stewardship (IBTrACS, 2014). Section 2.3.1 identified that IBTrACS provides three best track datasets for the South-West Indian Ocean. Following Rossouw (1999), Ho et al. (2006) and Mavume et al. (2009), the Joint Typhoon Warning Centre (JTWC) dataset has been chosen as the primary dataset for this study, as it is the most complete. This database contains all available observations on record up to and including the year 2012.

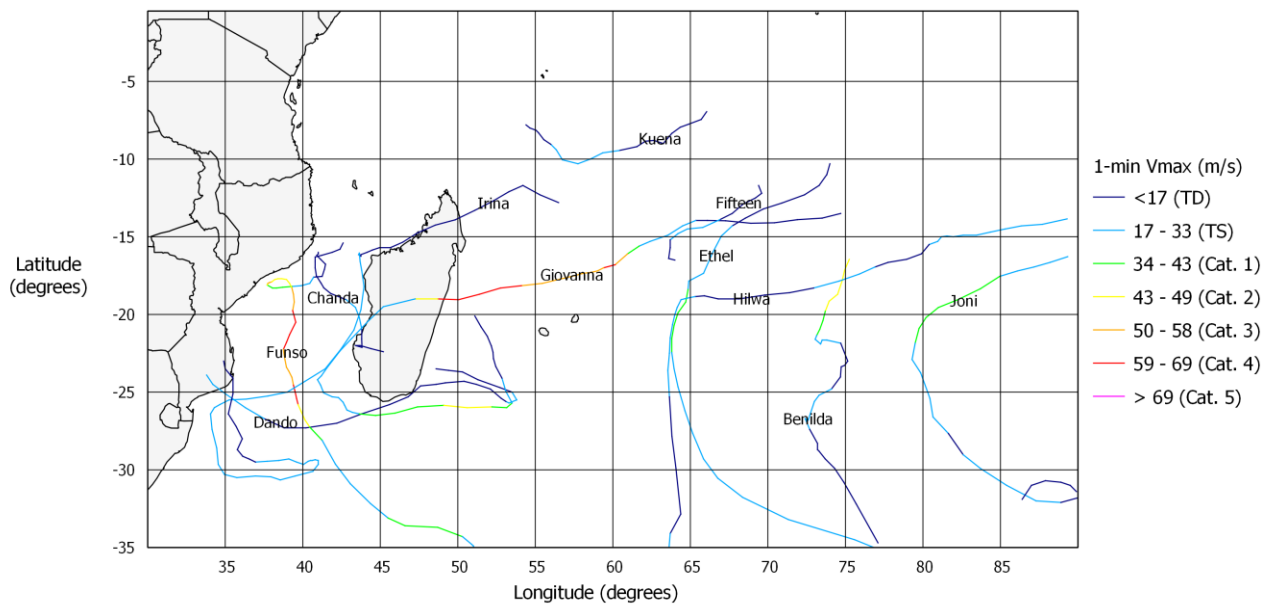
Table 4-1 provides an extract of the raw JTWC best track data archived during Tropical Cyclone Funso, which occurred over the Mozambique Channel during January 2012. JTWC best track data over the South-West Indian Ocean for the year 2012 is visually displayed in Figure 4-1. The presented tracks are colour coded to display the category of the V_{max} estimate according to the Saffir-Simpson scale (Table 2-1).

It is important to note that the JTWC has adopted the 1-min averaging period to define estimates of V_{max} . The 1-min average V_{max} has therefore been adopted as the standard averaging period for extreme wind speeds presented in this study.

Table 4-1: Extract from raw JTWC best track data (IBTrACS, 2014).

Name	Time	Latitude	Longitude	V_{max} (knots)	P_c (hPa)
Funso	2012-01-18 06:00	-16.7	41.4	20	1007
Funso	2012-01-18 12:00	-16.9	41.4	25	1004
Funso	2012-01-18 18:00	-17.2	41.4	25	1004
Funso	2012-01-19 00:00	-17.5	41.2	30	1000
Funso	2012-01-19 06:00	-17.5	40.8	35	996
Funso	2012-01-19 12:00	-17.9	40.5	45	989
Funso	2012-01-19 18:00	-18.2	39.9	55	982
Funso	2012-01-20 00:00	-18.2	39.3	75	967
Funso	2012-01-20 06:00	-18.3	38.7	75	967
Funso	2012-01-20 12:00	-18.3	38.3	75	967
Funso	2012-01-20 18:00	-18.3	38	80	963
Funso	2012-01-21 00:00	-18.1	37.7	85	959
Funso	2012-01-21 06:00	-18	37.7	100	948
Funso	2012-01-21 12:00	-17.9	37.8	100	948
Funso	2012-01-21 18:00	-17.8	38	90	956
Funso	2012-01-22 00:00	-17.7	38.2	90	956
Funso	2012-01-22 06:00	-17.7	38.4	90	956
Funso	2012-01-22 12:00	-17.7	38.6	90	956
Funso	2012-01-22 18:00	-17.8	38.9	90	956

Figure 4-1: JTWC best track data for the South-West Indian Ocean for the year 2012. Scale corresponds to the Saffir-Simpson scale.



4.3 Processing Methodology

In addition to the readily available parameters in best track data, it is necessary to calculate various other parameters important for the development of the synthetic track model described in Section 6. Processing of raw best track data has been carried out using a program written in the C# programming language. The main aspects of the best track data processing methodology are summarised below.

4.3.1 Identifying Relevant Data

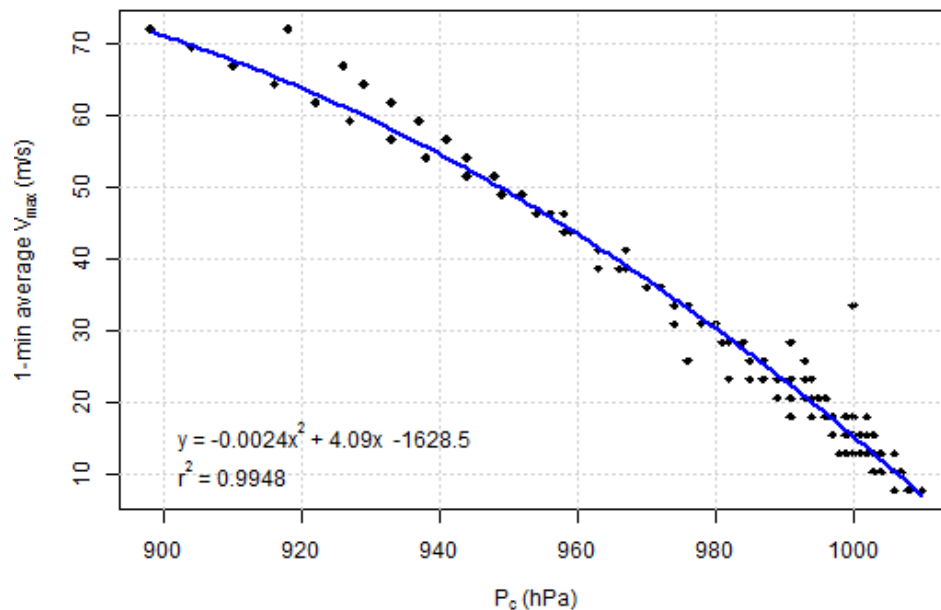
For the purposes of this study, the South-West Indian Ocean has been defined as the region of the Indian Ocean lying south of the equator and west of 90° E (see Figure 2-4). Data outside this region has been excluded from any analysis.

The best track archive for the region of interest extends as far back as the mid-nineteenth century. As discussed in Section 2.3.2, best track data prior to the development of radar in the 1940s is based entirely on vessel and land-based observations and is therefore considered unsuitable for defining average occurrence rates of tropical cyclones. Following Mavume et al. (2009), only best track data from the year 1952 onwards has been considered appropriate to provide an accurate account of tropical cyclone occurrence and spatial distribution. Data prior to the year 1952 has therefore been excluded from any analysis.

4.3.2 Gap-Filling for Missing Estimates of V_{max}

Although the JTWC best track dataset provides a fairly comprehensive record of historical events over the South-West Indian Ocean, there are some gaps in the estimation of V_{max} . It is desirable to have as large a database as possible for this parameter, particularly in the context of this study, therefore estimates of V_{max} have been inferred from other available data wherever possible, as described below.

For JTWC best track records, where the central pressure (P_c) is available, but V_{max} is not, the observed relationship between these two parameters in the JTWC dataset has been used to calculate V_{max} . This relationship is presented in Figure 4-2 and shows the quadratic equation providing the best fit to the data. It is noted that the near one-to-one relationship between V_{max} and P_c ($r^2 = 0.9948$) is a reflection of the wind-pressure relationship (WPR) adopted by the JTWC, rather than the true physical relationship (see Figure 2-3).

Figure 4-2: Wind-pressure relationship determined from JTWC best track data.

Estimates of V_{max} from Météo France La Réunion (MFR) have been used in instances when this parameter is available from MFR, but not the JTWC. MFR provides estimates of the 10-min average V_{max} , rather than the 1-min average V_{max} as provided by the JTWC. 10-min average wind speeds have therefore been converted to 1-min average wind speeds by applying the standard WMO (1993) correction factor of $1/0.88 = 1.14$ (Section 2.4.6).

4.3.3 Track Speed and Direction

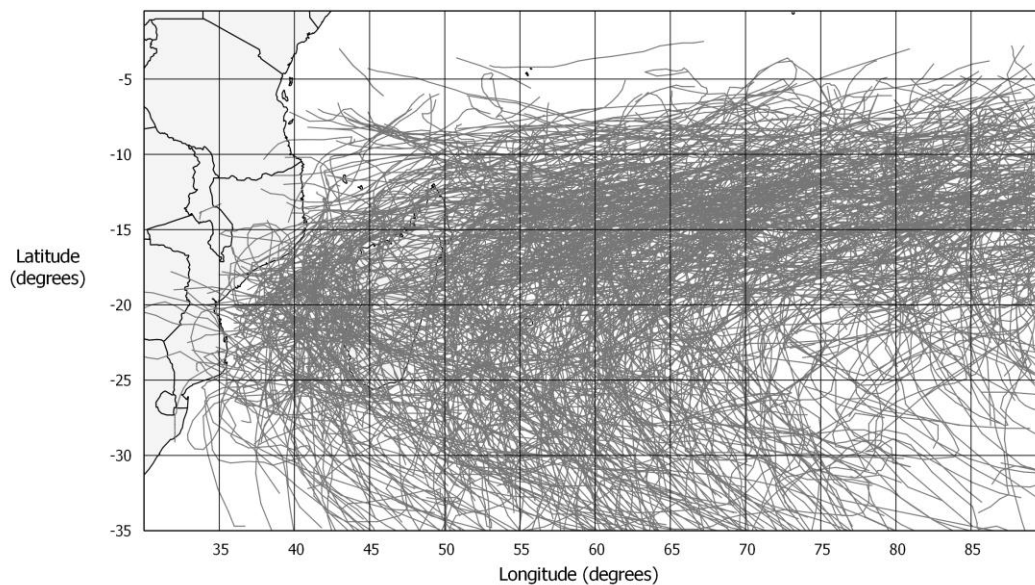
Track locations are provided in geographical coordinates (longitude, latitude), however the required parameters of track speed (c) and direction (θ) are best calculated in a local coordinate reference system so that distances in the units of meters can be calculated. The area of interest spans many Universal Transverse Mercator (UTM) zones, therefore the local UTM zone of any coordinate of interest has first been identified before transforming the geographical coordinates to the coordinates of the local UTM zone. All coordinate transformations were carried out using the datum conversion library supplied with the .NET Application Program Interface (API) provided with the 'MIKE by DHI' software (DHI, 2012a). The transformed coordinates allowed for the calculation of track speed and direction in the required units of m/s and ° TN respectively.

4.4 Summary Statistics

4.4.1 Annual Occurrence

The tracks contained in the 61 year (1952 to 2012) best track dataset for the South-West Indian Ocean forming the basis for this study are shown in Figure 4-3. This dataset constitutes the input to the components of the synthetic track model developed as part of this study (Section 6), for which intensity data are not required.

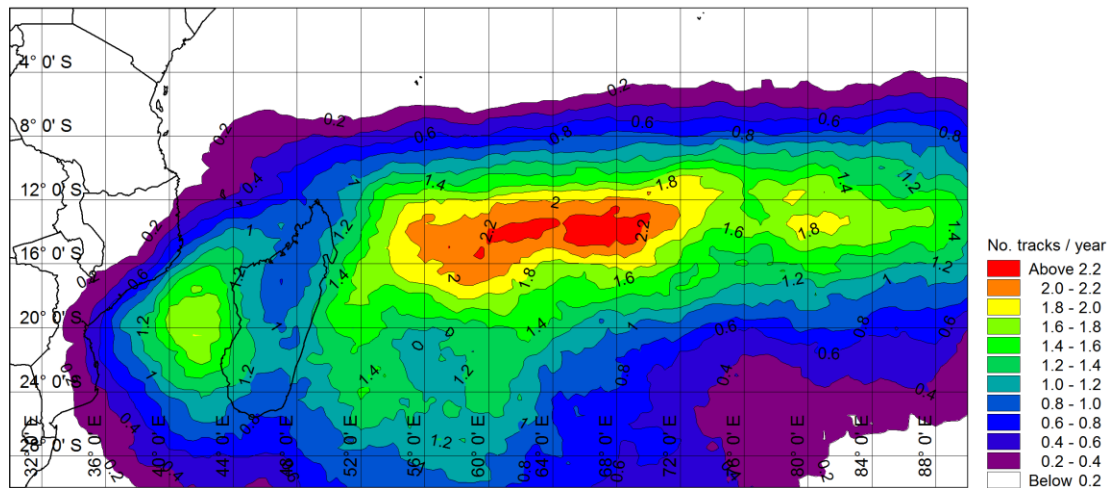
Figure 4-3: Best track data for the South-West Indian Ocean (1952 to 2012).



The average occurrence rate of tropical cyclone tracks over the South-West Indian Ocean from 1952 to 2012 is 14.0 tracks per year. The occurrence rate for tracks passing over the Mozambique Channel is 3.5 tracks per year. The Mozambique Channel has been defined for this study as the area west of Madagascar, contained within the latitudes of 10° S and 27° S. It must be noted that these occurrence rates include all tropical cyclones, including weak systems which may only have attained Tropical Depression status (Table 2-1).

The track density in areas of high activity (Figure 4-3) makes it difficult to infer little other than the outer extents of the tracks. Figure 4-4 presents the best track data in terms of the average number of tracks passing within 2 geographical degrees (approximately 200 km) of a given location per year on average, thus providing a clearer impression of trends in track occurrence over the region.

Figure 4-4: Average occurrence rate of tropical cyclone tracks over the South-West Indian Ocean (1952 to 2012). Contours represent the number of tracks passing within 2 geographical degrees (approximately 200 km) per year on average.

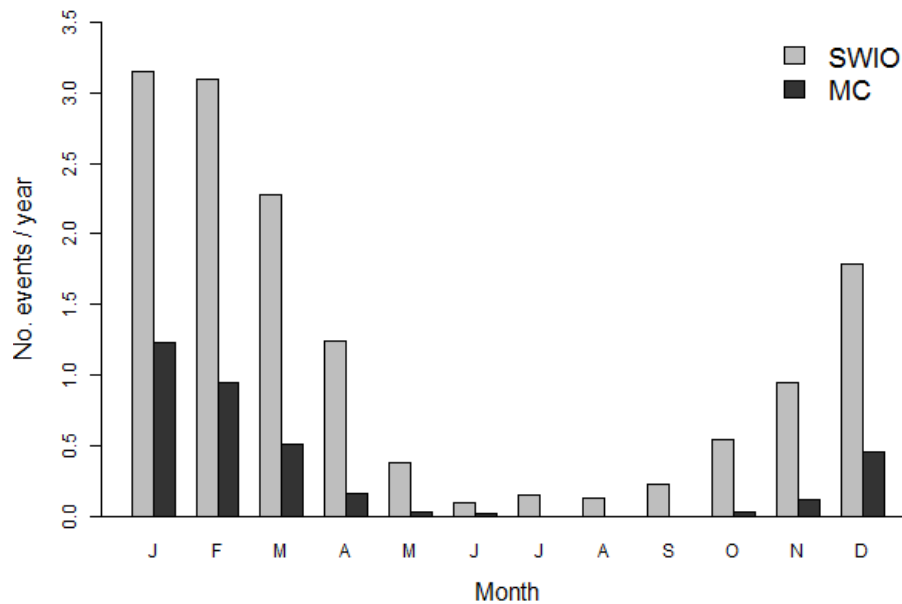


The spatial occurrence of historical tropical cyclones indicates that the most active region lies to the east of Madagascar, where there is a peak occurrence rate of about 2.2 events per year at a latitude of about 14° S. The influence of the land mass of Madagascar on track occurrence is significant, with many tracks veering away in a south to south-easterly direction before they reach Madagascar. A number of tracks do however pass over Madagascar and into the Mozambique Channel where a secondary occurrence peak of about 1.5 tracks per year is observed at about 42° E, 20° S. The increase in track occurrence over the Mozambique Channel is largely due to additional track genesis in this region. The outer extent of track occurrence to the west of the Mozambique Channel shows a strong resemblance to the Mozambique coastline, highlighting the influence of the land.

4.4.2 Seasonal Occurrence

The effect of the changing environmental conditions over the year has a significant effect on the occurrence rate of tropical cyclones. Figure 4-5 presents the occurrence rate of tropical cyclones by month for both the South-West Indian Ocean as well as for the Mozambique Channel. The data indicates that the tropical cyclone season coincides with the southern hemisphere summer, with a peak occurrence over the months of January and February. The observed annual occurrence rates for each month, as presented in Figure 4-5, form an important input to the modelling of the temporal occurrence of synthetic tracks (Section 6.3.2.1).

Figure 4-5: Average occurrence rates of tropical cyclones by month for the South-West Indian Ocean (SWIO) and the Mozambique Channel (MC) (1952 to 2012).

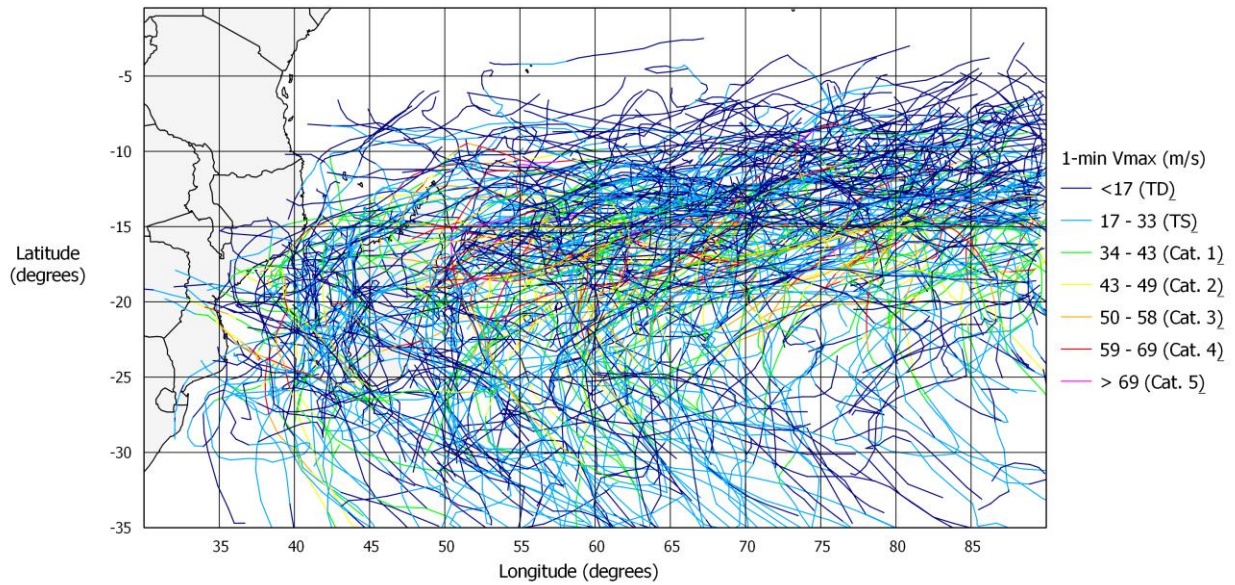


It has been well documented that there is noticeable inter-annual variability in tropical cyclone occurrence rates in the South-West Indian Ocean, attributed largely to the El Niño–Southern Oscillation (ENSO) and Madden-Julian Oscillation (MJO) effects (Ho et al., 2006; Mavume et al. 2009; Chang-Seng & Jury, 2010). Such variability is important for the seasonal forecasting of tropical cyclone activity, but has not been explicitly considered in the present study. It is argued that such seasonal variation will be averaged out when considering return periods of extreme events (e.g. 100 year return period), of importance for this study.

4.4.3 Intensity Data

Although the best track data for the South-West Indian Ocean is fairly complete from the early 1950s, estimates of tropical cyclone intensity are only available from 1980 onwards. The 33 year (1980 to 2012) best track dataset for which intensity data are available is shown in Figure 4-6. The presented tracks are colour coded to display the category of the V_{max} estimate according to the Saffir-Simpson scale (Table 2-1). These data form the input to the modelling of historical wind fields (Section 5), as well as the input to the components of the synthetic track model (Section 6) for which intensity data are required.

Figure 4-6: Best track data for the South-West Indian Ocean for which wind speed data are available (1980 to 2012). Scale corresponds to the Saffir-Simpson scale.



The annual occurrence rate by Saffir-Simpson scale category is shown in Figure 4-7. Only the highest intensity attained for each event has been used to generate the presented occurrence rates.

Figure 4-7: Average occurrence rates of tropical cyclones by Saffir-Simpson scale category for the South-West Indian Ocean (SWIO) and the Mozambique Channel (MC) (1980 to 2012).

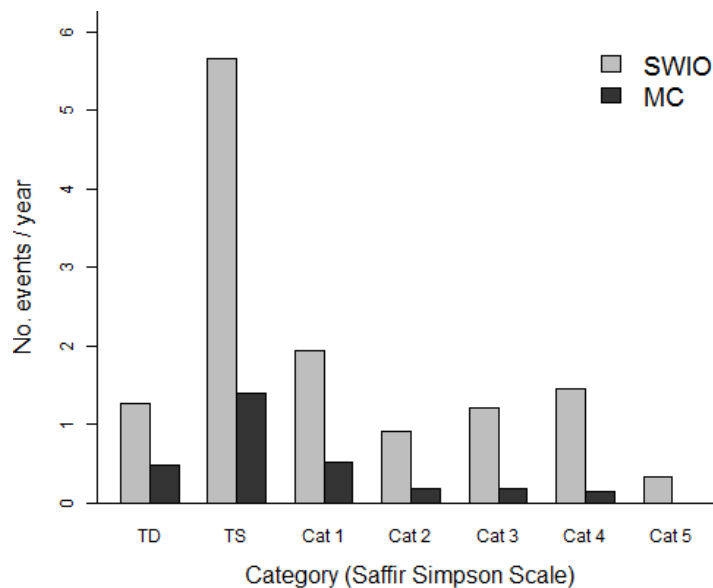


Figure 4-7 indicates that approximately half of the historical tropical cyclone events do not exceed Tropical Storm status ($V_{max} < 33$ m/s). The South-West Indian Ocean sees a Category 5

event ($V_{max} > 69$ m/s) 0.33 times per year on average (every third year). There has been no Category 5 event on record over the Mozambique Channel.

4.5 Summary and Conclusions

Best track data constitutes the most complete record of historical tropical cyclone activity across the globe. These data provide archived best estimates of the location of the tropical cyclone eye (ψ, φ), as well as an estimate of the intensity of the system (V_{max} and/or ΔP) at six hourly intervals over the duration of historical events. Best track data form the most appropriate basis upon which to develop tropical cyclone risk models.

The best track dataset from the Joint Typhoon Warning Centre (JTWC) has been adopted as the primary dataset for this study. The raw best track dataset has been processed to include gap-filling of missing estimates of V_{max} (wherever possible), as well as to include the calculation of parameters of track speed and direction, which are of particular importance to this study. Only data occurring in the South-West Indian Ocean, defined as the region of the Indian Ocean lying south of the equator and west of 90° E, has been considered for use in this study. Given the observational limitations of the early records, only best track data from the year 1952 onwards is considered to provide a reliable account of the geographical distribution and occurrence rates of tropical cyclones over the South-West Indian Ocean. Intensity data for the region are however limited to records from the year 1980 onwards.

The available data indicate an occurrence rate of 14.0 tropical cyclones per year on average over the South-West Indian Ocean. Only about half of these events are estimated to have exceeded Tropical Storm status ($V_{max} < 33$ m/s), during their lifetime. The presented geographical and temporal occurrences of historical tropical cyclones form an important input to the synthetic track model, presented in Section 6.

5. WIND FIELD MODEL

5.1 Introduction

Wind field models, as described in Section 2.4, are used to generate two dimensional surface wind fields which reasonably represent those of actual tropical cyclones. The wind field models considered as part of this study are simplistic parametric models, requiring only the limited parameters available in best track data archives as input parameters. Parametric wind field models are commonly used in tropical cyclone risk models for the estimation of extreme wind speeds as well as to drive ocean response models for determining extreme wave conditions and storm surge for the design of coastal infrastructure.

This section describes the application of both the Holland (1980) and Willoughby et al. (2006) parameteric wind field models, and compares their ability to reproduce measured wind speeds throughout the South-West Indian Ocean. The preferred parametric wind field model has been adopted for the estimation of extreme wind speeds for the South-West Indian Ocean, described in Section 7.

5.2 Description of the Model

Owing to their minimal computational requirements and comparable performance against more complicated dynamic models, only parametric wind field models have been considered as part of this study. The Holland (1980) model has historically been the most extensively adopted parametric wind field model in tropical cyclone risk assessments. The Willoughby et al. (2006) model is a promising alternative to the Holland (1980) model, based entirely on aircraft reconnaissance measurements of flight level wind speeds. Both of these models have been considered and compared as part of this study. Their application can be subdivided into the following general steps, described individually below:

- Calculation of the radius to maximum wind speed (R_{max}).
- Calculation of axisymmetric flight level wind speed profiles.
- Calculation of two-dimensional surface wind fields, allowing for planetary boundary layer corrections, forward motion asymmetry and wind inflow angle.

5.2.1 Radius to Maximum Wind Speed (R_{max})

The empirical relationship proposed by Willoughby & Rahn (2004) (Equation 2-2) has been used in this study for the calculation of R_{max} . This relationship is a function of latitude (φ) and

the axisymmetric (radially averaged) flight level wind speed (V_{Fmax}). As V_{max} is available in the best track data, rather than V_{Fmax} , the correct application of Equation 2-2 requires the conversion of V_{max} to V_{Fmax} . This requires the subtraction of the contribution of the forward motion of the storm from V_{max} , as well as the conversion from surface to flight level wind speeds. Following Mattocks & Forbes (2008), the following relationship has been adopted:

$$V_{Fmax} = \frac{(V_{max} - \delta c)}{K_F}$$

Equation 5-1

where:

δ = the fraction of the translation speed of the storm which contributes to V_{max} . Typical values of δ are 0.5 to 1, with higher values of δ leading to more asymmetric wind fields than lower values (Section 2.4.4). Following Xie et al. (2006), δ has been chosen as 0.5 for this study. Although the sensitivity of the model output to this parameter has not been formally assessed in this study, it is noted that the forward motion of the storm is typically a small proportion of V_{max} , particularly for more intense storms.

c = the translation speed of the storm (m/s) calculated from the raw best track data (Section 4.3.3).

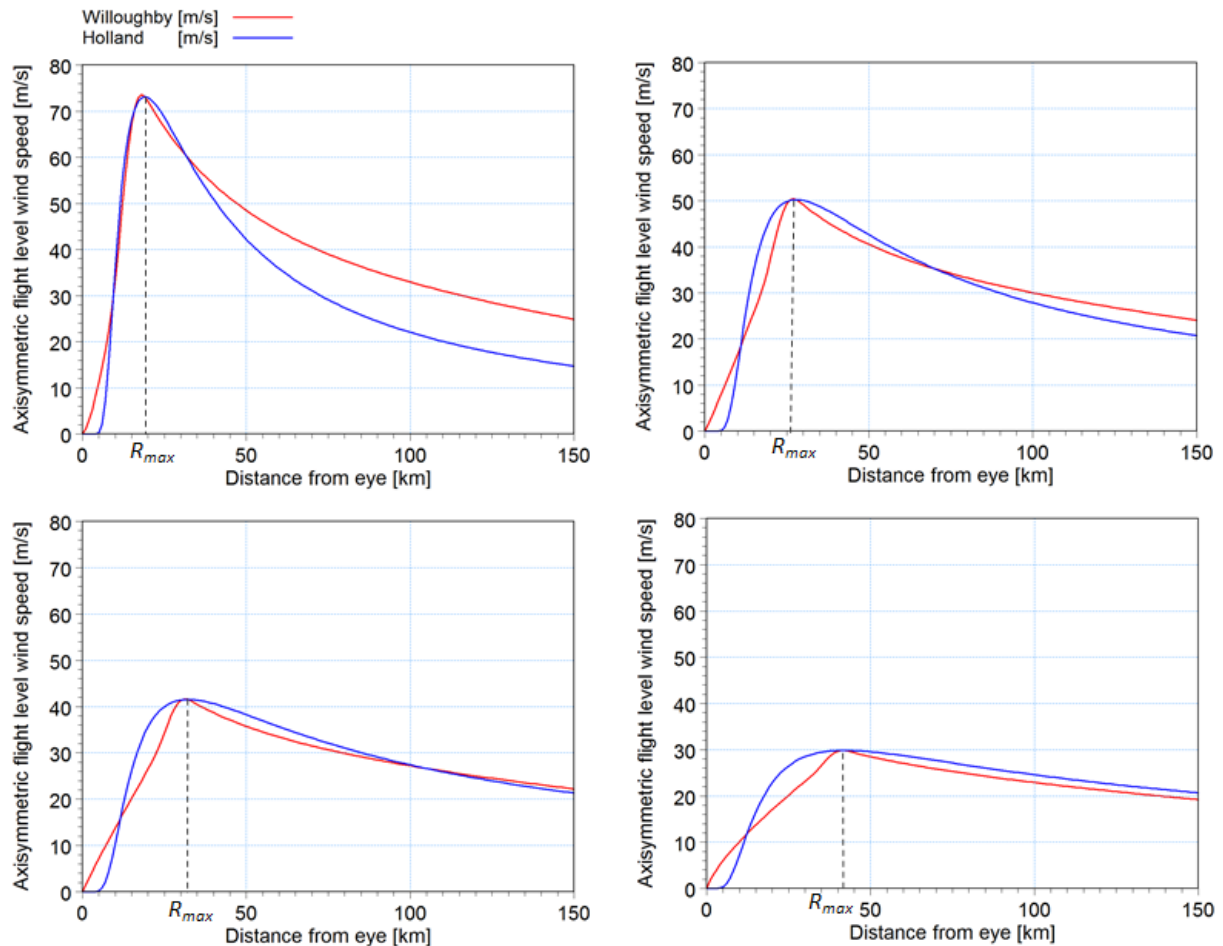
K_F = the conversion factor from flight level to surface wind speeds. Based on dropsonde observations, Franklin et al. (2003) proposed correction factors of 0.9 and 0.8 for eyewall and outer vortex regions respectively (Section 2.4.3). Sensitivity tests on this parameter showed that approximating K_F as a constant of 0.85 yielded favourable modelled wind speeds when compared with measurements (Section 5.3) and has therefore been adopted for this study.

5.2.2 Axisymmetric Flight Level Wind Speed Profiles

The application of the Holland (1980) wind field model requires the estimation of the shape parameter B . The empirical relationship proposed by Willoughby & Rahn (2004) (Equation 2-12) has been adopted for this study. This relationship has been derived from aircraft reconnaissance measurements and is a function of latitude (φ) and the axisymmetric flight level wind speed (V_{Fmax}). As such, the application of the Holland (1980) model (Equation 2-11) using the Willoughby & Rahn (2004) relationship for B , and replacing V_{Gmax} with V_{Fmax} , yields axisymmetric wind speed profiles at flight level. Axisymmetric flight level wind speed profiles as defined by the Willoughby et al. (2006) model have been calculated through the direct application of Equation 2-16 to Equation 2-22.

Figure 5-1 provides a comparison of the Holland (1980) and Willoughby et al. (2006) wind speed profiles for a range of intensities.

Figure 5-1: Comparison of Holland (1980) and Willoughby et al. (2006) wind speed profiles for a range of intensities (V_{Fmax}).



The Willoughby et al. (2006) model was developed in response to observed biases in the Holland (1980) model where it was found that the Holland (1980) model tended to over-predict wind speeds in the vicinity of the eyewall, while wind speeds further away from the eyewall were found to drop off too rapidly (Willoughby & Rahn, 2004). The observed differences in the Willoughby et al. (2006) and Holland (1980) wind speed profiles presented in Figure 5-1 are consistent with the differences between the Holland (1980) model and measured wind speed profiles from the Willoughby & Rahn (2004) study. This is to be expected as the Willoughby et al. (2006) model is the best statistical fit to these measured profiles.

The effect of the storm intensity on the shape of the wind speed profile in both parametric models is evident, with more intense systems tending to have considerably more peaked profiles than weaker systems. Figure 5-1 also highlights the tendency of R_{max} to decrease as the intensity of the system increases.

5.2.3 Asymmetric Surface Wind Fields

Two-dimensional surface (10 m elevation) wind speeds have been generated from the axisymmetric flight level wind speed profiles described above by applying the profile radially around the eye, while making the necessary adjustments for forward motion asymmetry and correcting from flight level to surface wind speeds. Surface wind speeds as a function of angle (θ measured counter-clockwise from the direction of the track) and distance (R) from the eye have been calculated as follows:

$$V(R, \theta) = K_F [V_F(R) + \delta c \cos(\theta_{max} - \theta)]$$

Equation 5-2

where:

$V_F(R)$ = axisymmetric flight level wind speed at a distance R from the eye, as determined from the parametric wind field model (Section 5.2.2).

θ_{max} = the angle to the maximum wind speed, measured counter-clockwise from the direction in which the cyclone is moving. θ_{max} has been chosen as 65° for this study (front left quadrant relative to the forward motion of the storm), following recommendations of Harper et al. (2001). The actual location of the maximum surface winds is highly variable (Harper et al., 2001), therefore fixing this parameter may lead to errors for individual events for which this is a poor assumption. The magnitude of this error is limited by the range of the asymmetry in the storm.

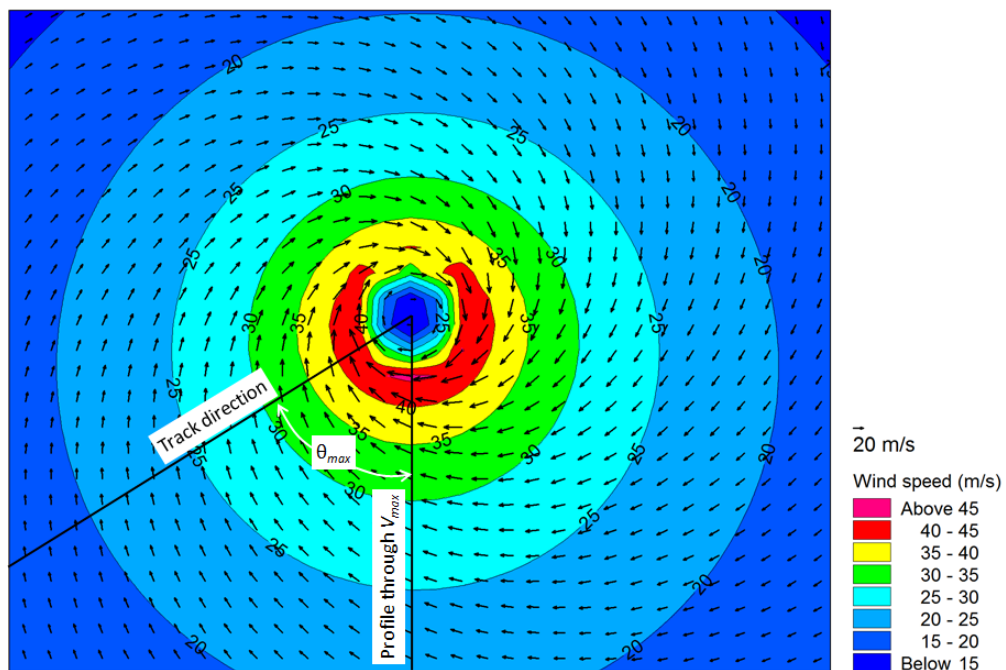
δ , c and K_F are as defined in Equation 5-1.

Figure 5-2 presents an example of an output parametric wind field. The example shows a track moving in a south-westerly direction, resulting in an asymmetric wind field with the strongest winds toward the left of the track direction. The figure indicates the profile through the location of the maximum wind speeds. At the location of maximum wind speed, i.e. when $\theta = \theta_{max}$ and $R = R_{max}$, Equation 5-2 is simply a rearrangement of Equation 5-1, therefore yielding a maximum wind speed anywhere in the wind field equal to the input V_{max} along this line. The input parameter of V_{max} is therefore always reproduced as the maximum wind speed in the

output asymmetric surface wind field. This is the desired result, given the definition of V_{max} as the maximum sustained surface (10 m elevation) wind speed anywhere in the storm (Section 2.2.3).

Following the recommendations of Harper et al. (2001) (Equation 2-24), wind directions have been turned inward toward the eye. The effect of this adjustment is clearly evident in the arrangement of wind vectors around the eye.

Figure 5-2: Example of a parametric wind field, including the effect of forward motion asymmetry.



5.3 Validation of the Model

The parameterisation of the tropical cyclone wind field, as described above, will naturally lead to errors when compared with actual wind fields. These errors can be expected to be large for individual events as some events are less 'well behaved' than others. Rather than reproducing individual historical events with a high degree accuracy, the parametric wind field model is intended to generate wind fields which are statistically unbiased when compared to actual events. This is particularly important within the context of this study as a model which systematically over-predicts (or under-predicts) wind speeds will result in extreme wind speeds which will be too high (or too low). The model validation presented below provides an

assessment of the ability of both the Holland (1980) and Willoughby et al. (2006) models to reproduce wind speed measurements throughout the South-West Indian Ocean.

5.3.1 Description of Data

Wind measurements informing this study have been kindly provided by Mr Francois Bonnardot of Météo France. The measurements have been undertaken at eight land based measurement stations located throughout the South-West Indian Ocean as shown in Figure 5-3. The names, coordinates and timespan covered by each measurement station are provided in Table 5-1.

Each dataset provides measurements of 10-min average wind speed, 10-min average wind direction, maximum instantaneous wind speed within the last hour, and direction at maximum instantaneous wind speed. Measurements are typically provided at hourly or three hourly intervals.

Figure 5-3: Locations of wind speed measurement stations.

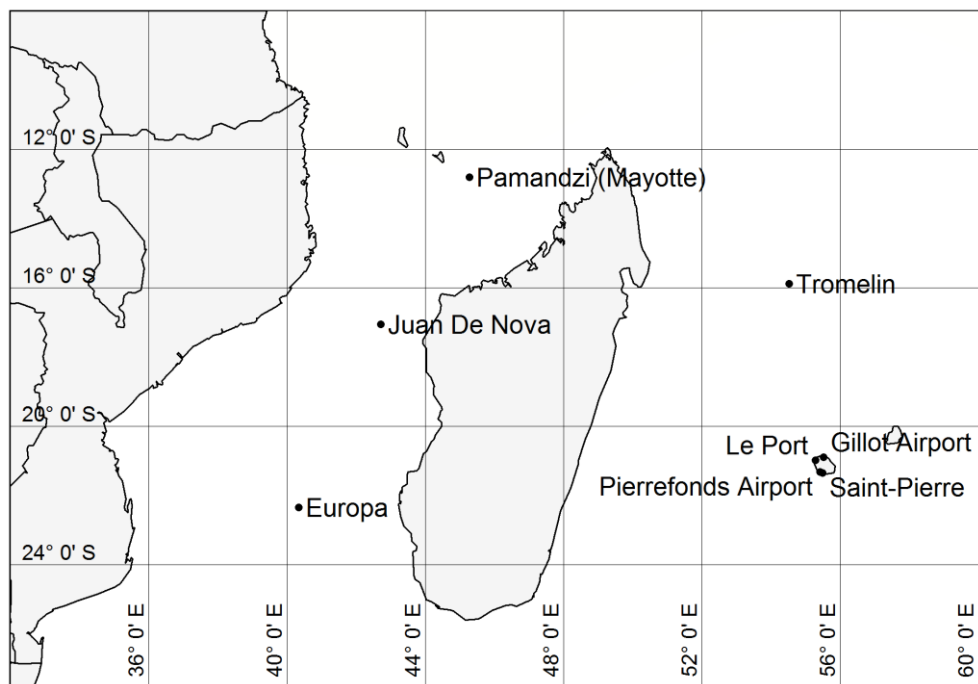


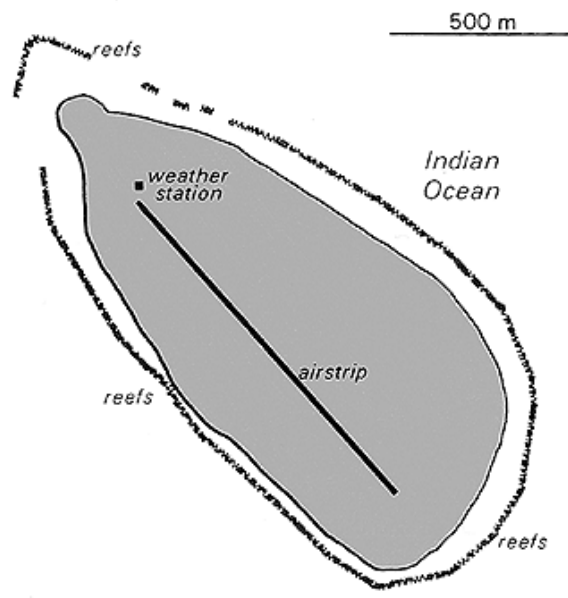
Table 5-1: Details of wind measurement stations

Name	Longitude (degrees)	Latitude (degrees)	Timespan
Gillot Airport	55.528	-20.892	1981 - 2014
Pierrefonds Airport	55.425	-21.32	1999 - 2014
Le Port	55.282	-20.976	1982 - 2014
Saint-Pierre	55.487	-21.344	1981 - 2002
Tromelin	54.52	-15.887	1981 - 2014
Juan De Nova	42.712	-17.054	1981 - 2014
Europa	40.34	-22.344	1981 - 2014
Pamandzi (Mayotte)	45.283	-12.805	1981 - 2014

The applicability of wind measurements for the validation of the parametric wind field model is influenced by the extent to which the measurements may have been affected by local land based features, such as mountains or buildings. Depending on the offshore wind direction, such features may cause wind speeds to be higher (due to funnelling) or lower (due to blocking) than those offshore. As the parametric wind field model does not allow for these adjustments, measurement stations far from mountains or developed areas are preferable for the purposes of this study. Furthermore, measurement stations which are located in areas which are more exposed to tropical cyclone events, and for which there are long records of measurements, are also naturally more useful for the purposes of this study. Given these considerations, Tromelin Island provides the most useful individual dataset for this study and is given particular attention in the model validation presented herein.

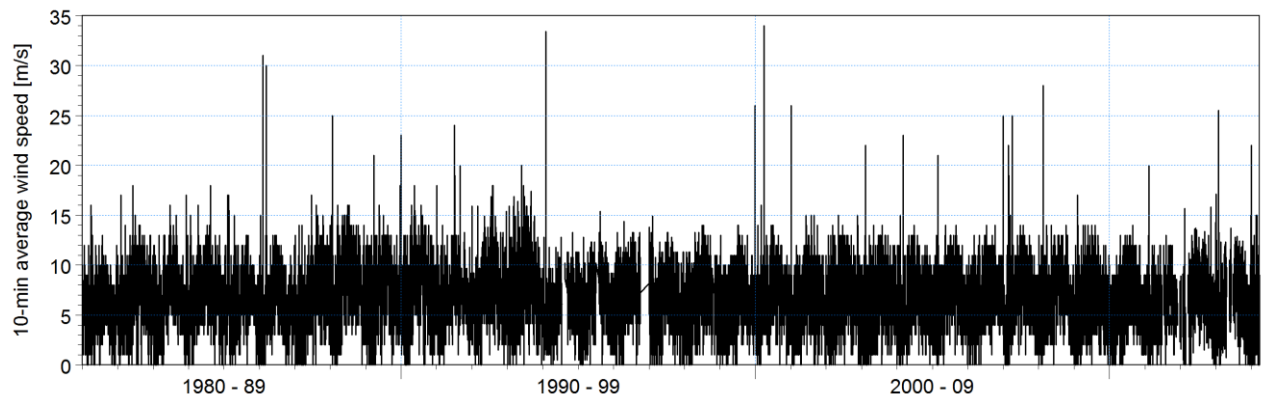
Tromelin Island is particularly small, with a land area of approximately 1 km². The island is flat and sandy, making it free from any notable land based features. Wind measurements on the island are therefore likely to be fairly representative of open ocean winds. A diagram of the island, highlighting the size of the island and location of the measurement station is shown in Figure 5-4.

Figure 5-4: Plan view of Tromelin Island, indicating the size of the island and the location of the measurement station (Penn State, 2014).



The measurement station at Tromelin Island is particularly relevant when considering measurements of tropical cyclone winds, as it is located in a region which experiences an occurrence rate of tropical cyclones close to the peak occurrence rate for the South-West Indian Ocean (see Figure 4-4). The dataset is also almost entirely complete, containing approximately 32 years of valid data. Figure 5-5 presents a time-series of measured 10-min average wind speeds at Tromelin over the full duration of the dataset. The time-series indicates a number of extreme wind speed events which clearly stand out from the other measurements in the time-series. Most (but not all) of these events are due to passing tropical cyclones, providing a good source of ground truth data for the validation of the parametric wind field models.

Figure 5-5: Time-series of 10-min average wind speed measured at Tromelin Island. See Figure 5-3 for the location of the measurement station.



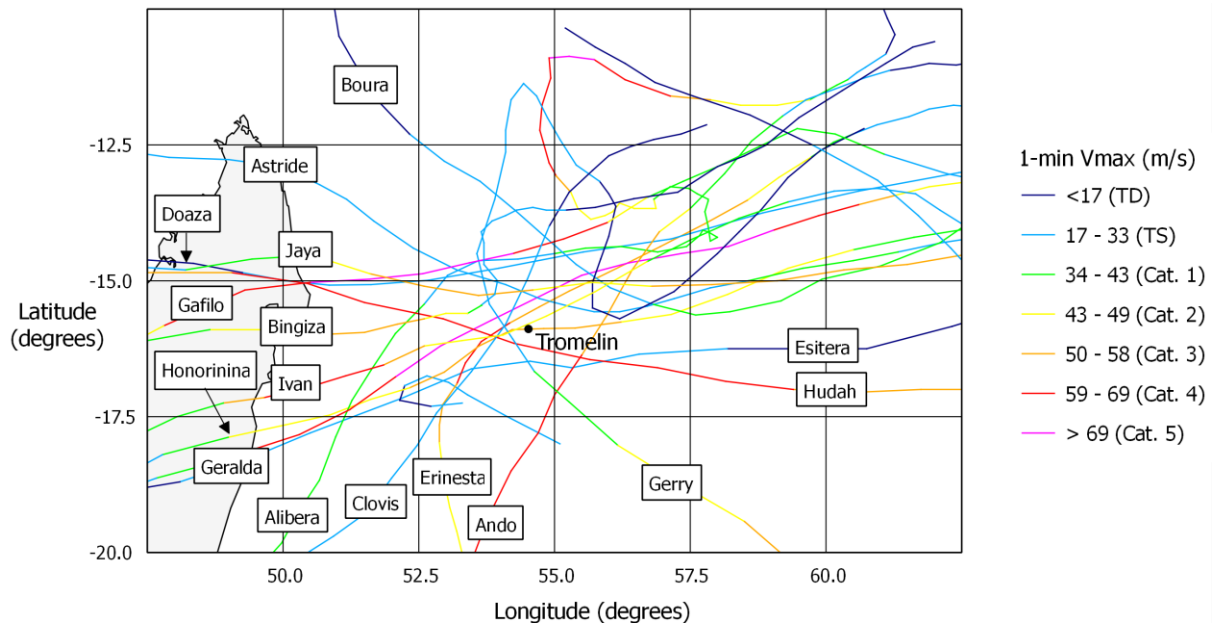
5.3.2 Methodology

The validation of wind field models involves the comparison of modelled wind speeds with those of wind speed measurements at the available measurement stations. It is important to note that parametric wind field models are only expected to provide representative wind fields near the eyewall, where the uniformity of the intense vortex can be reasonably approximated by a simple parametric model. Only historical tracks passing within 2 geographical degrees (approximately 200 km) of the respective measurement stations have therefore been considered for the validation of the parametric wind field models. It is the extreme wind speeds which are of particular interest for this study, therefore only historical tracks which have at least one best track V_{max} entry greater than 25 m/s, within the 2 geographical degrees threshold distance, have been considered. The comparison has been further restricted to tropical cyclone events for which the peak measured 10-min average wind speed exceeds 15 m/s. This has again been done to limit the focus of the validation process on the ability of the model to reproduce only the extreme wind speeds as it is these events which are of particular interest to this study.

Considering all measurement stations (Figure 5-3), there are in total 60 measured extreme events which satisfy the above criteria for comparison. Not all of these events are independent as in some instances individual tropical cyclones have been recorded by more than one measurement station. At the Tromelin measurement station there are 16 historical independent tropical cyclones which satisfy the above criteria for comparison. These tracks,

including their intensity, are shown in Figure 5-6. The intensity scale corresponds to the Saffir-Simpson scale as defined in Table 2-1.

Figure 5-6: Historical tropical cyclone tracks used to compare modelled vs measured wind speeds at Tromelin.

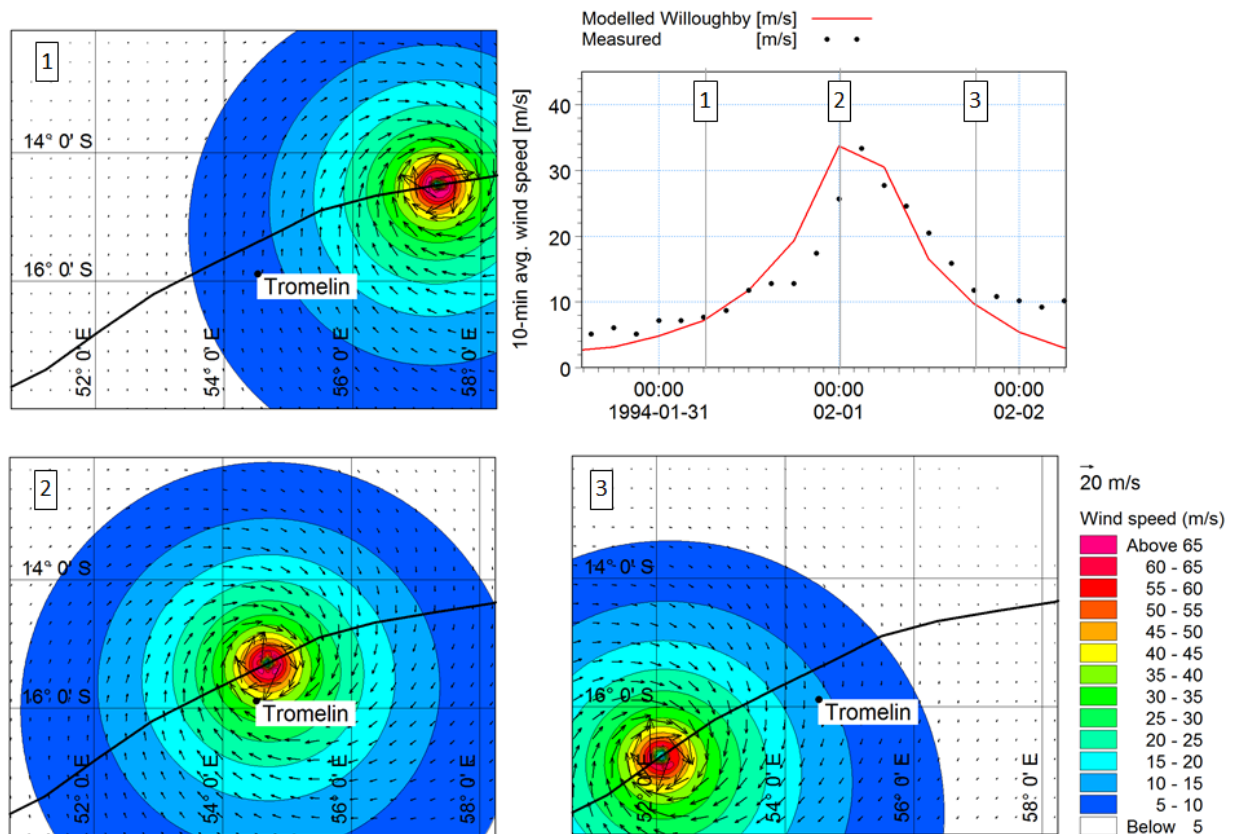


The application of the Holland (1980) and Willoughby et al. (2006) parametric wind field models, as described in Section 5.2, has been applied along each of the relevant historical tropical cyclone tracks using a program written in the C# programming language. Figure 5-7 provides an example of the extraction of a time-series of modelled wind speeds at Tromelin for Tropical Cyclone Geralda (1994).

The presented two-dimension wind fields have been calculated on a 10 km regular grid for presentation purposes only. The calculated time-series at the measurement station is not dependent on the spatial resolution of this grid, being calculated directly from the actual distances and angles between the measurement station and the eye at each time-step. In this way no errors due to the assumed spatial resolution of the grid are introduced.

Modelled wind speeds have been converted from 1-min average to 10-min average wind speeds for direct comparison with the measurements. The WMO (1993) correction factor of 0.88 has been applied for this purpose (Section 2.4.6).

Figure 5-7: Example of the extraction of modelled wind speeds at Tromelin for Tropical Cyclone Geralda (1994). The time-series indicates the measured wind speeds at Tromelin over the same period of time.



5.3.3 Results

5.3.3.1 Time-series of Wind Speeds

Figure 5-8 presents time-series plots of modelled and measured 10-min average wind speeds at Tromelin. Both the Willoughby et al. (2006) and Holland (1980) parametric wind field model results are presented for comparison. The name of each historical tropical cyclone corresponding to the extreme wind speed event is provided for reference. The corresponding tracks from which the modelled wind speeds shown in Figure 5-8 were derived are shown in Figure 5-6.

In addition to the Tromelin measurement station, the methodology described above has been applied to all of the other available measurement stations (shown in Figure 5-3). Time-series comparisons between modelled and measured wind speeds at all of these measurement stations are provided in Appendix A for reference.

Figure 5-8: Time-series of modelled vs measured 10-min average wind speeds at Tromelin.

The name of each corresponding tropical cyclone is provided for reference. Figure 5-6 shows the best track data used as input to the parametric wind field models.

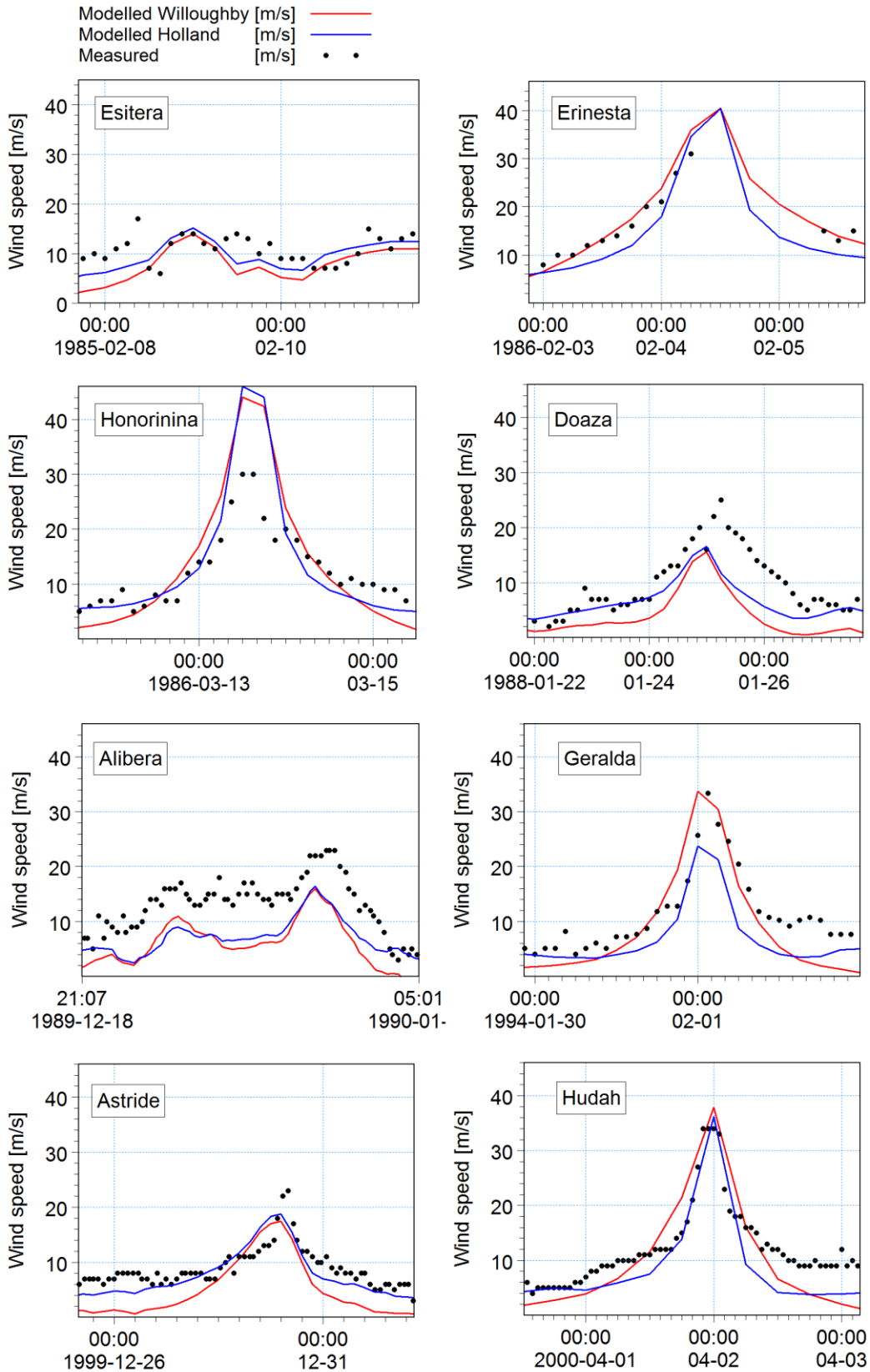
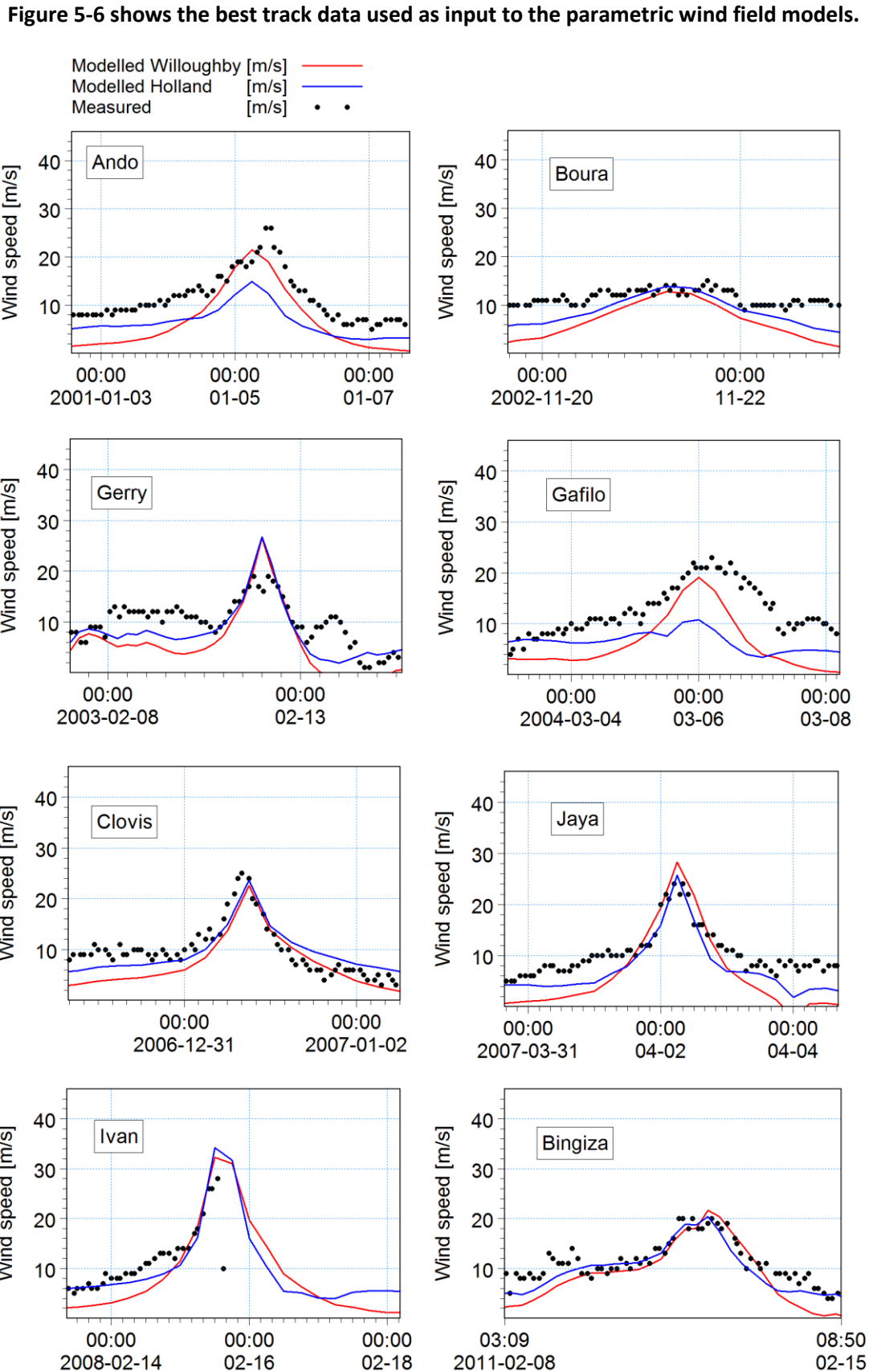


Figure 5-8 (continued): Time-series of modelled vs measured 10-min average wind speeds at Tromelin. The name of each corresponding tropical cyclone is provided for reference.



5.3.3.2 Comparison of Peak Wind Speeds

As described above, parametric wind field models are not expected to provide accurate wind speeds far away from the eyewall. The validation of the parametric wind field models therefore focusses only on the ability of the model to reproduce measurements of the peak wind speed generated by passing tropical cyclones. Figure 5-9 compares the peak modelled wind speeds for the relevant historical tropical cyclone events (shown in Figure 5-8) with those of the corresponding peak measurements at the Tromelin measurement station. Comparing only the peak values also ensures that timing errors between the model and measurements do not contribute to the observed errors.

Figure 5-9: Scatter plots of modelled vs measured peak 10-min average wind speeds at Tromelin using both the Willoughby et al. (2006) and Holland (1980) parametric wind field models.

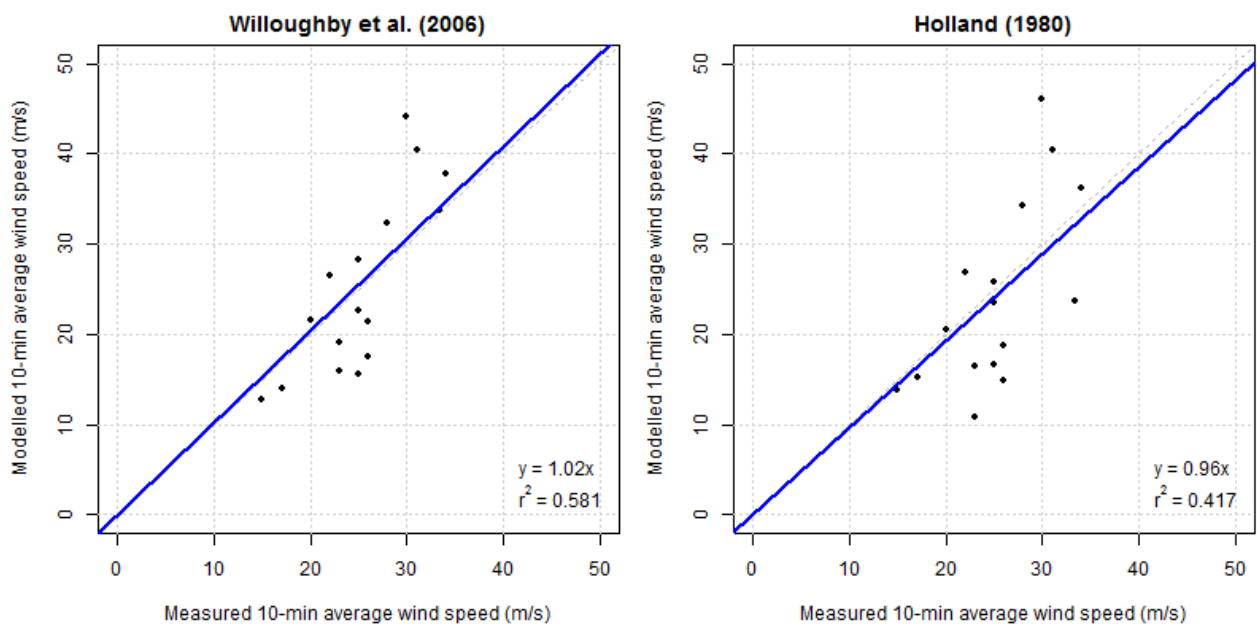


Figure 5-9 displays the straight line resulting in a least squares fit through the plotted data (in blue), while forcing the straight line to pass through the origin. The gradient of the fitted straight line indicates the extent of the overall bias in the model. A gradient which is greater than one indicates a model which tends to over-predict wind speeds, while the opposite is true for gradients less than one. The coefficient of determination (r^2) is a measure of how well the model is able to reproduce the measurements. $r^2 = 0$ is equivalent to a model which is no better than the mean of the measurements, while $r^2 = 1$ is equivalent to a model which reproduces the variation of the measurements exactly.

The comparison of the model results with measurements at Tromelin Island indicates that both the Willoughby et al. (2006) and Holland (1980) models show little overall bias. Both models do however show a tendency to under-predict the lower wind speeds, while over-predicting the higher wind speeds. Of the two parametric wind field models, the Willoughby et al. (2006) model provides a better overall fit to the measurements ($r^2 = 0.581$ as opposed to $r^2 = 0.417$).

Although there are four measurement stations located on Réunion Island (Figure 5-3), the island is relatively large, mountainous, and fairly developed around the locations of the measurement stations. It is therefore suggested that the wind measurements on Réunion Island may be more influenced by land based features than the other measurement stations, which are located on smaller islands. By including data from Pamandzi (Mayote), Juan de Nova and Europa (Figure 5-3) with the data already presented for Tromelin (Figure 5-9), the number of peak wind speeds for comparison is extended from 16 to 29. The resulting relationship between modelled and measured peak 10-min average wind speeds are shown in Figure 5-10.

Figure 5-10: Scatter plots of modelled vs measured peak 10-min average wind speeds for all measurement stations, excluding those on Réunion Island, using both the Willoughby et al. (2006) and Holland (1980) parametric wind field models.

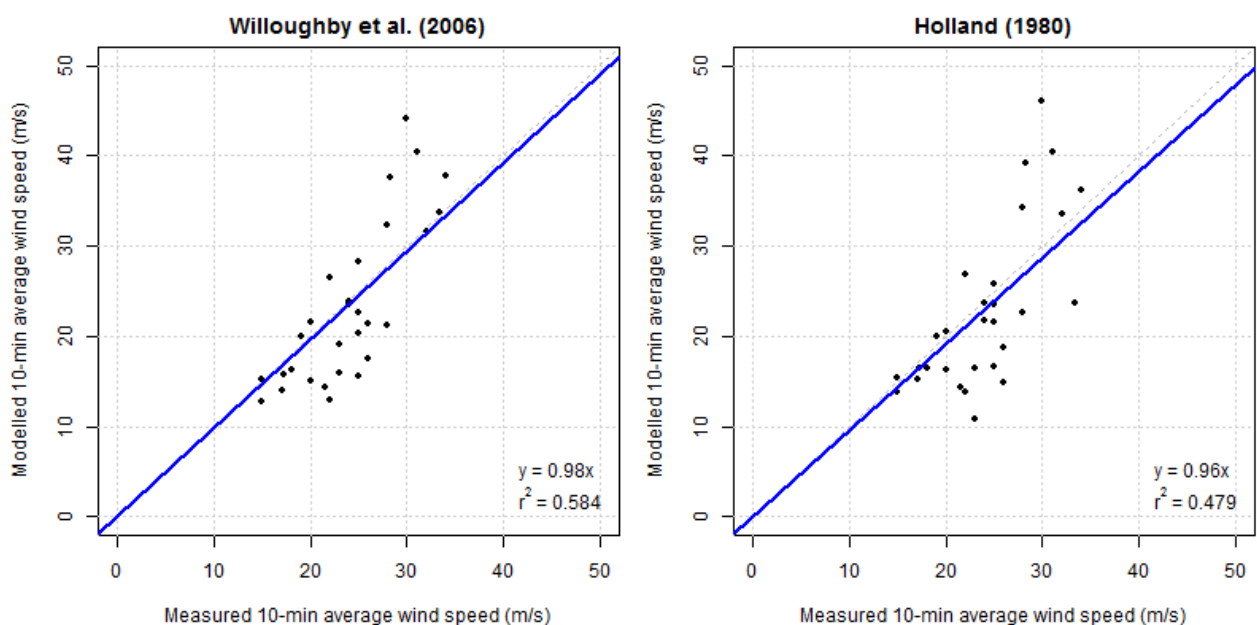


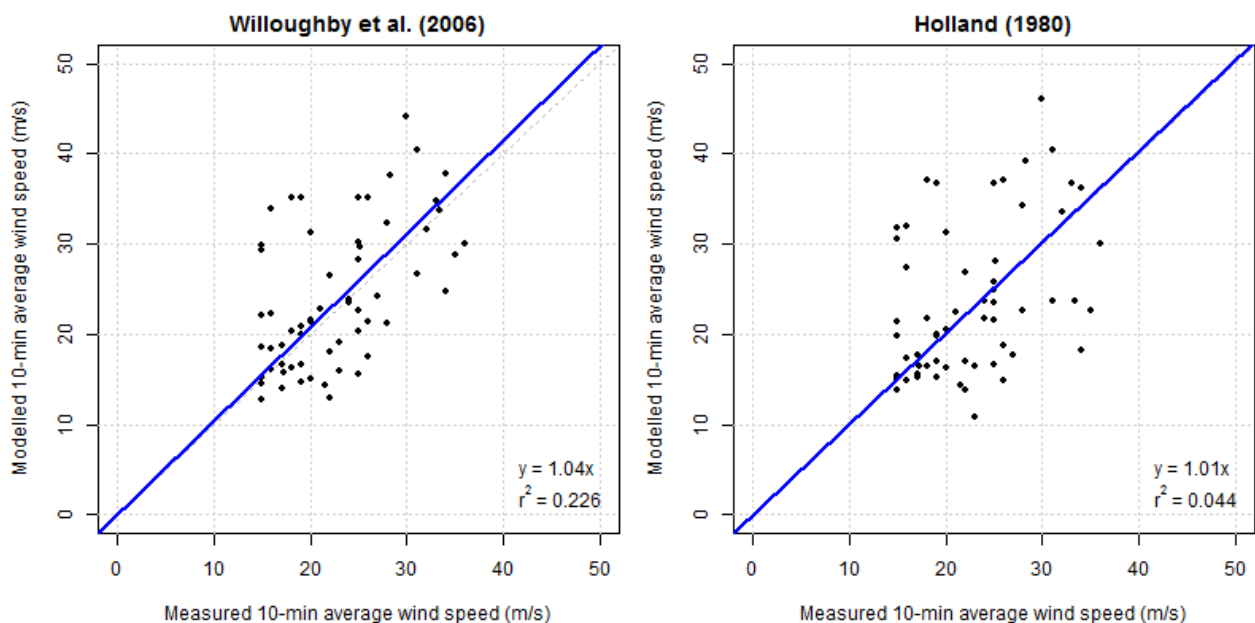
Figure 5-10 indicates that including data from all measurement stations, excluding those on Réunion Island, yields a relationship between modelled and measured peak wind speeds which is very similar to that presented in Figure 5-9. The models show little overall bias,

however there does again appear to be a tendency for lower peak wind speeds to be under-predicted, while higher peak wind speeds are over-predicted.

Using data from all measurements stations, including those on Réunion Island, extends the number of peak wind speeds for comparison from 29 to 60. The resulting relationship between modelled and measured peak 10-min average wind speeds are shown in Figure 5-11.

Figure 5-11 indicates that including data from Réunion Island significantly reduces the fit of the model to the measurements. The r^2 value for the Holland (1980) model reduces to just 0.044, implying that the model performance is only marginally better than a horizontal straight line through the mean of the measurements. As already suggested, the poorer performance of the models may be due to land based features which are likely to be more influential on Réunion Island than on the other measurement stations. These features have the potential to both increase as well as decrease wind speeds when compared to nearby open ocean winds. It is therefore suggested that Figure 5-10 provides a more realistic depiction of the ability of the parametric wind field models to reproduce actual open ocean wind speeds due to tropical cyclones than Figure 5-11.

Figure 5-11: Scatter plots of modelled vs measured peak 10-min average wind speeds at all measurement stations using both the Willoughby et al. (2006) and Holland (1980) parametric wind field models.



5.3.3.3 *Time-series of Wind Directions*

Although extreme wind speeds are the direct output of this study, the ability of the parametric wind field model to reasonably reproduce measured wind directions becomes relevant if the model is to be used for modelling ocean response. In this case the correct arrangement of both wind speeds and directions around the eye is vitally important for the modelling of waves, currents and storm surge.

Figure 5-12 presents time-series plots of modelled and measured wind directions at Tromelin. Wind direction is measured clockwise relative to True North, and is the direction from which the wind is blowing. There is no distinction between the Willoughby et al. (2006) and Holland (1980) parametric wind field models in terms of wind direction, therefore the presented results apply to both models. Of the 16 events for which wind speed measurements are available at Tromelin (Figure 5-8), only 13 of these have valid wind direction measurements for comparison.

The results indicate that the model reproduces the observed trends in wind directions around the peak wind speed, where wind directions show dramatic changes as the track passes the measurement station. The presented results are encouraging, although it is acknowledged that there does appear to be a bias in modelled wind directions, with wind directions tending to be too high prior to the storm peak and too low after the storm peak.

While the importance of wind directions in the context of ocean response modelling is acknowledged, the model results are considered reasonable, and are not discussed in any more detail as part of this study.

Figure 5-12: Time-series of modelled vs measured wind directions at Tromelin. The name of each corresponding tropical cyclone is provided for reference. Figure 5-6 shows the best track data used as input to the parametric wind field models.

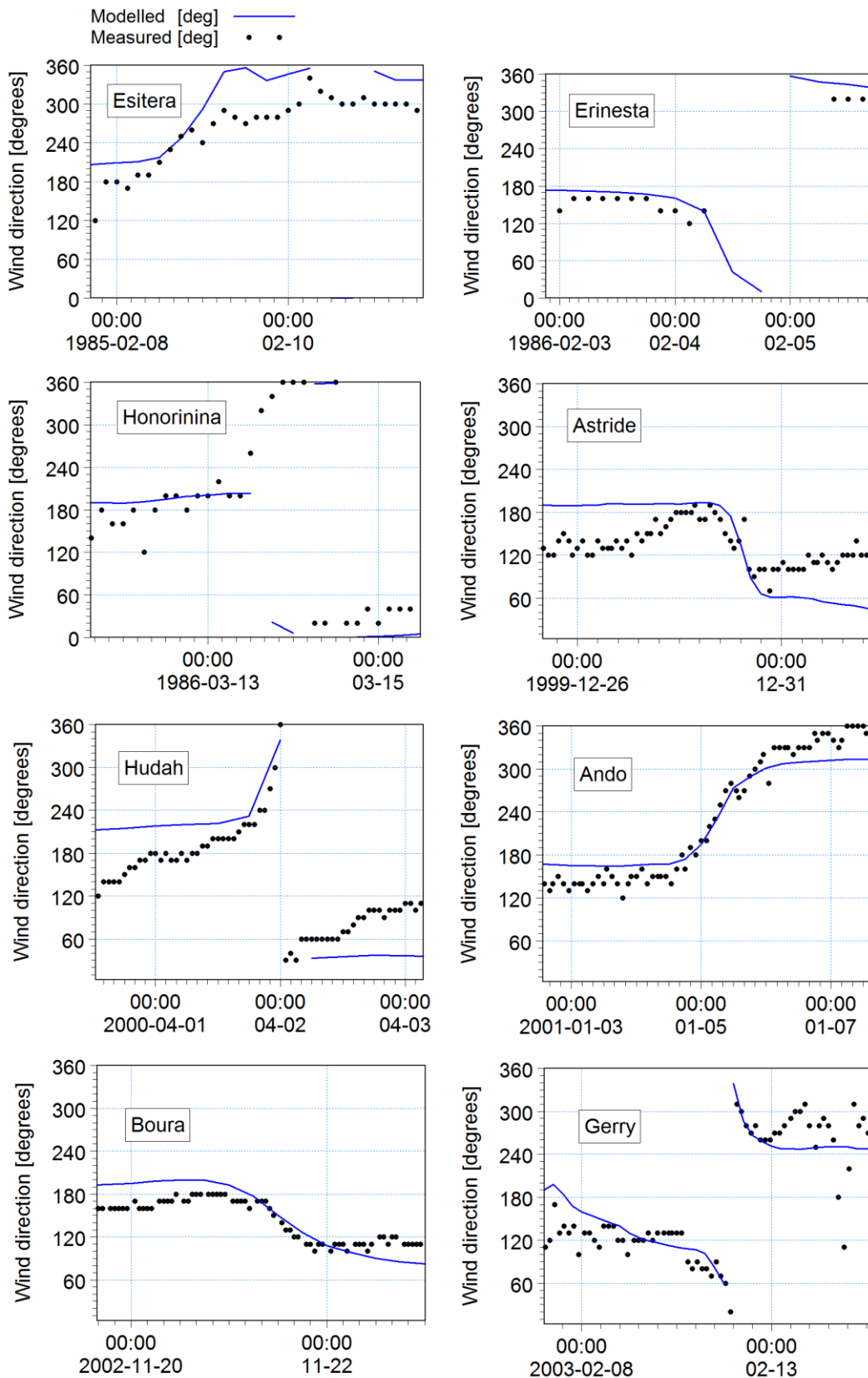
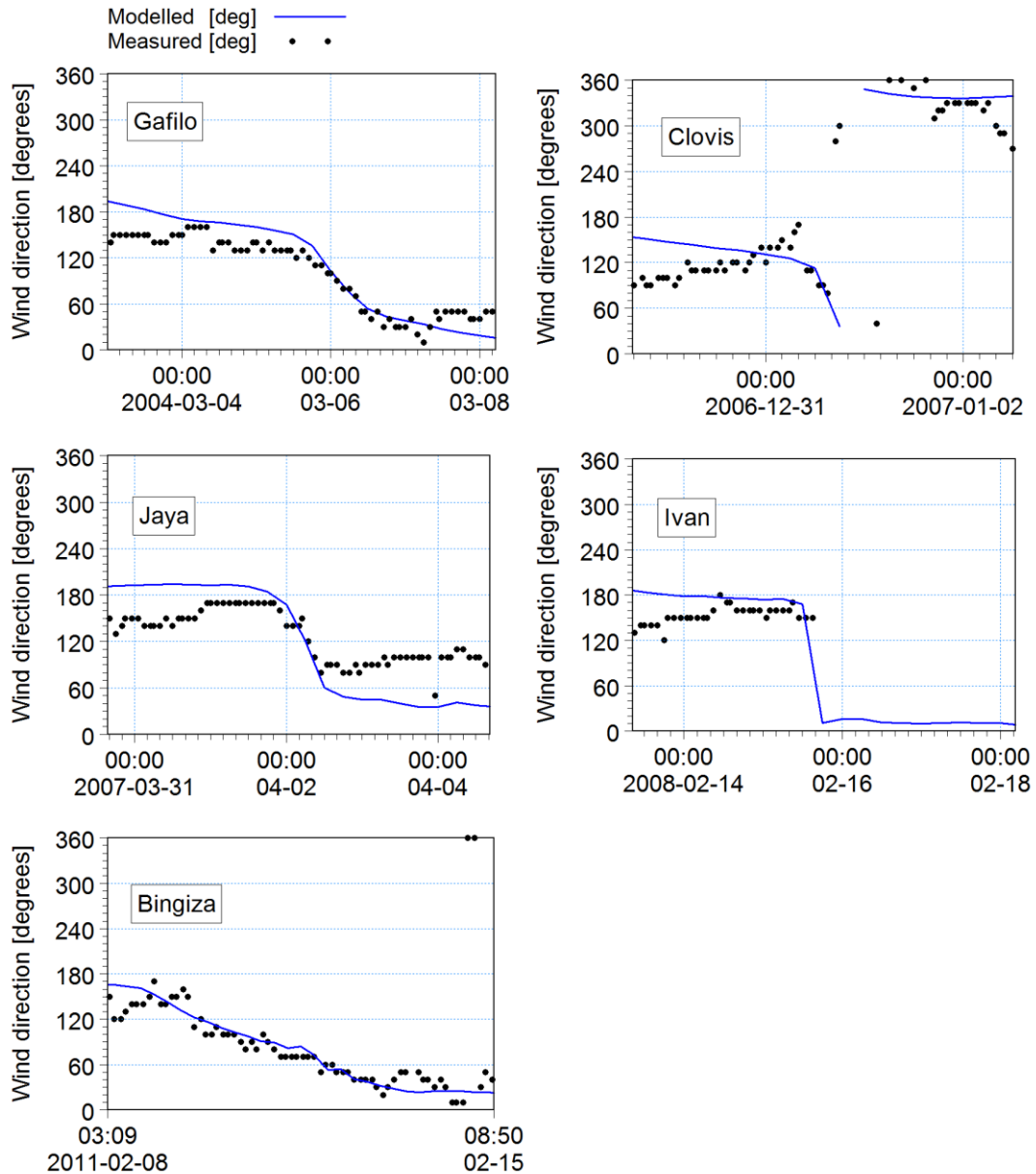


Figure 5-12 (continued): Time-series of modelled vs measured wind directions at Tromelin.

The name of each corresponding tropical cyclone is provided for reference. Figure 5-6 shows the best track data used as input to the parametric wind field models.



5.3.4 Discussion

The ultimate objective of parametric wind field models is to provide statistically unbiased predictions of wind fields near the vicinity of the eyewall, given the limited available data in the best track archives. Due to the simplistic formulation of these models, large errors between modelled and measured wind speeds are to be expected for individual events. Possible reasons for the observed differences between the modelled and the measured wind speeds include the following:

- There are errors associated with the maximum sustained wind speed (V_{max}) estimates provided in the best track data. The root mean square error in this parameter is in the order of 6 m/s (see Section 2.3.3).
- Parametric wind field models have been largely based on observations of tropical cyclones over the North Atlantic Ocean. Errors will be introduced if characteristics of storms over the South-West Indian Ocean are different to those over the North Atlantic Ocean.
- The radius to maximum wind speed (R_{max}) has been estimated using an empirical relationship. Given the rapid change in wind speed around the eyewall (Figure 5-1), a small error in the estimation of R_{max} could potentially lead to a large error in the estimation of wind speed at a given location. Such errors would also be exacerbated by errors in the estimation of the location of the eye (see Section 2.3.3).
- There is natural variation in tropical cyclone structure with individual events being less 'well behaved' than others. Even if the parameters of V_{max} and R_{max} are known to a high degree of accuracy, the best fit parametric model may still yield large errors at a given location of interest.
- There are errors introduced in the conversion of 1-min to 10-min average wind speeds required for the direct comparison of model results with the available measurements.
- Even on remote islands with few land based features, measurements will be affected to some extent by the increased friction on the earth's surface due to the island. Measurements are therefore not expected to be identical to open ocean winds, which the model is intending to reproduce.
- Wind speed measurements are typically provided at hourly or three hourly time intervals, while best track data are provided at six hourly intervals. Variations in wind speed measurements on a time scale of less than six hours will not be resolved by the model.
- The wind data have been manually scanned for any obviously spurious measurements, however there will inevitably be some errors inherent in any long record of measurements (e.g. due to faulty instrumentation) which will influence the comparison between modelled and measured wind speeds.

Given the possible reasons for observed differences between the model results and measurements discussed above, the model validation results presented in Section 5.3.3 are

pleasing in that both the Holland (1980) and Willoughby et al. (2006) models have been shown to produce peak wind speeds which are in reasonable agreement when compared to measurements. The tendency of parametric wind field models to under-predicted lower wind speeds and over-predict higher wind speeds is however noted. It is suggested that this observation deserves further investigation which has not been undertaken as part of this study. This would best be done through analyses of aircraft reconnaissance data over the South-West Indian Ocean.

Of the two considered models, the Willoughby et al. (2006) model provides wind speeds which are more in line with the observed measurements. This result is to be expected as the model has been based entirely on aircraft reconnaissance measurements, making it a better fit to measured wind speeds by definition. The Willoughby et al. (2006) model has therefore been selected as the preferred model to be used for the estimation of extreme wind speeds calculated as part of this study.

5.4 Summary and Conclusions

Parametric wind field models use the limited information available in best track archives to produce two dimensional surface wind fields which reasonably resemble those of actual storms. The Holland (1980) model has become the most widely adopted parametric wind field model for use in tropical cyclone risk models. The Willoughby et al. (2006) model, based entirely on measured flight level axisymmetric wind speed profiles, provides a promising alternative to the Holland (1980) model.

The application of parametric wind field models requires an estimation of the radius to maximum wind speed (R_{max}). The empirical relationship proposed by Willoughby & Rahn (2004) (based on reconnaissance measurements of flight level wind speeds) has been adopted for this study. The relationship between flight level and surface (10 m elevation) wind speeds has been approximated through a constant factor of 0.85, in line with dropsonde measurements from Franklin et al. (2003). Wind field asymmetry has been included through the vector addition of the forward motion of the system to the wind field. The adopted approach ensures that the V_{max} estimate provided in the best track data is reproduced in the output wind field as the maximum wind speed anywhere in the storm (in line with the definition of V_{max}).

The ability of the parametric wind field models to reproduce actual wind speeds of historical tropical cyclones has been assessed. This has been carried out through a comparison of the

modelled wind speeds with measured wind speeds undertaken on a number of islands throughout the South-West Indian Ocean. Both the Holland (1980) and Willoughby et al. (2006) models have been shown to produce peak wind speeds which are in reasonable agreement when compared to measurements, although a tendency for the models to under-predicted lower wind speeds and over-predict higher wind speeds has been noted. The Willoughby et al. (2006) model has been shown to provide a better fit to the measurements, and has therefore been selected as the preferred model to be adopted for the estimation of extreme wind speeds for the region, as described in Section 7.

6. SYNTHETIC TRACK MODEL

6.1 Introduction

Synthetic track modelling, as described in Section 2.5, forms an important component of the tropical cyclone risk model developed as part of this study. The ultimate aim of synthetic track modelling is to generate thousands of years of tropical cyclone tracks that are statistically consistent with those in the historical best track data. For this study, 5 000 years of synthetic tropical cyclone tracks for the South-West Indian Ocean have been generated. These data form an important input to the estimation of extreme wind speeds for the region, as described in Section 7.

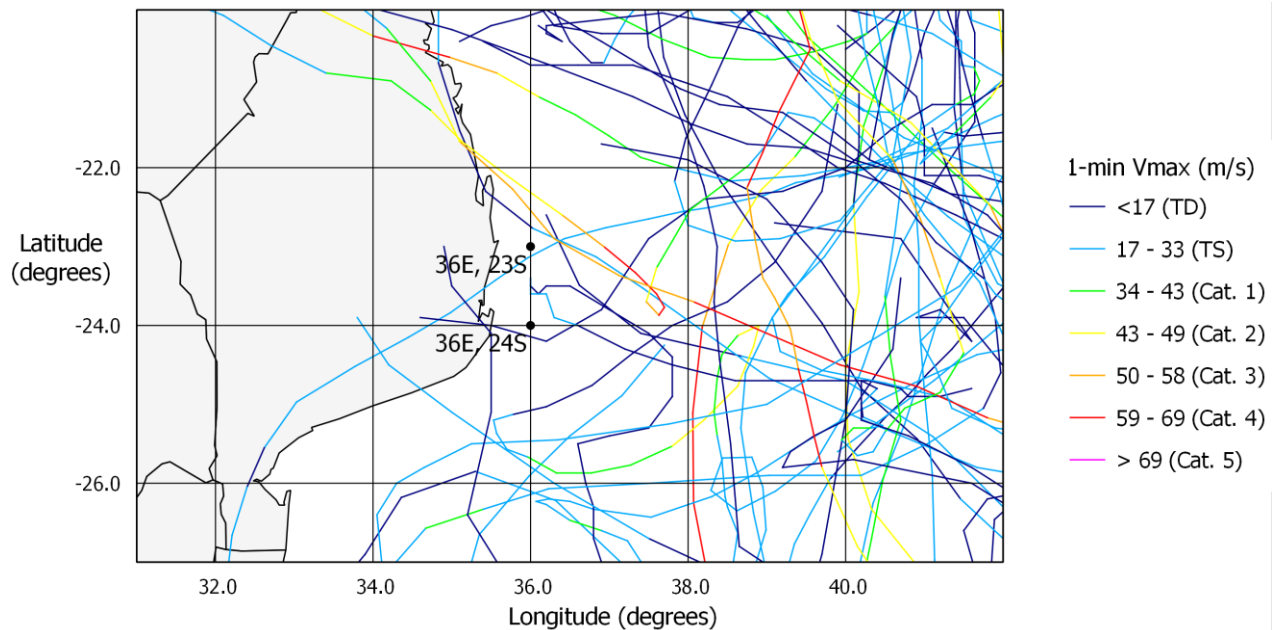
This section begins by discussing the motivation behind the use of a synthetic track model for the estimation of extreme wind speeds due to tropical cyclones. The synthetic track model adopted for this study is then described in detail, and the capability of the model to produce synthetic tracks which are statistically consistent with those in the historical records is presented and discussed.

6.2 Motivation for Synthetic Track Modelling

The requirement for a probabilistic approach to tropical cyclone risk analysis is underpinned by the notion that the available records are insufficiently long to infer extreme conditions required for engineering design. Small sample sizes may lead to unrealistic extreme value distributions and ultimately large errors in the estimation of extreme wind speeds at return periods of interest (e.g. 100 years). It is natural to test this hypothesis through the calculation of extreme wind speeds at locations in close proximity to one another, from the historical data alone. Large variations in calculated extreme wind speeds at nearby locations are likely to be unphysical, highlighting the effect of small sample sizes, and the need for a probabilistic approach.

As an illustration, Figure 6-1 presents the historical tracks for which intensity data are available (1980 – 2012) in the vicinity of two hypothetical locations of the Mozambique coastline. Given the close proximity of these two locations one would expect the true physical risk exposure to tropical cyclones to be similar.

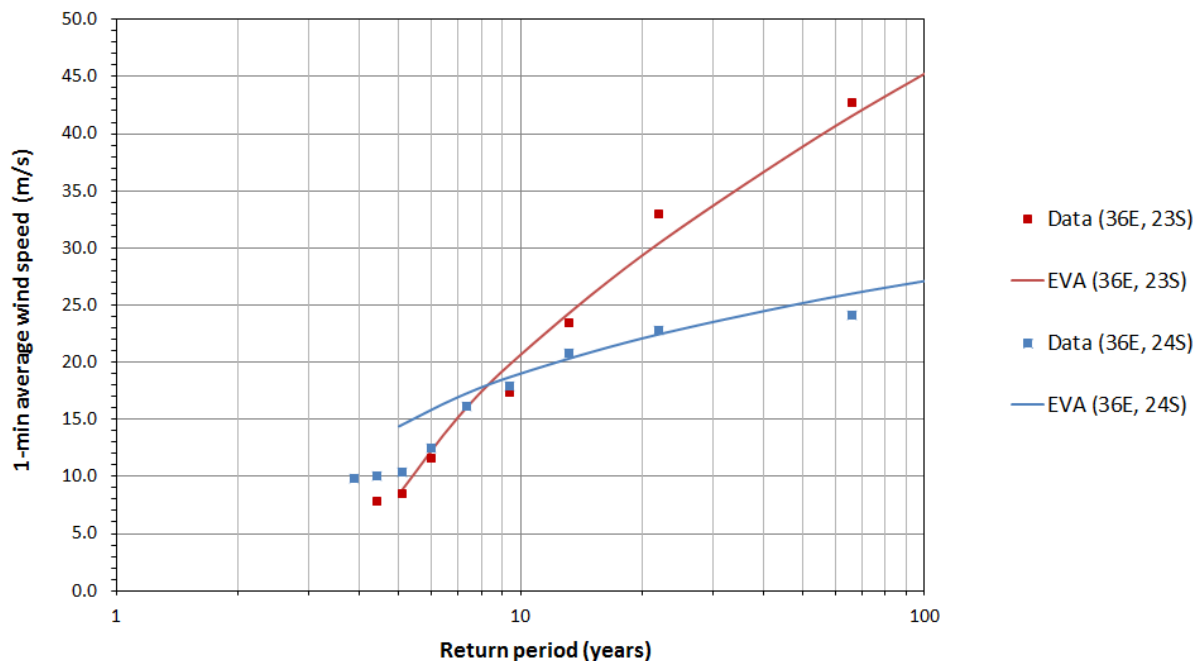
Figure 6-1: Historical tracks for which intensity data are available (1980 – 2012) in the vicinity of two hypothetical locations on the Mozambique coastline.



Time-series of modelled wind speeds at each location have been calculated through the application of the Willoughby et al. (2006) parametric wind field model along the tracks shown in Figure 6-1. For reasons described in the wind field model validation (Section 5.3.2), the modelled tracks have been limited to those passing within two geographical degrees of each location of interest. Only the peak modelled wind speed for each independent event has been extracted and used as the input to an extreme value analysis (EVA) of peak wind speeds at each location.

EVA at the two hypothetical locations have been carried out using the EVA toolbox of the MIKE by DHI suite of models developed by Danish Hydraulics Institute (DHI). The application of the model is described in the User Manual (DHI, 2012b), while full details of the statistical basis for the model is described in the Technical Reference and Documentation (DHI, 2012c). Given an extreme value time-series of peak modelled wind speeds, and the duration over which the series was extracted (33 years in this case), the EVA tool provides a selection of extreme value distributions which can be fitted to the data. The analysis carried out for this example comprised fitting a three parameter Weibull distribution using the Method of Moments. The best estimate results of the EVA at both hypothetical locations are shown in Figure 6-2. Return periods corresponding to the individual data points have been assigned according to the Hazen plotting position formula.

Figure 6-2: Extreme value analysis of modelled wind speeds at two hypothetical locations on the Mozambique coastline (see Figure 6-1 for model output locations).



It is acknowledged that the use of different extreme value distributions may result in the calculation of different extreme wind speeds, however the emphasis of the example is not on the selection of the most appropriate theoretical distribution, but rather on the difference in the results at the two hypothetical locations. It is suggested that the presented results are reasonable and serve to highlight the intention of the example.

The results indicate a significant difference between the extreme wind speeds at the two hypothetical locations, with the 100 year return period 1-min average wind speed varying from 27 m/s at the southerly location to 45 m/s at the northerly location. The EVA at the northerly location is clearly significantly influenced by two intense tropical cyclones which passed just to the north of the location, resulting in high modelled wind speeds (43 m/s and 33 m/s) for these events respectively. The southerly location happened to have no such events which passed sufficiently close to have produced equivalent wind speeds. This example serves to highlight the potential for errors due to the small sample sizes in the historical data, and underlines the need to extend the length of the historical best track dataset to many more years through a probabilistic approach. Synthetic track models have been developed for exactly this purpose.

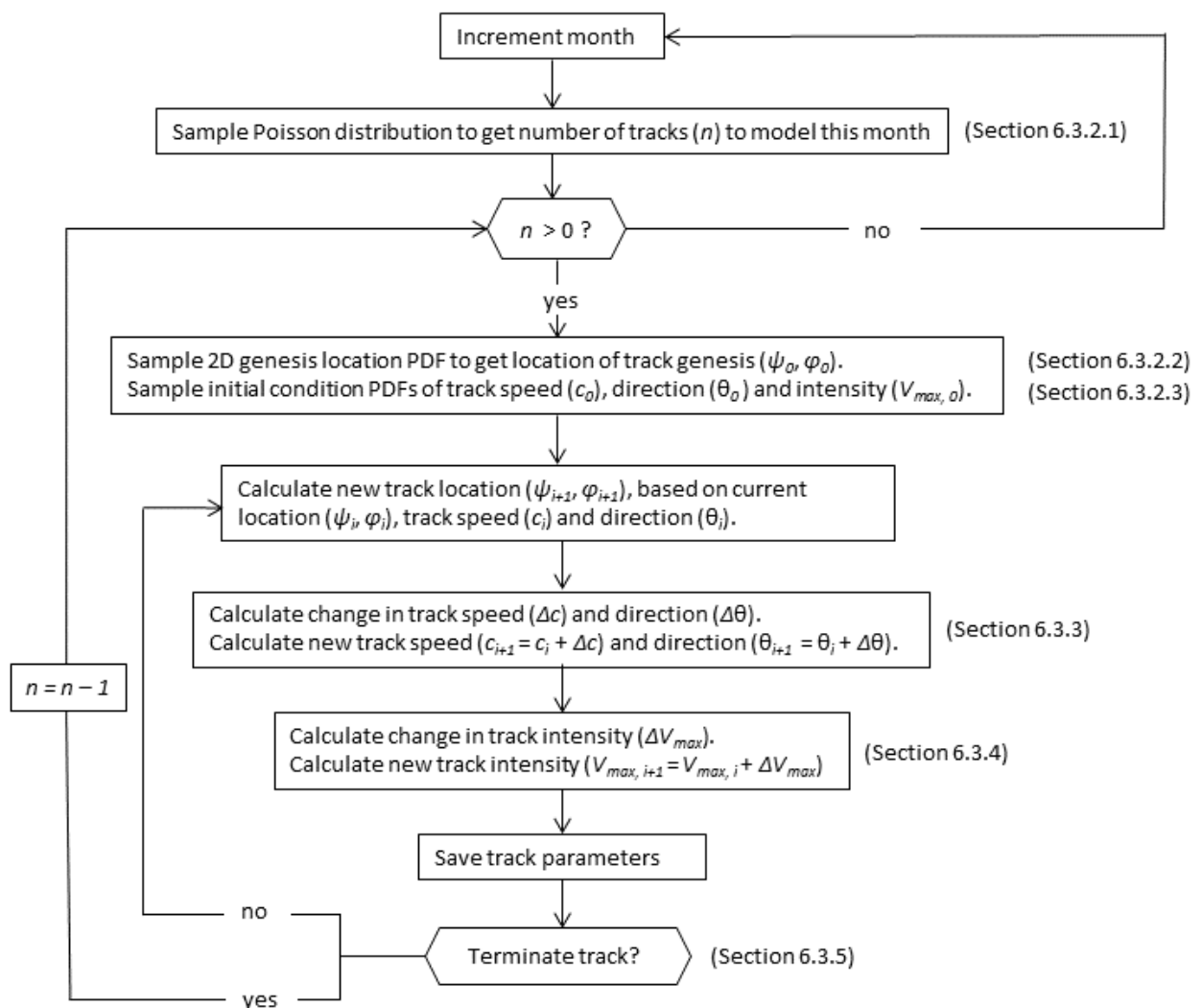
6.3 Description of the Model

6.3.1 Overview

The supporting literature for synthetic track modelling (Section 2.5) describes a number of approaches which have been adopted to date. The synthetic track model developed as part of this study can be described as a Markov chain model, largely following the methods described by Powel et al. (2005) and Emanuel et al. (2006).

The structure of the synthetic track model is presented in Figure 6-3. The various components of the model are described in more detail in the following subsections.

Figure 6-3: Flow diagram of synthetic track model.



The statistical components of the synthetic track model have been developed using the programming language R, a widely used software environment for statistical computing and graphics (R Core Team, 2013).

6.3.2 Genesis

Genesis refers to the initial formation of a tropical cyclone track. The modelling of track genesis requires the simulation of the temporal occurrence, spatial occurrence and initial conditions of each track. Each of these components of track genesis are discussed individually below.

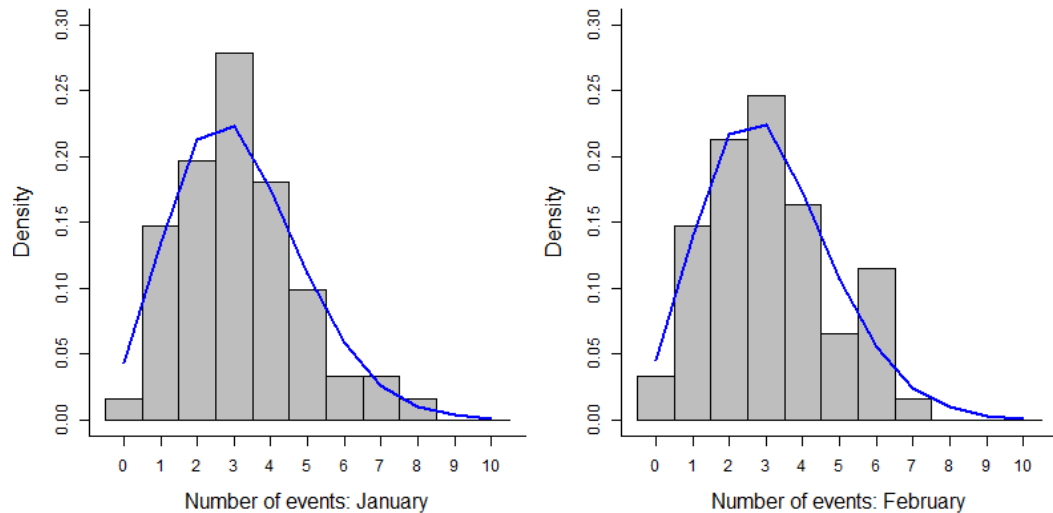
6.3.2.1 Temporal Occurrence

The temporal occurrence of synthetic tracks has been modelled on a monthly, rather than an annual basis, as this allows for the inclusion of the natural variability in track properties as a function of the changing environmental conditions throughout the year. In particular, the month in which the track occurs has an influence on the potential intensity which the track can attain (discussed in Section 6.3.4.1).

The number of events to be modelled for each month has been determined through the sampling of the relevant Poisson distribution for the month of the year. The Poisson distribution is described in Section 2.6.1.1. The Poisson distribution for each month of the year has been defined according to the historical mean monthly occurrence rates for the entire South-West Indian Ocean, as presented in Figure 4-5. Sampling of Poisson distributions has been carried out using the 'rpois' function of the base R package (R Core Team, 2013).

Figure 6-4 presents bar charts of the number of historical events occurring in the South-West Indian Ocean for the months of January and February (the peak of the tropical cyclone season) from 1952 to 2012, as well as the theoretical Poisson distribution (in blue). The calculated densities are normalised so that the sum of all densities for each graph is equal to one. The theoretical Poisson distribution is derived from the mean occurrence rate alone. The results confirm that the Poisson distribution is indeed a good representation of the historical temporal occurrence of tropical cyclones in the region.

Figure 6-4: Bar charts of the number of historical events occurring in the South-West Indian Ocean for the months of January and February from 1952 to 2012. The plots include the theoretical Poisson distribution (in blue) for the respective months.



6.3.2.2 Spatial Occurrence

The spatial occurrence of tropical cyclone genesis has been modelled through the sampling of a two-dimensional binned kernel density estimate based on historical genesis locations in the best track data. Historical genesis events have been identified in the best track archives as the first data entry for a given event. In practical terms, this is when the meteorological organisation archiving the best track data started tracking the event. The generation of the two-dimensional binned kernel density estimate was carried out using the 'KernSmooth' package (Wand & Ripley, 2013), which provides functions for kernel smoothing according to Wand & Jones (1995).

The domain of interest has been subdivided onto a 0.5 degree geographical grid, and based on the density of historical genesis points in the vicinity of each grid point, the density of each grid point was computed. The dimensionless density at each grid point is automatically normalised so that the integral of all densities over the domain is equal to one. The smoothness of the output density is dependent on the kernel bandwidth smoothing parameter. Larger values of bandwidth make smoother estimates, while smaller values of bandwidth make less smooth estimates. The bandwidth smoothing parameter was manually adjusted until a visually pleasing density distribution was obtained.

The binned kernel density estimate used for simulating genesis locations for this study is shown in Figure 6-5. Sampling of the two-dimensional density estimate for track genesis has

been carried out using a 'hit and miss' algorithm, analogous to the one-dimensional version described in Appendix B.

Figure 6-5: Binned kernel density estimate of genesis locations. Historical genesis locations from which the density is derived are shown as black points.

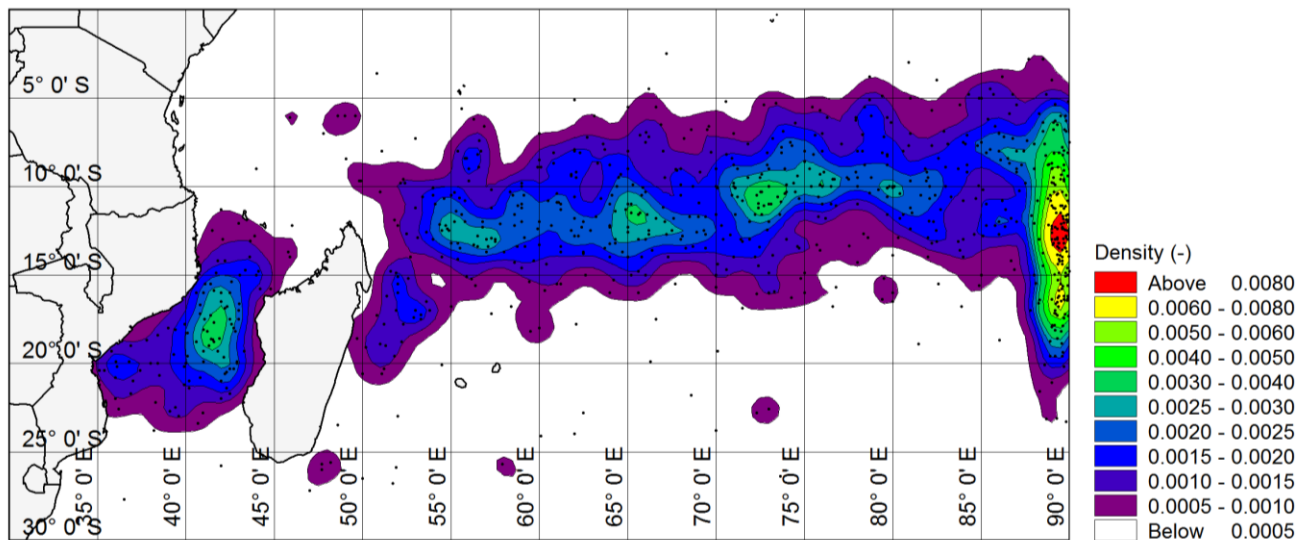


Figure 6-5 indicates that conditions most favourable for tropical cyclone genesis over the South-West Indian Ocean occur in a band which spans the region. The genesis density peaks to the east of Madagascar, between latitudes of 5° S and 15° S, with genesis tending to shift southward at lower longitudes. Within the Mozambique Channel, genesis density shows an observed peak between latitudes of 15° S and 20° S. The eastern extent of the domain indicates high genesis density, although this is due to a large number of fully developed tracks which enter the domain from the east. As these are not explicitly genesis events, initial conditions for these events are modelled separately (as discussed in Section 6.3.2.3 below).

6.3.2.3 Initial Conditions for Track Speed, Direction and Intensity

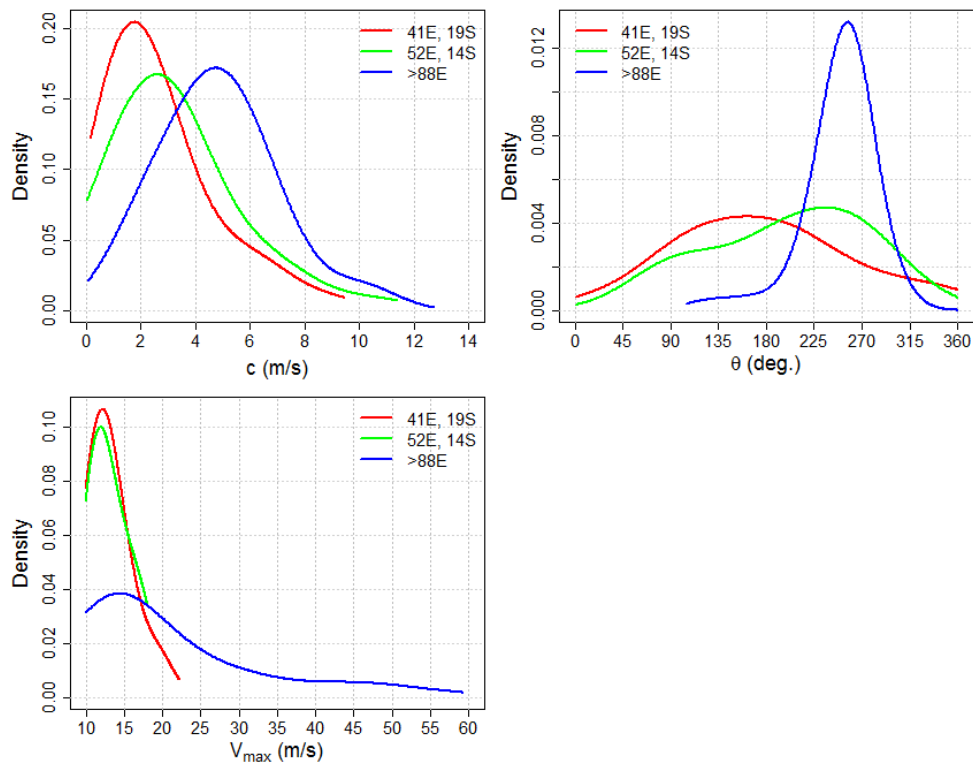
Initial conditions for track speed (c), track direction (θ) and intensity (V_{max}) have been modelled by sampling non-parametric probability density functions (PDFs) of these parameters, which are derived from initial conditions contained in the historical best track data. Details of the generation and sampling of non-parametric PDFs are discussed in Appendix B. Initial conditions for c and θ have been based on the entire 61 year (1952 to 2012) best track dataset for the region, while those for V_{max} are reliant on the 33 year dataset (1980 to 2012) for which intensity data are available.

PDFs of initial conditions have been defined on a 0.5° geographical grid. For each grid point, only genesis data in the immediate vicinity of the grid point have been used in the generation of the PDF of interest. Qualitative inspection of generated PDFs indicated that a threshold of at least 30 observations is required to obtain a robust PDF. Selection of data at each grid point begins by considering data with a search radius of two geographical degrees (approximately 200 km) of the grid point. If the threshold of 30 observations is not attained, then the search radius is extended in one degree increments until the threshold is attained. This leads to very large search areas for remote genesis locations, which is favoured over the generation of PDFs from fewer observations.

The exception to the methodology described above is when the modelled genesis location lies east of 88° E. In this case only data east of 88° E is used to compute the PDFs for initial conditions as these genesis data contain fully developed events entering the domain from the east, rather than actual genesis events.

The location of each genesis event determines which PDFs are sampled to generate the initial conditions for the event. Figure 6-6 presents examples of initial condition PDFs at three locations within the domain. One location lies in the Mozambique Channel (41° E, 19° S), one lies to the east of Madagascar (52° E, 14° S) and one is at the eastern extent of the domain ($> 88^\circ$ E). The figure highlights the variation of initial conditions across the domain. In particular, the initial conditions for locations $> 88^\circ$ E are notably different, being more typical of fully developed events rather than actual genesis events.

Figure 6-6: Non-parametric probability density functions (PDFs) for initial conditions of track speed (c), track direction (θ) and intensity (V_{max}). Three locations are compared.



6.3.3 Track Propagation

Once a track has been initiated, it is propagated through space through the sampling of non-parametric PDFs for incremental changes in track direction ($\Delta\theta$) and track speed (Δc). The track propagation component of the model has been based on the entire 61 year (1952 to 2012) best track dataset for the region.

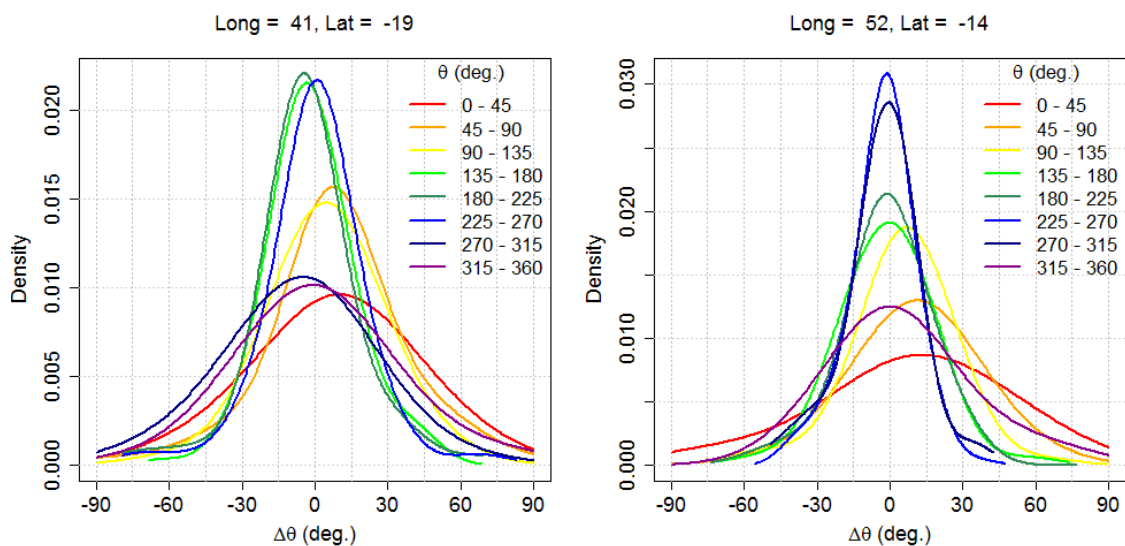
As for the genesis conditions, PDFs for track propagation have been defined on a 0.5° geographical grid spanning the domain. For each grid point, relevant data within a search radius of two geographical degrees (approximately 200 km) is checked to see if the threshold number of observations for a robust PDF is attained or not. If not, then the search radius is extended in one degree increments until the threshold is achieved.

6.3.3.1 Track Direction

Changes in track direction ($\Delta\theta$) at each six hour time-step have been modelled as a function of the direction of the track (θ) at the preceding time-step. Following Powel et al. (2005), eight directional bins (45° increments) have been adopted for this purpose. This takes the effect of the current direction on the change in track direction into account. Figure 6-7 presents PDFs

of $\Delta\theta$ at two locations in the study domain. One location lies in the Mozambique Channel (41° E, 19° S) and the other lies to the east of Madagascar (52° E, 14° S). Track direction is measured clockwise from true north, such that a heading of 270° implies a track heading in a westerly direction. Positive (or negative) changes in track direction represent clockwise (or anti-clockwise) rotations in track direction. More peaked distributions indicate a tendency for the track to maintain its current direction. In general, the derived density functions display the expected trends. For instance, at coordinates 52° E, 14° S (east of Madagascar), tracks moving in a westerly direction show a strong tendency to maintain their heading. The same can be said for tracks moving in a southerly direction at coordinates 41° E, 19° S (in the Mozambique Channel).

Figure 6-7: Non-parametric probability density functions for change in track direction ($\Delta\theta$) for various track directional bins. Two locations are compared.



Initial tests showed that the purely statistical model for change in track direction described above is insufficient to model the physical limits imposed by the equator, with the model yielding too many synthetic tracks nearing, or even passing over the equator. For this reason, an additional constraint was applied to the track directions whereby for latitudes north of 10° S, the northerly component of $\Delta\theta$ is checked and only accepted if negative. This ensures that tracks north of 10° S will always tend to move away from the equator.

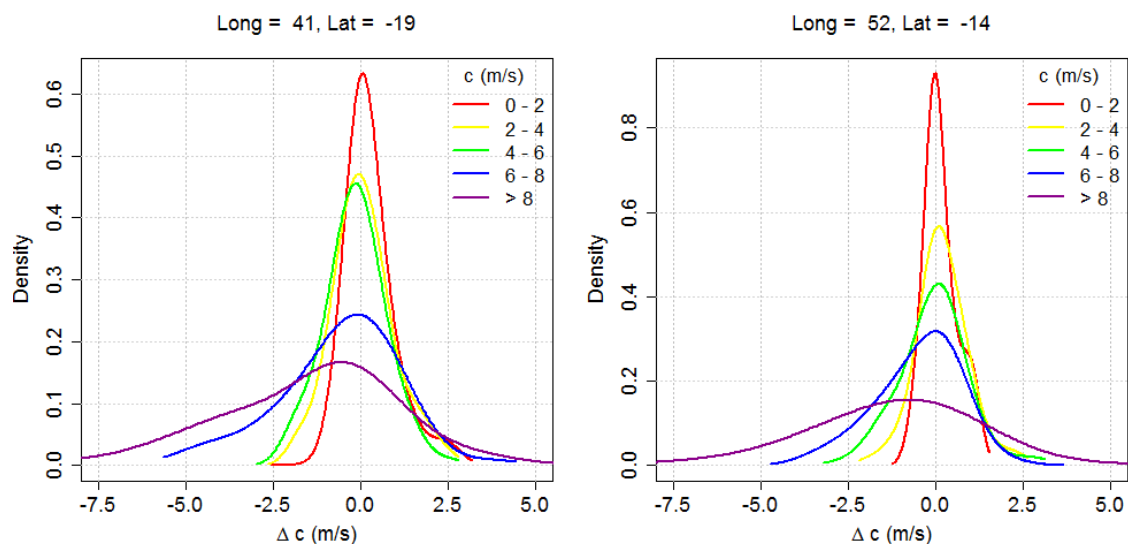
6.3.3.2 Track Speed

Changes in track speed (Δc) have been modelled as a function of the track speed (c) at the preceding time-step. Five track speed bins, at 2 m/s increments, have been adopted for this

purpose. Figure 6-8 presents density functions of Δc at the same two locations as shown in Figure 6-7. In general, the derived density functions show the expected trends, with faster track speeds showing a wider range of possible changes in track direction and an increased tendency to slow down.

The track propagation model requires an upper limit to track speed so as to ensure that physical limits for this parameter are not exceeded. Based on observed track speeds in the historical best track data, a nominal upper limit to track speed of 15 m/s has been adopted for the track propagation model.

Figure 6-8: Non-parametric probability density functions for change in track speed (Δc) for various track speed bins. Two locations are compared.



6.3.4 Intensity Evolution

The intensity evolution model is comprised of two components; namely an at-sea model and a land-filling model. The selection of the intensity evolution model depends on whether the synthetic track is over land or over the ocean. A land mask defined on a 0.25° geographical grid has been used to define whether a given track is defined as being at-sea or over land.

6.3.4.1 At-Sea Model

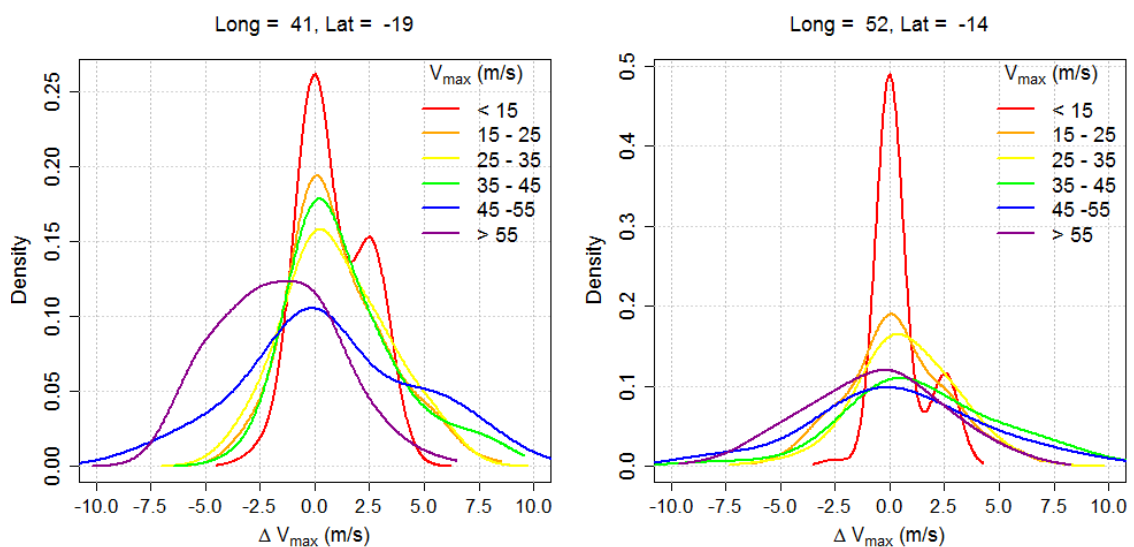
When the location of the track is defined as at-sea, then the change in track intensity at each six hour interval is modelled in a statistical approach analogous to the track propagation component of the model. The at-sea intensity model has been based on the 33 year (1980 to 2012) best track dataset for which intensity data are available. Only at-sea historical data has

been used as the basis of the model. Data over land has been excluded as these intensity data show an increased tendency to decay with time, which is not desirable if the track is over water.

PDFs for intensity evolution have been defined on a 0.5° geographical grid spanning the domain. For each grid point, relevant data within a search radius of two geographical degrees (approximately 200 km) is checked to see if the threshold number of observations for a robust PDF is attained or not. If not, then the search radius is extended by one degree increments until the threshold is achieved.

Changes in track intensity (ΔV_{max}) have been modelled as a function of the intensity (V_{max}) at the preceding time-step. Six intensity bins, at 10 m/s increments, have been adopted for this purpose. Figure 6-9 presents density functions of ΔV_{max} at the same two locations as shown in Figure 6-7 and Figure 6-8. In general, the derived density functions show the expected trends, with higher intensities showing a wider range of possible changes in intensity and very intense systems showing more of a tendency to decay. The PDFs for the lowest intensity bin ($V_{max} < 15$ m/s) show two peaks, which is due to the 5 kt (2.6 m/s) resolution of the historical intensity data. At this intensity bin there are only data at two discrete values of ΔV_{max} , leading to the observed two peaked density estimates.

Figure 6-9: Non-parametric probability density functions for change in track intensity (ΔV_{max}) for various intensity bins. Two locations are compared.



The concept of maximum potential intensity (MPI) as an upper physical limit to tropical cyclone intensity was discussed in Section 2.6.3.3. Mean monthly estimates of MPI, defined

on a 2.5° global geographical grid, have been kindly supplied by Professor Kerry Emanuel of the Massachusetts Institute of Technology for this study (personal communication). The details of the calculation procedure of the MPI estimates follows Emanuel (1988, 1995), and is summarised online by Bister & Emmanuel (n.d.). Appendix C shows these mean monthly MPI maps for the region of the South-West Indian Ocean.

At each time-step the coordinates of the track, and the month in which the track has occurred, are used to obtain the theoretical mean monthly MPI. Due to the relatively coarse grid of the raw MPI data, an inverse distance weighting algorithm has been used to interpolate between the gridded MPI data to obtain MPI estimates at the specific coordinates of the track being modelled. These space and time-varying MPI estimates have been used as the upper limits in the modelling of synthetic track intensity. As such, at each time-step, ΔV_{max} is checked and only accepted if the resulting V_{max} is less than the calculated MPI for the track location and month in which the track has occurred.

As for the track propagation model, initial tests showed that the purely statistical intensity model described above is insufficient to model the physical limits imposed by the equator, with the model tending to over-predict track intensities near the equator. For this reason an additional constraint was applied to the intensity model whereby for latitudes north of 10° S and V_{max} greater than 25 m/s, ΔV_{max} is checked and only accepted if negative. The suitability of this rather crude adjustment to the model is confirmed in the comparison of the modelled and historical distributions of track intensity (Figure 6-16).

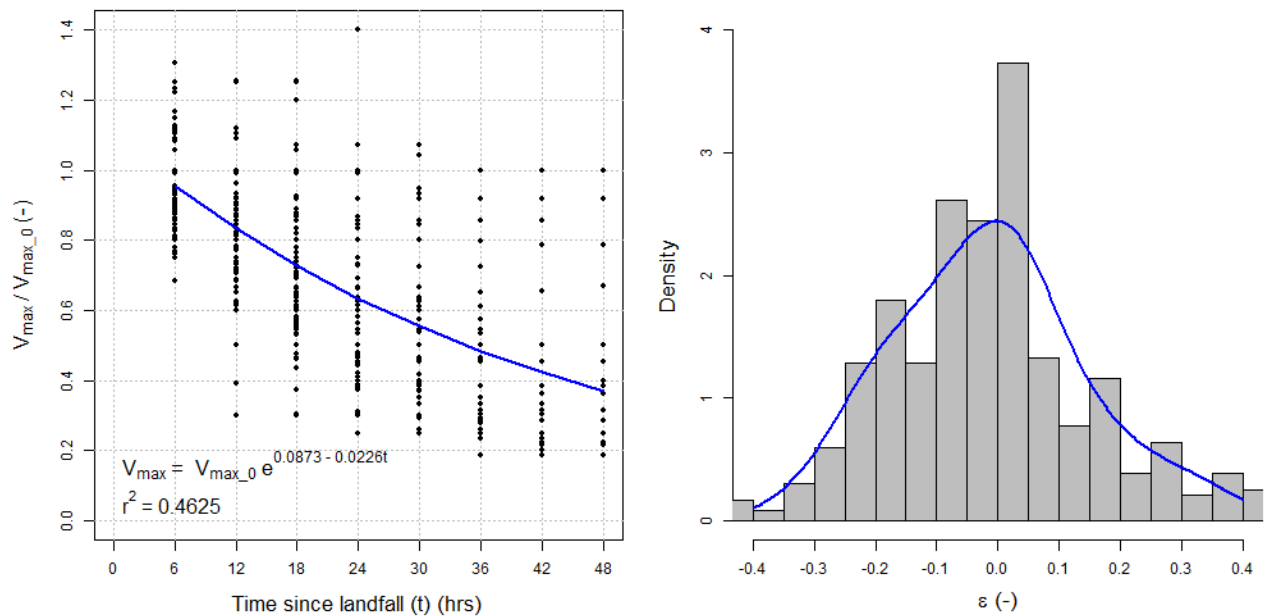
6.3.4.2 Land-Filling Model

As tropical cyclones move over land the heat source of the ocean which drives the system is no longer available, and so their intensity tends to weaken as a function of time. The intensity evolution of synthetic tracks over land is governed by a land-filling model, which is particularly important in the context of this study as many tracks pass over Madagascar and into the Mozambique Channel. A poorly formulated land-filling model will therefore lead to unrealistic intensity estimates in the Mozambique Channel.

The land-filling model is based on the 33 year (1980 to 2012) best track dataset for which intensity data are available, but considers only data with locations over land. These data have been processed to extract the observed reduction of tropical cyclone intensity as a function of time over land. The left window of Figure 6-10 presents the change of the ratio of V_{max}/V_{max_0} with time after landfall, where V_{max_0} is V_{max} at the time of landfall. The right

window of Figure 6-10 presents the model residuals ($\varepsilon = \text{observed} - \text{model}$) resulting from the best fit exponential curve to the historical data.

Figure 6-10: Land-filling model. Left window shows the best fit to the historical landfall events, while the right window shows the residuals from the best fit model.



When a synthetic track makes landfall, the intensity at the time of landfall (V_{max_0}) is saved. For as long as the track remains over land, the intensity of the track (V_{max}) is determined from the land-filling model as follows:

$$V_{max} = V_{max_0}(e^{0.0873 - 0.0226t} + \varepsilon)$$

Equation 6-1

The residual term ε is determined from sampling the distribution of model residuals shown in Figure 6-10 at the time of landfall and is kept constant throughout the landfall event. Sampling the results in this manner ensures that the observed variation in intensity reduction as a function of time over land is well reproduced by the model.

6.3.5 Termination

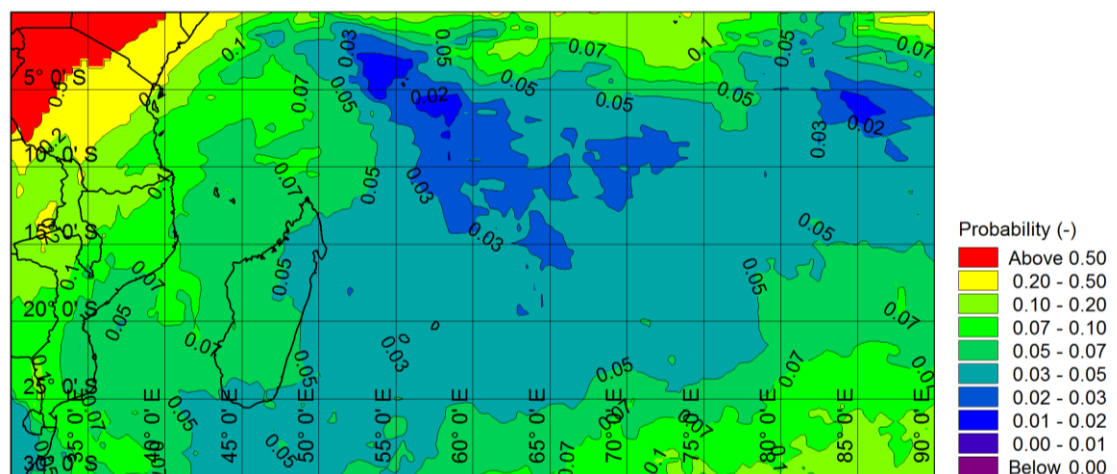
Each 6 hour time-step ends with a check on whether the track should be terminated or not. The termination component of the model has been based on the 33 year (1980 to 2012) best track dataset for which intensity data are available. The probability of track termination has been calculated as the ratio of the number of historical termination events, divided by the number of historical non-termination events in the vicinity of the location of the track.

Termination probabilities have been defined on a 0.5° geographical grid. Due to the wide distribution of historical termination locations, the search radius for each grid point is necessarily large. After some sensitivity tests to determine the minimum required search radius which would result in robust termination probabilities for each grid point, a search radius of 10 geographical degrees was chosen.

It was found that the termination algorithm was important in the generation of realistic occurrence rates of tropical cyclones throughout the domain. If track lifetimes are over-predicted, then the average occurrence rate of modelled synthetic tracks at a given location will be too high. The reverse is true if track lifetimes are under-predicted. It was found that best results were achieved by making termination probabilities a function of track duration as well as track intensity. Duration bins of < 80 hours, 80 hours to 160 hours, 160 hours to 240 hours and > 240 hours were used for this task. From physical arguments, termination should also be dependent on the intensity of the event, where weaker systems will be more likely to terminate than stronger systems. Different termination probabilities have therefore been calculated for intensity bins of $V_{max} \geq 20$ m/s as well as $V_{max} < 20$ m/s.

Figure 6-11 presents an example of a termination probability map for $V_{max} < 20$ m/s and track duration between 160 hours and 240 hours. By way of an example, a location with a termination probability of 0.05 implies that passing tracks under these conditions will terminate on average every 20th time-step. Figure 6-11 serves to highlight the expected trends, whereby in general, the termination probabilities tend to increase close to and over land, as well as near the equator and at the southern extremity of the domain.

Figure 6-11: Probability of track termination for $V_{max} < 20$ m/s and track duration between 160 hours and 240 hours.



It is acknowledged that termination probabilities may become inaccurate in areas where there are particularly few historical termination locations from which to derive the probabilities. For example, one might expect higher termination probabilities near 55° E, 5° S than those shown in Figure 6-11, as this area is near the equator. Such discrepancies were considered acceptable, given that the model results in desired track durations and therefore occurrence rates, as confirmed by the validation of the synthetic track model below.

6.4 Validation of the Model

As described in Section 6.2, the relatively small sample sizes of historical tropical cyclones leads to potentially large errors in the estimation of extreme wind speeds. The synthetic track model described above can be used to generate thousands of years of data, thus eliminating errors introduced by small sample sizes. Such a model will however naturally introduce errors of its own, as synthetic tracks will never replicate the properties of actual tracks exactly. A synthetic track model which introduces errors in extreme wind speed estimates greater than those introduced by small sample sizes is of little value. It is therefore important to validate the synthetic track model to ensure that the statistical properties of the historical tracks are well reproduced.

The validation of the synthetic track model is comprised of a number of comparisons of the statistical properties of the synthetic tracks with those of the historical tracks. The analysis is comprised of two components, namely the comparison of the spatial and temporal occurrence of historical and synthetic tracks, as well as the comparison of the various track parameters of interest (track speed, direction and intensity).

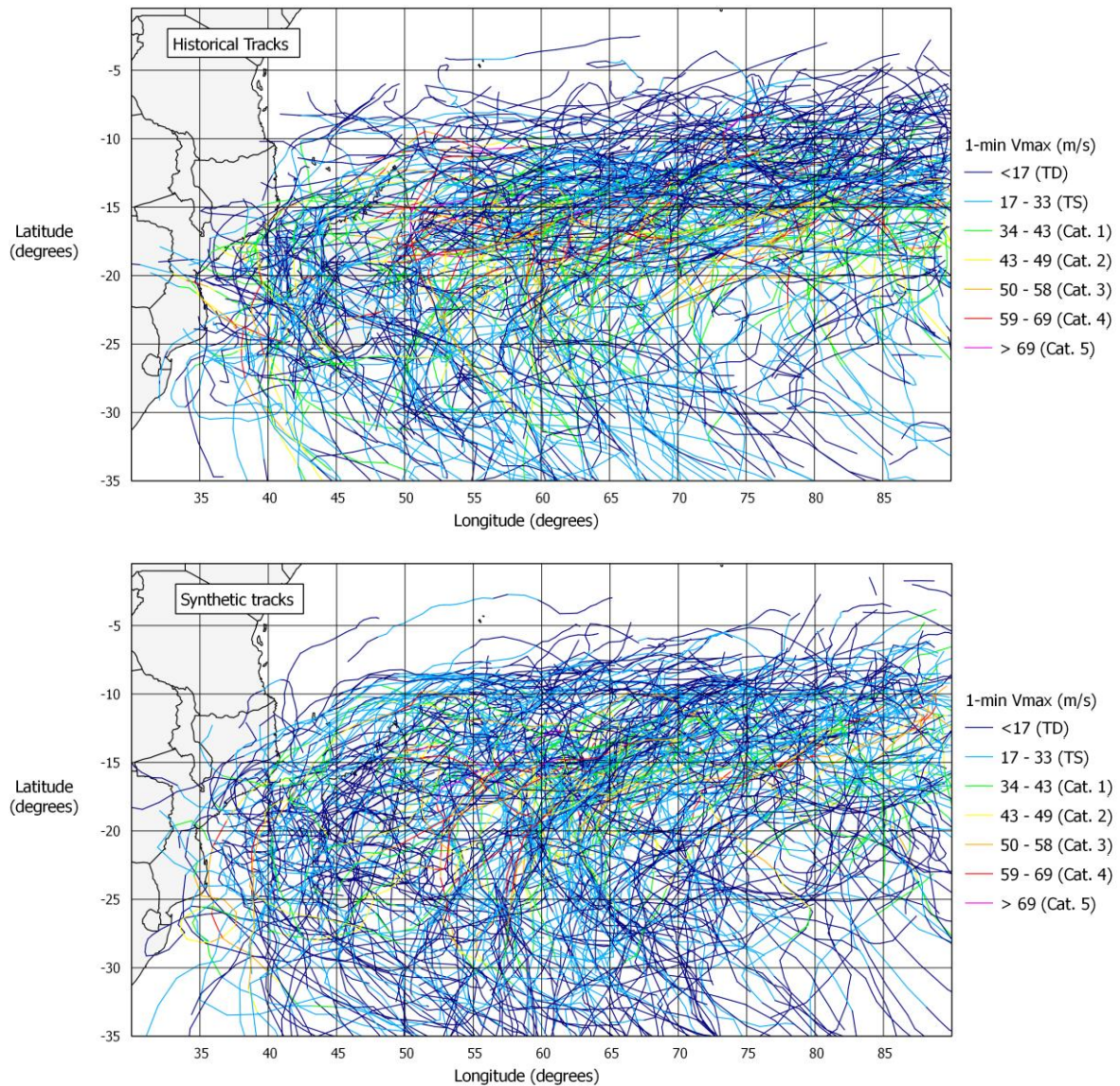
6.4.1 Spatial and Temporal Occurrence

Figure 6-12 compares the 33 year (1980 to 2012) historical best track dataset for which intensity data are available (as shown in Figure 4-6) with 33 years of randomly selected synthetic tracks. The track colour denotes the intensity of the track, according to the Saffir-Simpson scale (Table 2-1).

Figure 6-12 provides a qualitative impression of the ability of the synthetic track model to generate tracks which reasonably resemble those in the historical data. It must however be noted that there can be significant variation in the qualitative impression of the synthetic tracks, depending on which 33 years are selected for comparison. This again points to the small sample size of the 33 year historical dataset in terms of tropical cyclone occurrence. It is therefore suggested that little can be inferred from Figure 6-12 in terms of the validation of

the synthetic track model. The figure does however serve as an example of the raw output of the synthetic track model.

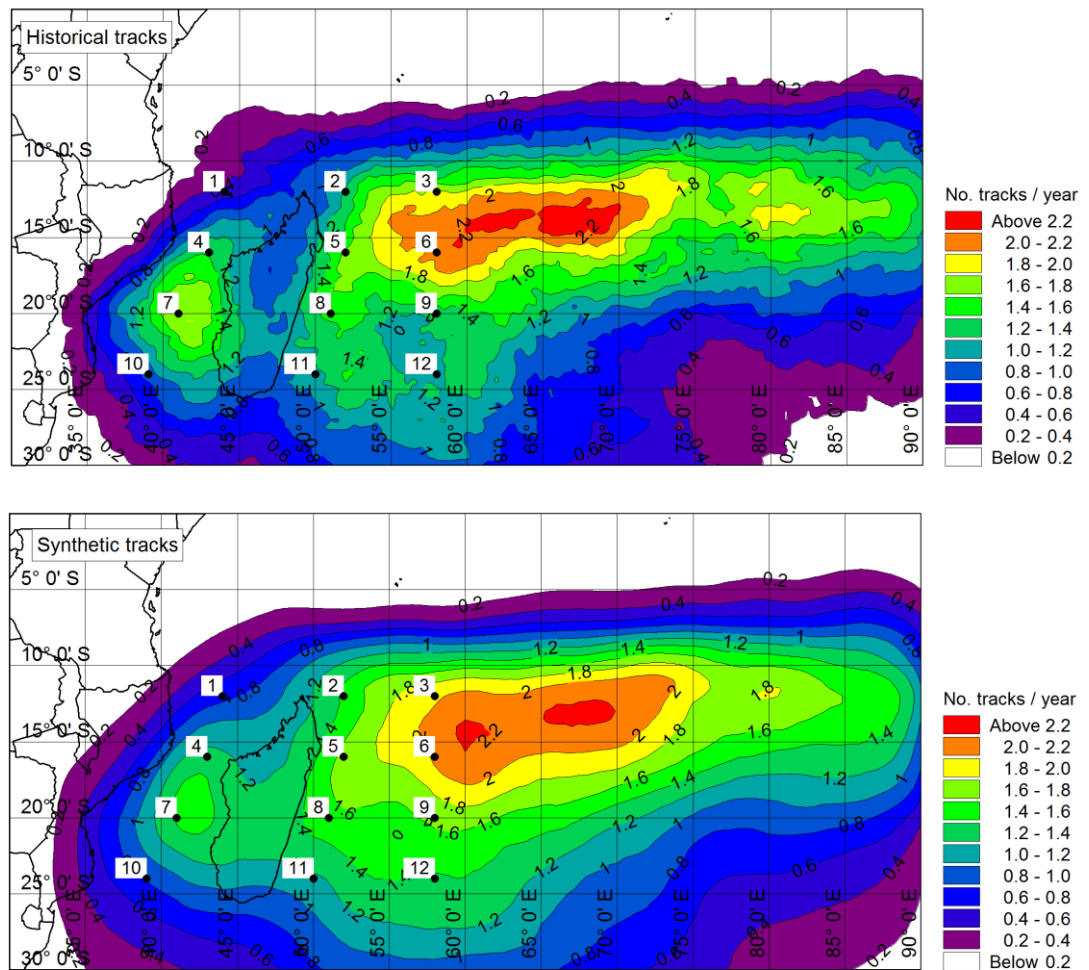
Figure 6-12: Comparison of 33 years of historical tracks (1980 to 2012) with 33 years of randomly selected synthetic tracks. The scale corresponds to the Saffir-Simpson scale.



A more quantitative representation of the ability of the synthetic track model to reproduce the spatial and temporal occurrence of historical tracks is presented in Figure 6-13. In this figure the best track data are presented in terms of the average number of tracks passing within 2 geographical degrees (approximately 200 km) of a given location per year on average. The contours for the historical tracks have been derived from the full 61 year (1952 to 2012) historical dataset for which track occurrence and location are available. The contours for the synthetic tracks have been derived from 5 000 years of data generated by the model. The

numbered points in the plots refer to control points which have been used in the comparison of synthetic and historical distributions of track parameters (Section 6.4.2).

Figure 6-13: Comparison of average occurrence rates of tropical cyclones from 61 years (1952 to 2012) of historical tracks and 5 000 years of synthetic tracks. Contours represent the number of tracks passing within 2 geographical degrees (approximately 200 km) per year on average. Numbered points refer to control points for the comparison of track parameters.



The results indicate that the synthetic track model generates occurrence rates of tropical cyclones similar to the observed occurrence rates over much of the South-West Indian Ocean. The model displays skill in reproducing occurrence rates around the outer extents of the region influenced by tropical cyclones (areas of low occurrence), as well as reproducing the observed peak occurrence rates to the east of Madagascar.

A potential shortcoming of the model is lower than observed occurrence rates over the central Mozambique Channel, where a synthetic peak occurrence rate of 1.5 tracks/year is achieved as opposed to the historical peak occurrence rate of about 1.8 tracks/year. The opposite is true over Madagascar, where the model yields higher than observed occurrence rates. This discrepancy may be explained by the inability of the model to simulate subtle influences of land masses. This is discussed further under Section 6.5.

A notable observation from Figure 6-13 is that the contours of occurrence rate for the synthetic tracks are far smoother than those for the historical tracks. This difference is due to the fact that the synthetic occurrence rates have been derived from 5 000 years of data, while the historical occurrence rates have been derived from just 61 years of data. This underlines the fact that 61 years is a relatively small sample size when tropical cyclone occurrence is considered. It is suggested that at least some of the observed differences between the model and historical results are as a direct result of the small sample size from which the historical occurrence rates have been derived.

Based on the presented results, it is suggested that the synthetic track model can be described as satisfactory in its ability to generate the desired spatial and temporal occurrence of tropical cyclone tracks.

6.4.2 Distributions of Track Speed, Direction and Intensity

Figure 6-14, Figure 6-15 and Figure 6-16 compare historical and synthetic cumulative density distributions for the parameters of track direction (θ), track speed (c) and intensity (V_{max}) respectively. Historical distributions of θ and c have been derived from the 61 year (1952 to 2012) historical dataset for which track occurrence and location are available, while historical distributions of V_{max} have been derived from the 33 year (1980 to 2012) historical best track dataset for which intensity data are available. Synthetic parameter distributions have all been derived from 5 000 years of modelled tracks.

Each figure presents data occurring within 2 geographical degrees (approximately 200 km) of twelve selected control points. The locations of the control points are shown in Figure 6-13, while their coordinates are provided in Table 6-1. Four control points are located in the Mozambique Channel, while the remaining eight control points are located east of Madagascar. Control points have been limited to the western extent of the domain, as this is where there is the greatest threat to loss of life and infrastructure, and therefore where the results are of greatest importance.

Table 6-1: Coordinates of control points used to compare distributions of synthetic and historical track parameters.

Control Point	Longitude (degrees)	Latitude (degrees)
1	44	-12
2	52	-12
3	58	-12
4	43	-16
5	52	-16
6	58	-16
7	41	-20
8	51	-20
9	58	-20
10	39	-24
11	50	-24
12	58	-24

Figure 6-14: Comparison of historical and synthetic distributions of track direction (θ) occurring within 2 geographical degrees (approximately 200 km) of selected control points. Locations of control points are shown in Figure 6-13.

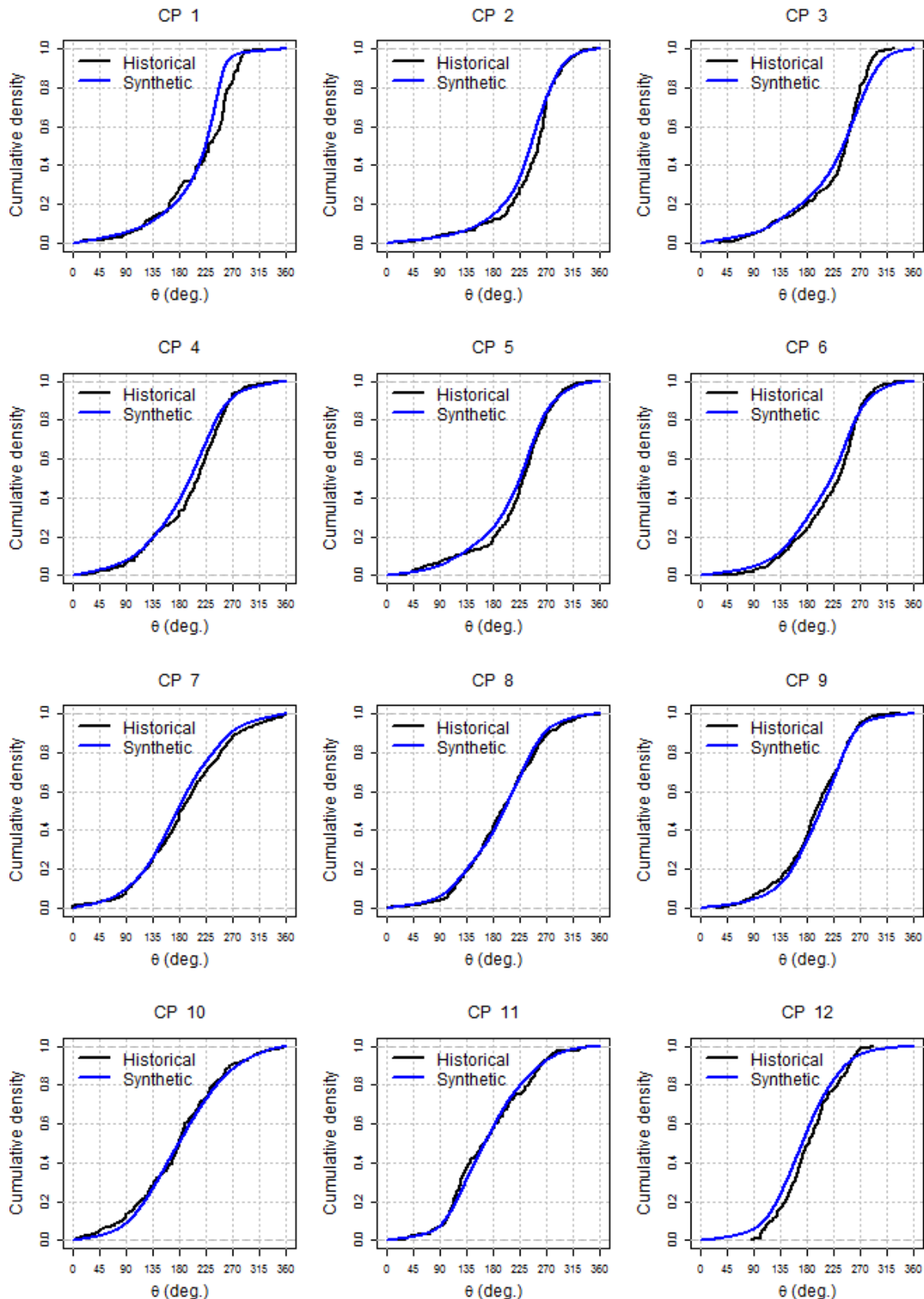


Figure 6-15: Comparison of historical and synthetic distributions of track speed (c) occurring within 2 geographical degrees (approximately 200 km) of selected control points. Locations of control points are shown in Figure 6-13.

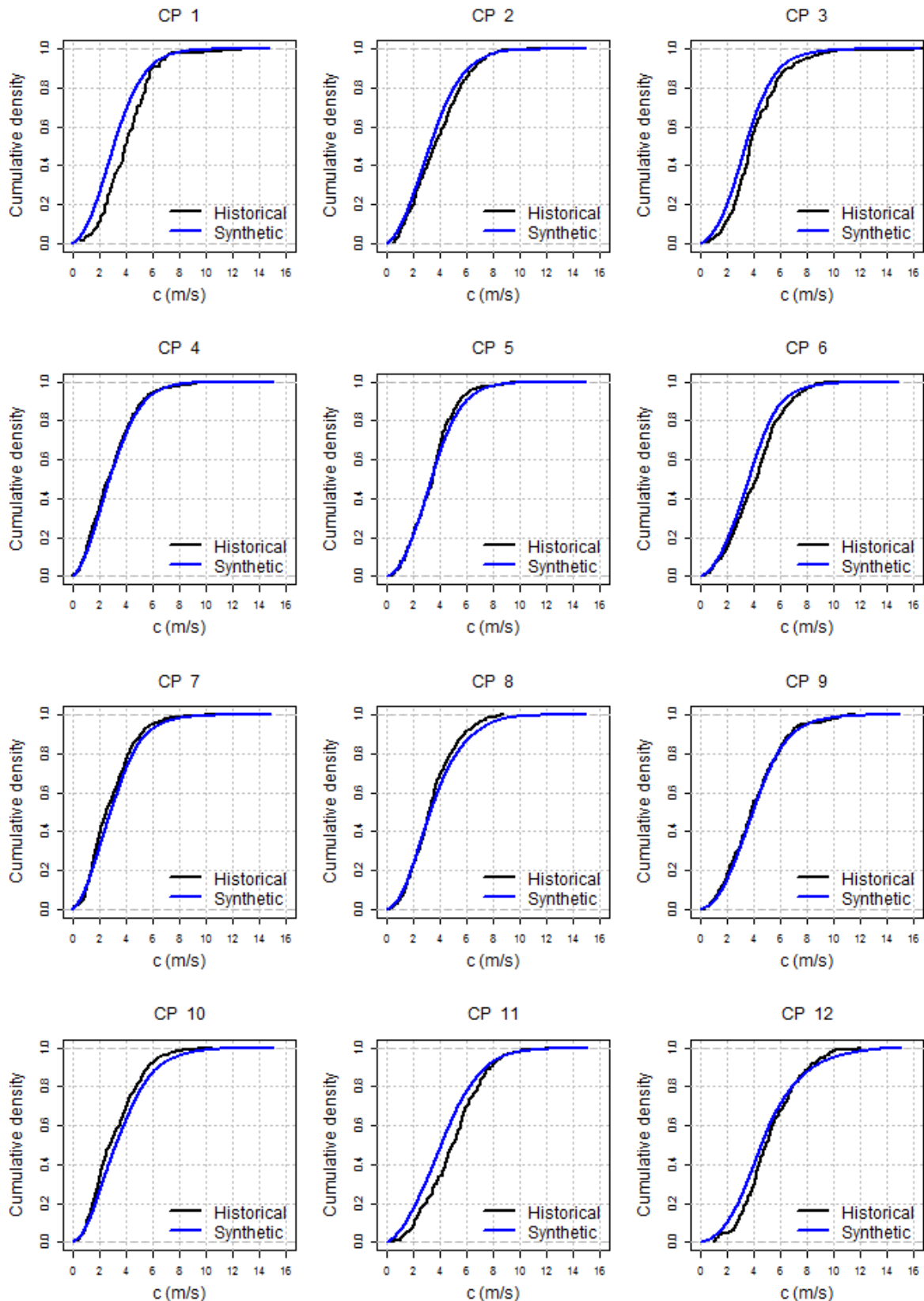
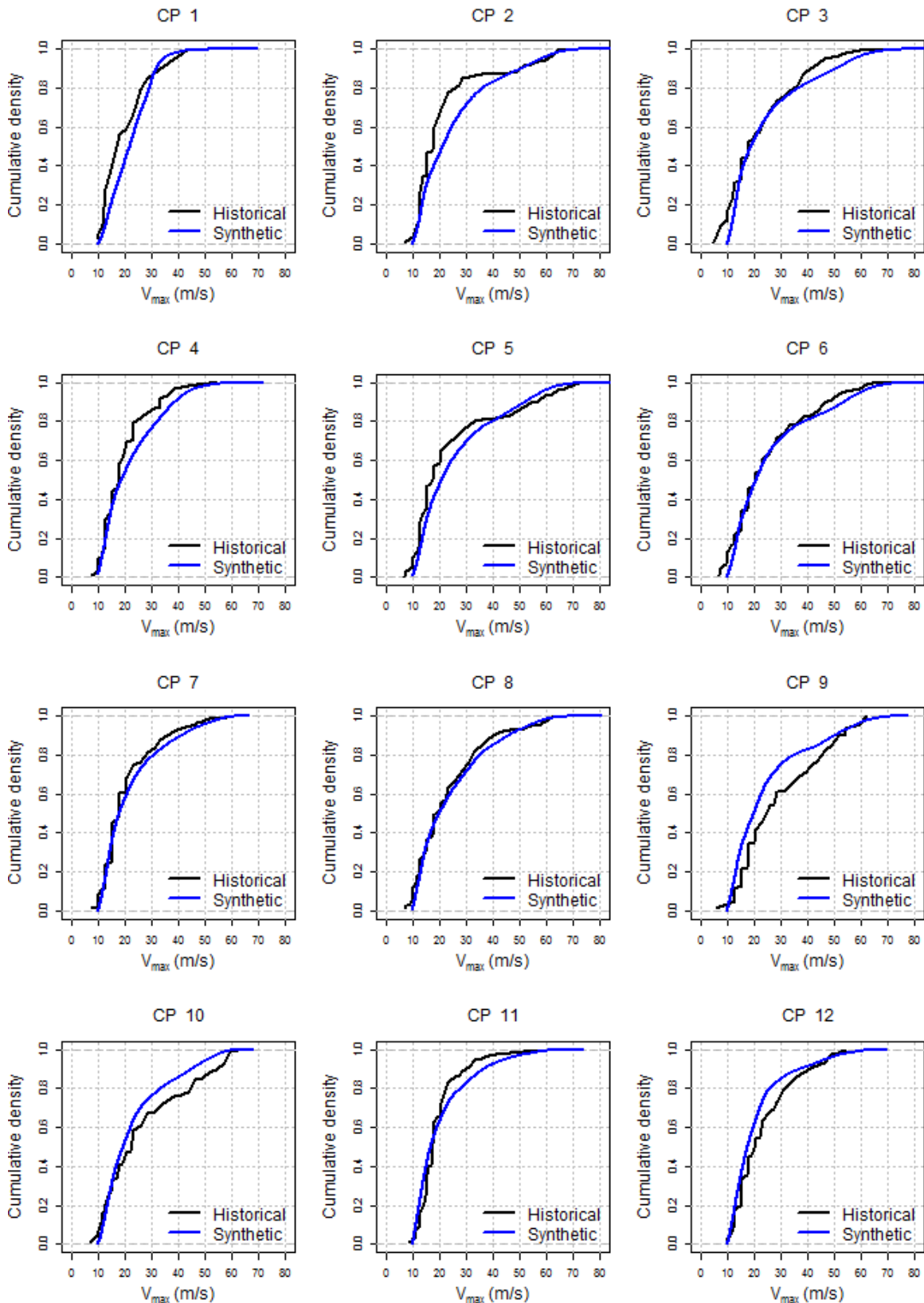


Figure 6-16: Comparison of historical and synthetic distributions of track intensity (V_{max}) occurring within 2 geographical degrees (approximately 200 km) of selected control points. Locations of control points are shown in Figure 6-13.



In general, the modelled distributions of synthetic track parameters compare well with those of the historical data. Although the model performance may appear to be more favourable at some locations when compared to others, an important observation is that the model shows no clear bias in any of the parameters.

Historical distributions of track direction (θ) and track speed (c) are notably smoother than those for intensity (V_{max}). This is partly because distributions of θ and c have been derived from 61 years, as opposed to just 33 years of data, as well as due to the fact that historical records of V_{max} are at a resolution of 5 kt (2.6 m/s), resulting in steps in the calculated distribution rather than a continuous curve. Many of the observed differences in the synthetic and historical distributions of V_{max} are therefore likely to be due to shortcomings in the historical data, rather than shortcomings in the model.

It is important to note that the distributions of storm intensity shown in Figure 6-16 do not represent the distributions of wind speed at the given locations, but rather the distributions of maximum wind speed anywhere within 2 geographic degrees of the given locations. A wind field model (Section 5) is needed to calculate distributions of the actual wind speed which would be experienced at a given location of interest.

Based on the presented results, it is suggested that the synthetic track model can be described as satisfactory in its ability to generate track parameters which are statistically consistent with those in the historical data.

6.5 Limitations to the Model

While the validation of the synthetic track model presented above is considered to be reasonable, it is important to note some limitations to the approach, including the following:

- The track propagation component of the model is based solely on observed changes in track speed and direction in the historical 61 year best track data. It is therefore possible that very unusual tracks, which may be physically possible but not contained in the historical data, may not be produced by the synthetic track model.
- As explained in Section 6.3.3, at least 30 historical observations are required for the generation of robust PDFs, requiring a search radius of at least 2 geographical degrees. The physical influence of land masses may not be well reproduced using this approach, as data points far away from the land mass are required as the basis for the model. It is suggested that the observed discrepancies between modelled and measured track

occurrence over the Mozambique Channel and Madagascar can be largely attributed to this model shortcoming.

- The statistical modelling of intensity evolution experiences the same shortcomings as the track propagation component of the model, however these shortcomings are exacerbated by the smaller duration over which intensity data are available - 33 years as opposed to 61 years.
- The modelling approach has assumed that the underlying statistical properties of tropical cyclone occurrence and intensity have been constant over the duration of the historical data, and will continue to be constant into the future. The potential impact of climate change on tropical cyclone activity over the South-West Indian Ocean has not been considered in this study.

6.6 Summary and Conclusions

It has been shown that the estimation of extreme wind speeds from historical best track data alone can lead to large errors. These errors are due to the small sample sizes of extreme events available in the historical data. A probabilistic approach is therefore required to circumvent the problems imposed by the limited historical best track data. Synthetic track modelling is the current state-of-the-art methodology available to carry out this task.

A synthetic track model, largely following the methods described in Powel et al. (2005) and Emanuel et al. (2006) has been developed. The model is purely statistical and is based on properties derived from the historical best track data. The temporal occurrence of tropical cyclone genesis has been modelled by sampling Poisson distributions defined for each month of the year. The spatial occurrence of tropical cyclone genesis has been modelled through the sampling of a two dimensional probability density estimate derived from historical genesis locations. Track propagation in space has been modelled by sampling conditional probability density functions of change in track direction and speed, defined on a 0.5 degree geographical grid spanning the domain. The evolution of intensity along tracks over the ocean has been modelled in a statistical approach analogous to that described for the track propagation model. The evolution of track intensity over land has been modelled using a land-filling model, whereby intensity reduces as a function of time over land. The statistical model has been adjusted to account for physical limitations, such as those imposed by the equator, and the maximum potential intensity which an event can attain, given the surrounding environmental conditions.

It has been identified that the applicability of any synthetic track model depends on the ability of the model to reproduce the statistical properties of the historical tracks. It has been shown that the synthetic track model developed as part of this study is able to reasonably reproduce both the spatial and temporal occurrence of historical tracks, as well as the distributions of track parameters (i.e. track speed, direction and intensity).

7. EXTREME WIND SPEEDS FOR THE SOUTH-WEST INDIAN OCEAN

7.1 Introduction

The objective of this thesis is to produce maps of tropical cyclone induced wind speeds at various return periods of interest for the entire South-West Indian Ocean (Section 1.2). This objective has been achieved through the development of a tropical cyclone risk model comprised of two main components; namely a parametric wind field model (described in Section 5) and a synthetic track model (described in Section 6).

This section describes the methodology as to how the wind field and the synthetic track models have been used to calculate extreme wind speeds due to tropical cyclones. Extreme wind speed maps for the South-West Indian Ocean at 50, 100, 200 and 500 year return periods are presented, and some guidance as to how these results might be used to infer conditions for input to engineering design is discussed.

7.2 Methodology

The output of the synthetic track model (Section 6) is 5 000 years of best track data for the South-West Indian Ocean. These data contain parameters of track location (ψ , φ), speed (c), direction (θ) and intensity (V_{max}) along each track at six hourly time-steps. Given these parameters at each time-step, the Willoughby et al. (2006) parametric wind field model, selected as the preferred model for use in this study (Section 5), is capable of providing estimates of wind speed at any arbitrary location of interest. The methodology described below has been applied through the application of a program written in the C# programming language.

For the purposes of calculating extreme wind speed estimates, the domain of the South-West Indian Ocean has been subdivided onto a 1 degree geographical grid. The Willoughby et al. (2006) parametric wind field model has been applied along synthetic tracks passing within 2 geographical degrees of each grid point, saving the peak modelled wind speed at each grid point due to each track. This process effectively produces a 5 000 year extreme value series of tropical cyclone wind speeds at each grid point in the domain.

Given the 5000 year duration of the synthetic data, wind speeds with return periods in the order of 100 years are by definition contained within the extreme value series. There is therefore no need to fit a theoretical extreme value distribution to the data for the estimation of wind speeds at return periods of interest for engineering design. Assuming a Poisson

distribution for tropical cyclone occurrence, extreme wind speed can be related to return period through the following expression (Vickery et al., 2000b):

$$\frac{1}{RP} = 1 - \exp(-\lambda \Pr(V > V_{RP}))$$

Equation 7-1

where:

RP = return period (years).

λ = mean recurrence rate per year of tropical cyclones passing within 2 geographical degrees of the location of interest.

V_{RP} = wind speed with an average recurrence interval of RP years.

$\Pr(V > V_{RP})$ = probability that V_{RP} is exceeded for any given event passing within 2 geographical degrees of the location of interest.

For a given return period of RP years, the exceedance probability $\Pr(V > V_{RP})$ is solved for through Equation 7-1. The wind speed associated with this exceedance probability (V_{RP}) is then obtained by interpolating from the rank ordered extreme value series. By way of an example, if $\Pr(V > V_{RP})$ is determined to be 0.05 (i.e. an exceedance probability of 5%), then V_{RP} is the 95th percentile wind speed contained in the extreme value series.

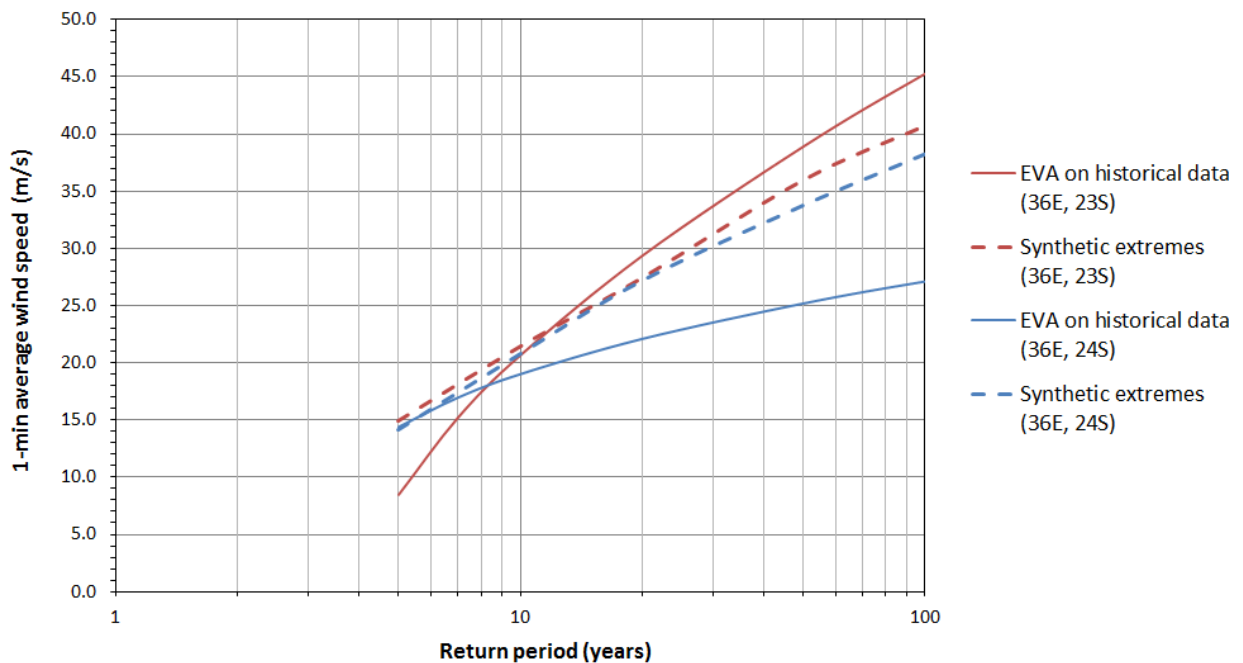
Repeating this processes for each grid point over the domain of the South-West Indian Ocean allows for the generation of extreme wind speed maps for the region at any return period of interest.

7.3 Results

7.3.1 Comparison with EVAs on Historical Data

Before results for the entire South-West Indian Ocean are presented, it is prudent to assess whether the results are in line with what might be expected from the model. Figure 7-1 compares the results of the tropical cyclone risk model developed as part of this study with extreme wind speeds derived from the historical data alone. The two considered locations are those which were used to motivate for the use of a synthetic track model (Section 6.2).

Figure 7-1: Comparison of extreme wind speeds calculated from historical data and synthetic data at two hypothetical locations on the Mozambique coastline.



Of the two hypothetical locations, the northerly location (36° E, 23° S) was relatively 'unlucky' over the 33 year duration for which historical data are available, being affected by two particularly strong events. The southerly location (36° E, 24° S), while having a similar physical risk exposure to tropical cyclones (owing to its close proximity), experienced no such events. One would therefore intuitively expect the true physical risk exposure at these two locations to be somewhere in-between what was predicted by the EVAs at these locations. Figure 7-1 indicates that the extreme wind speeds generated by the tropical cyclone risk model show exactly this expected result, providing some confidence that the output of the model is indeed realistic.

7.3.2 Extreme Wind Speed Maps

Figure 7-2 to Figure 7-5 present best estimate extreme wind speed maps for the South-West Indian Ocean at return periods of 50, 100, 200 and 500 years respectively.

Figure 7-2: 50 year return period 1-min average wind speeds due to tropical cyclones for the South-West Indian Ocean.

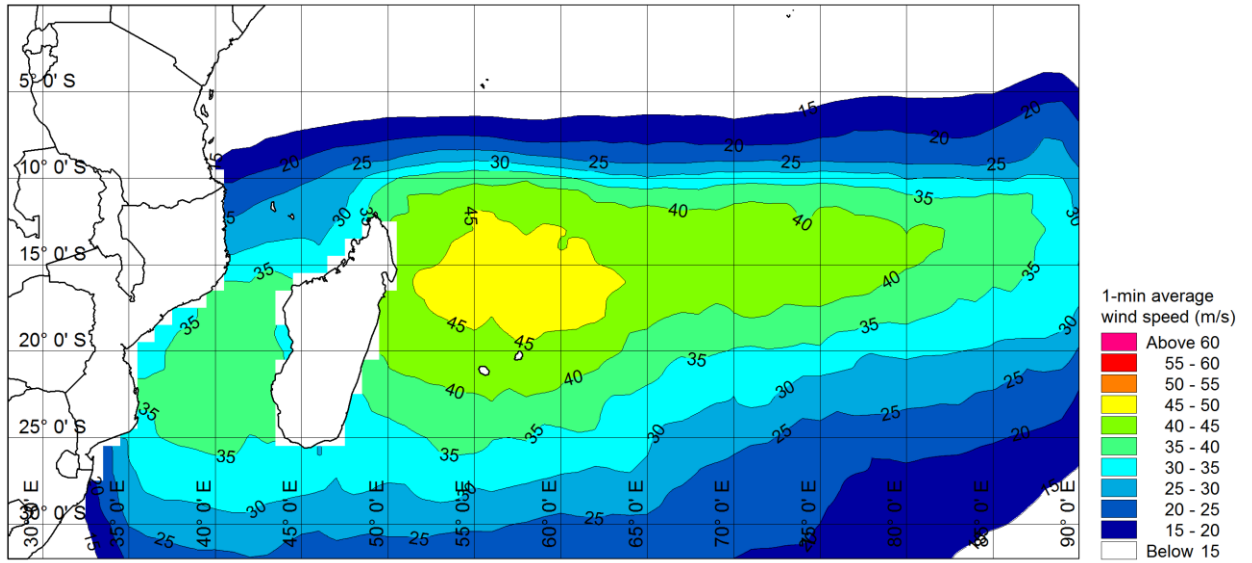


Figure 7-3: 100 year return period 1-min average wind speeds due to tropical cyclones for the South-West Indian Ocean.

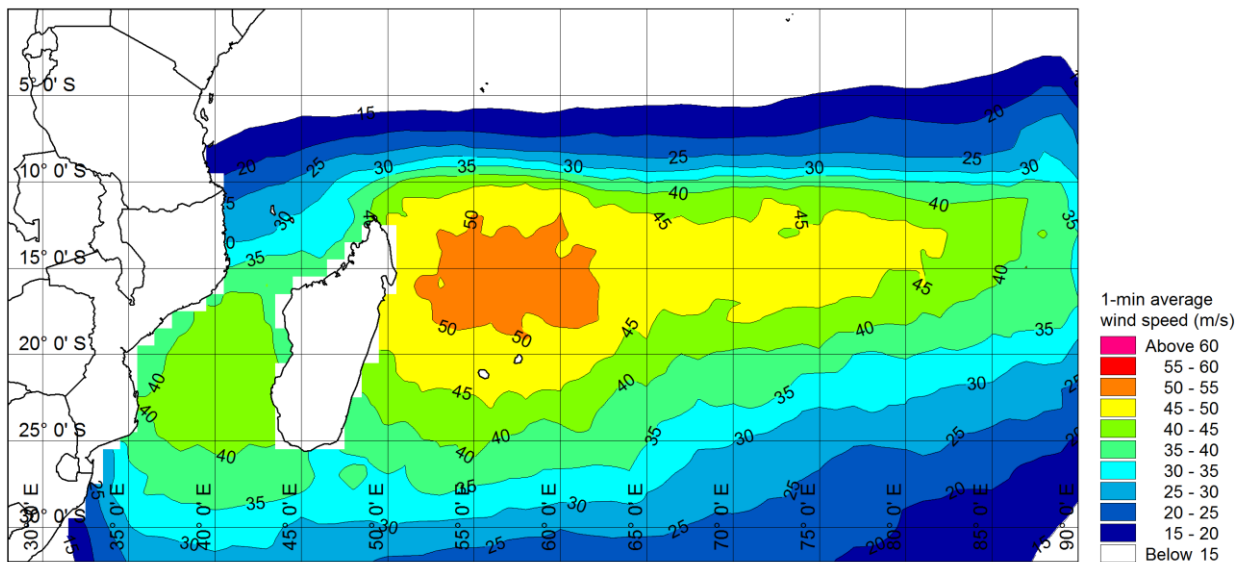


Figure 7-4: 200 year return period 1-min average wind speeds due to tropical cyclones for the South-West Indian Ocean.

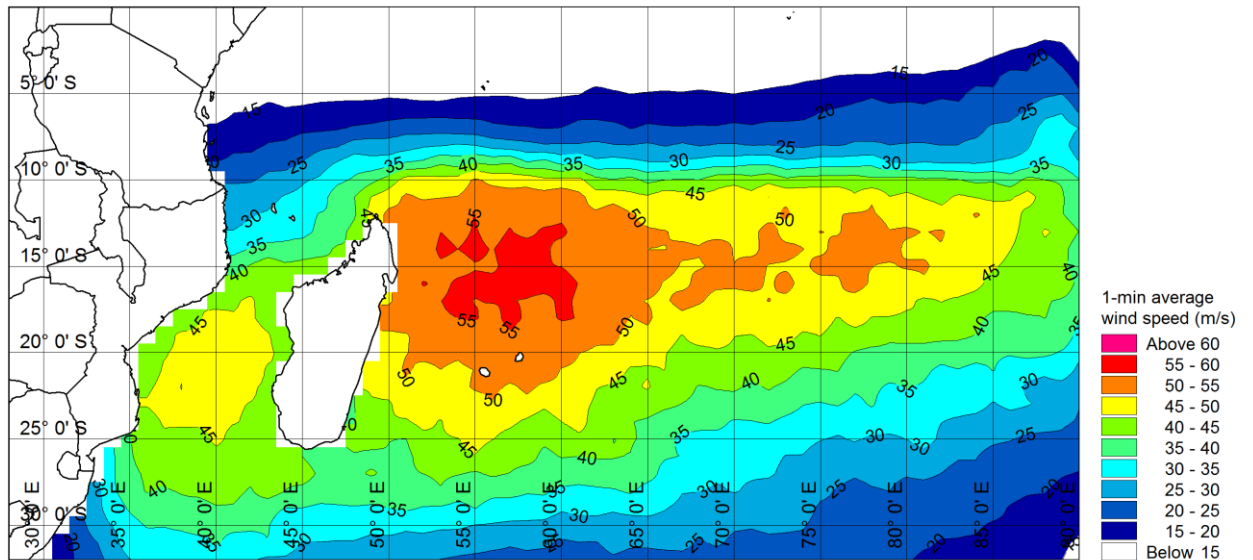
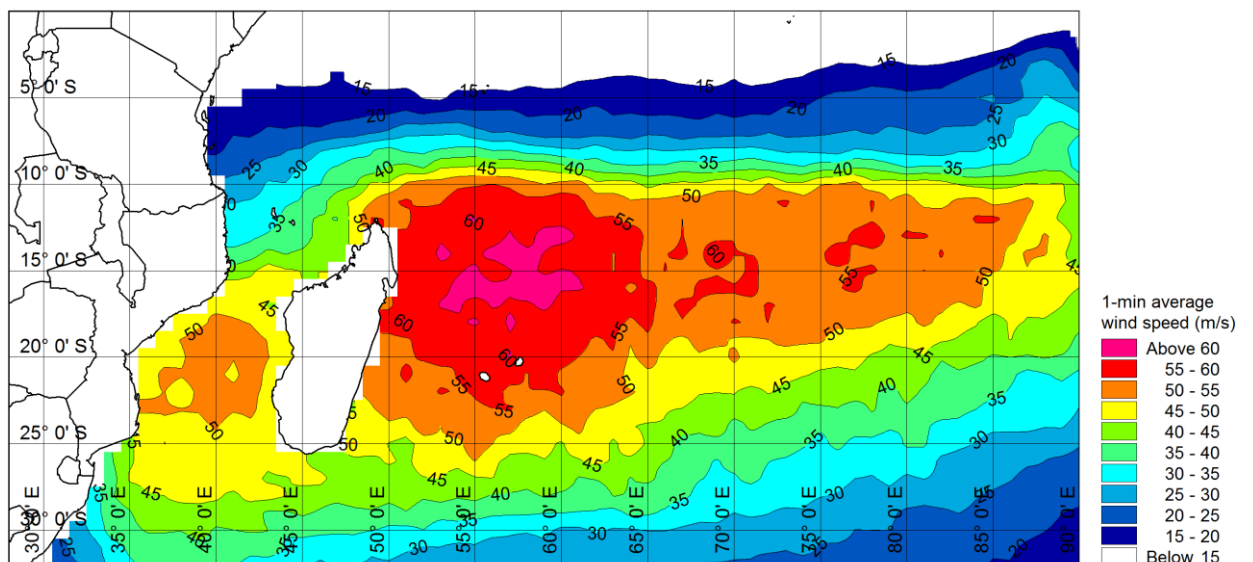


Figure 7-5: 500 year return period 1-min average wind speeds due to tropical cyclones for the South-West Indian Ocean.



The parametric wind field model adopted for this study makes use of a simple correction factor to convert from flight level to surface wind speeds, which is applicable for open ocean conditions only. Wind speeds over land would be affected by the increased roughness of the terrain and funnelling/blocking effects due to large features, which have not been explicitly

considered in this study. The presented wind speed maps are therefore limited to open ocean conditions.

7.4 Application to Coastal Engineering

7.4.1 Design Wind Speeds for the Southern African Coastline

Figure 7-6 presents estimated 1-min average wind speeds as a function of latitude along the southern African coastline for various return periods. The results have been extracted from those presented in Figure 7-2 to Figure 7-5 above, using the most westerly grid cell for which estimates have been made. The presented results are therefore representative of the coastline of mainland south-east Africa, excluding Madagascar and other islands.

Figure 7-6: 50, 100, 200 and 500 year return period 1-min average wind speeds due to tropical cyclones as a function of latitude along the south-east African coastline.

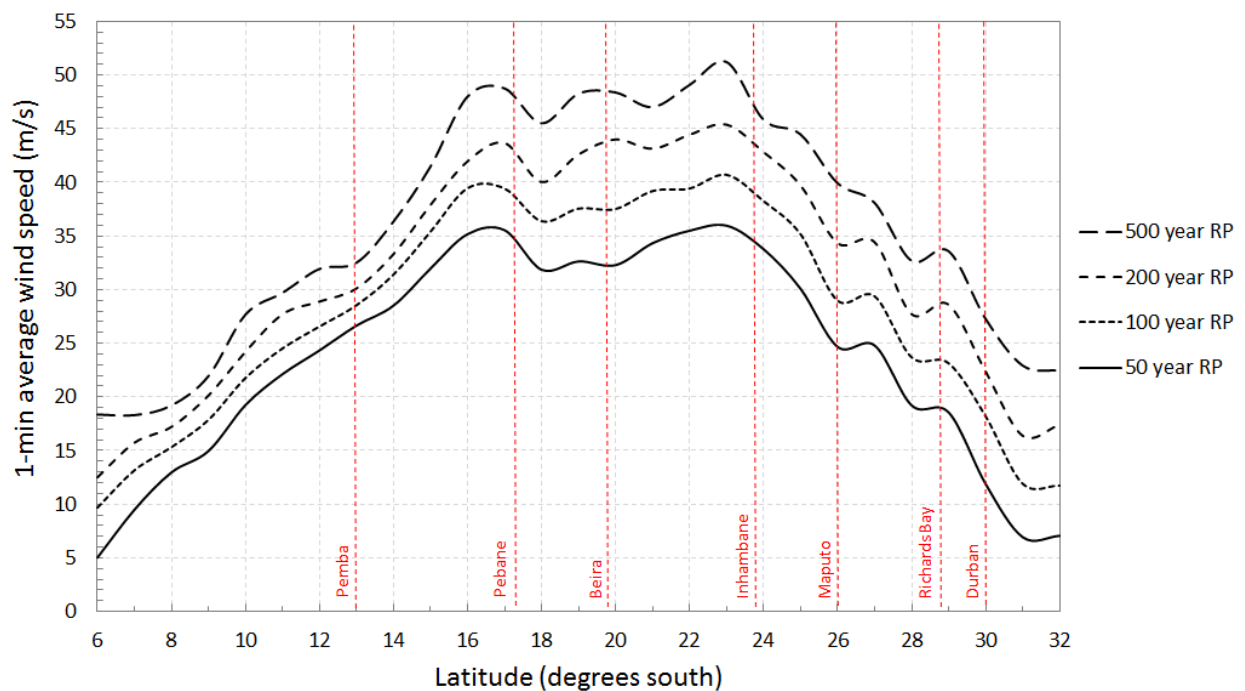


Figure 7-6 indicates that for the south-eastern African coastline, extreme wind speeds increase approximately linearly with increasing southerly latitudes until about 16° S. Between 16° S and 24° S the results indicate relatively similar risk exposure to tropical cyclones, implying that there is little scope for optimising site selection along this stretch of coastline to minimise the impacts due to tropical cyclones. South of 24° S risk exposure to tropical cyclones reduces rapidly with increasing southerly latitudes.

At Richards Bay, South Africa's most northerly port, the estimated 1-min average 100 year return period wind speed is about 24 m/s, which would be classified as an average intensity tropical storm according to the Saffir-Simpson scale (Table 2-1). The 100 year return period tropical cyclone induced wind speed reduces to about 18 m/s at the latitude of Durban, corresponding to the lower end of tropical storm category wind speeds. It is suggested that the risk of damaging impacts due to tropical cyclone winds can be considered negligible south of Durban, as these would be overshadowed by the effects of systems such as frontal systems and cut-off lows.

7.4.2 Ocean Response Modelling

In addition to extreme wind speeds, the engineering design of coastal structures in regions prone to tropical cyclones requires the estimation of extreme waves, water levels and currents due to these events. This is typically carried out through the application of an ocean response model (coupled hydrodynamic and spectral wave model), using space and time-varying tropical cyclone wind and pressure fields as input to the model. The coupling of hydrodynamics with wave generation can be particularly important as increased storm surge (due to low atmospheric pressure near the eye, and wind setup due to onshore winds) leads to reduced depth-induced wave breaking and therefore higher wave heights at the structure of interest. Higher wave heights in turn lead to increased water levels in the form of wave setup.

The approaches used to define extreme ocean response parameters can be broadly classified as deterministic and probabilistic. Each approach is briefly described below.

7.4.2.1 Deterministic Approach

The results of this thesis provide a good basis for the selection of "design storm" parameters, which are the required input to an ocean response model. In this approach, the extreme wind speed estimates (V_{max}), as defined above, are used to estimate the other storm parameters. While deterministic relationships are available for the estimation of the associated minimum central pressure (P_c) and radius to maximum wind speed (R_{max}), the parameters of track speed (c) and direction (θ) are however less well correlated with storm intensity. As it is not possible to define a unique design storm from extreme wind speed estimates alone, a small set of candidate design storms are rather defined, so that the sensitivity of the model results to these candidate storms can be ascertained. These storms are often referred to as "screening storms" (Resio et al., 2007). For example, the 100 year return period 1-min average wind

speed at Maputo Bay is estimated to be 29 m/s (Figure 7-6). Typical associated design storm parameters for this extreme wind speed are provided in Table 7-1.

Table 7-1: Example of 100 year return period design storm parameters off the coastline of Maputo Bay.

Parameter	Value	Basis
Maximum sustained 1-min average wind speed (V_{max})	29 m/s	Figure 7-6
Minimum central pressure (P_c)	982 hPa	Figure 4-2
Radius to maximum wind speed (R_{max})	42 km	Equation 2-2
Track speed (c)	Test sensitivity	-
Track angle (θ)	Test sensitivity	-

Ocean response models require the mean wind speed as the model input, rather than the 1-min average wind speeds estimates provided above. It is therefore important to correct the extreme wind speeds presented in this thesis before being used directly for the estimation of extreme ocean response parameters. The correction of wind speeds for various averaging periods is discussed in Section 2.4.6.

It must be borne in mind that the modelling of design storms for the inference of extreme ocean response parameters is hampered by limitations. Notably, modelled wave heights at a given site would be particularly sensitive to the time history of storm intensity prior to landfall. Assigning a constant design wind speed estimate over the duration of the storm may lead to unrealistic wave heights at the site of interest, as in reality storms build up and decay over time. Furthermore, certain sites may be particularly sensitive to the choice of design storm parameters. For example, a protective headland would lead to large sensitivity in track angle. Choosing the worst case design storm parameters may therefore be an overly conservative approach.

7.4.2.2 Probabilistic Approach

The pitfalls of the deterministic approach to ocean response modelling described above can be circumvented through a probabilistic approach, analogous to that used to calculate extreme wind speeds in this study. In this approach, a coupled hydrodynamic and spectral wave model is applied along each synthetic track passing within a defined threshold distance of a given site of interest. Saving the modelled waves, water levels and currents at the site due to each synthetic track, it is possible to generate thousands of years of synthetic ocean response parameters from which extreme values can be derived. An example of the

application of this methodology - to the Australian east coast - is provided by Harper et al. (2004). This approach is however limited by the significant computational requirements of modelling ocean response due to thousands of years of synthetic tracks.

7.5 Uncertainty

There is naturally some uncertainty associated with the extreme wind speed results presented above. Reasons for the uncertainty can be attributed to the following:

- Uncertainty in the best track data forming the basis of the tropical cyclone risk model, discussed in Section 2.3.3.
- Uncertainty in the parametric wind field model, discussed in Section 5.3.4.
- Uncertainty in the synthetic track model, discussed in Section 6.5.

No attempt has been made to quantify the cumulative effect of these uncertainties on the ultimate uncertainty in the results of this study. Attention is however drawn to the sources of uncertainty, highlighting that while the presented results have been generated through the sound application of best practise techniques in the field of tropical cyclone risk modelling, there will always be errors in the estimates due to data inaccuracies and model approximations. Engineering judgement should therefore be used in the application of the results.

7.6 Summary and Conclusions

Extreme wind speeds for the South-West Indian Ocean have been calculated by coupling the Willoughby et al. (2006) parametric wind field model to 5 000 years of tropical cyclone tracks produced by a synthetic track model developed as part of this study. This allows for the generation of a 5 000 year extreme value series at any location of interest. Extreme wind speeds at return periods of interest are by definition contained within the extreme value series, therefore no theoretical extreme value distribution is required to be fitted to the data. Wind speeds corresponding to return periods of interest have been calculated following the method described in Vickery et al. (2000b).

By carrying out calculations on a 1 degree geographical grid, extreme wind speed maps have been produced for the entire South-West Indian Ocean at return periods of 50, 100, 200 and 500 years. The results have also been presented in terms of the variation of extreme wind speeds as a function of latitude along the southern African coastline. The presented results

are intended to provide much needed guidance for the engineering design of coastal infrastructure in the region.

8. CONCLUSIONS AND RECOMMENDATIONS

8.1 Conclusions

The quantification of the risk exposure to the impacts of tropical cyclones is vitally important for planning and design of infrastructure in regions prone to these events. Although there has been substantial research carried out in the field of tropical cyclone risk modelling, there has been relatively little research into the quantification of risk exposure over the South-West Indian Ocean. The objective of this thesis is to generate extreme wind speed maps for this region at various return periods of interest. This objective has been achieved through the development of a tropical cyclone risk model, using state-of-the-art techniques.

Best track data for the South-West Indian Ocean, as archived by the Joint Typhoon Warning Centre (JTWC), has been used as the primary dataset for this study. These data provide best estimates of the location (ψ , φ) and intensity (V_{max} and/or ΔP) of historical tropical cyclones, at six hourly intervals. The data from the year 1952 onwards have been considered to provide a reliable account of the geographical distribution and occurrence rates of tropical cyclones. Intensity data are however limited to records from the year 1980. The data indicates an occurrence rate of 14.0 events per year on average, although only about half of these exceed Tropical Storm status according to the Saffir-Simpson Scale.

Parametric wind field modelling has been undertaken to generate representative tropical cyclone wind fields, using the limited data available in the best track data archives as model input. Both the Holland (1980) and Willoughby et al. (2006) parametric wind field models have been considered for this purpose. The empirical relationship proposed by Willoughby & Rahn (2004) has been adopted for the estimation of R_{max} , an important input parameter for the wind field models. The ability of the wind field models to reproduce actual wind fields has been assessed through the comparison of modelled and measured wind speeds at a number of measurement stations throughout the South-West Indian Ocean. Although both considered models were shown to produce peak wind speeds which are in reasonable agreement when compared to measurements, the Willoughby et al. (2006) model was found to yield a better fit to the measurements and was consequently adopted as the preferred model for this study.

Through an extreme value analysis of modelled historical wind speeds at two nearby locations it has been shown that the small sample sizes of historical data can lead to potentially large errors in estimated extreme wind speeds. This finding highlights the need for a probabilistic approach to the estimation of extreme tropical cyclone induced wind speeds. A synthetic track

model has been developed, capable of generating thousands of years of tropical cyclone tracks over the South-West Indian Ocean. The model is a Markov chain model, largely following methods described in Powel et al. (2005) and Emanuel et al. (2006). The synthetic track model is purely statistical with its properties derived from the historical best track data. Adjustments have however been made to account for physical limitations such as those imposed by the equator and the maximum potential intensity which an event can attain. It has been shown that the synthetic track model developed as part of this study is able to reasonably reproduce both the spatial and temporal occurrence of historical tracks, as well as the distributions of track parameters (i.e. track speed, direction and intensity).

Coupling the Willoughby et al. (2006) parametric wind field model with the synthetic track model developed as part of this study has allowed for the generation of 5 000 years of tropical cyclone induced wind speeds at any location of interest. By carrying out calculations on a 1 degree geographical grid, extreme wind speed maps have been produced for the entire South-West Indian Ocean at return periods of 50, 100, 200 and 500 years, thus satisfying the objective of the thesis.

8.2 Recommendations

Due to the long period of time over which best track data are archived, these data can be hampered by inconsistencies in analysis techniques over time, leading to non-physical trends in the data. For this reason, Météo France La Réunion is currently undertaking a reanalysis of its best track data archives to provide a homogenous dataset for the region, free of these inconsistencies. It is recommended that the results of this study be revised using the reanalysed best track dataset once it becomes available.

The comparison of wind speeds produced by parametric wind field models with land based wind speed measurements showed that the models show a tendency to under-predict low wind speeds while similarly showing a tendency to over-predict high wind speeds. It is recommended that this observation be further investigated to assess whether wind field models based on observations largely over the North Atlantic Ocean are indeed applicable to tropical cyclones occurring over the South-West Indian Ocean. This would best be done through analyses of aircraft reconnaissance data over the South-West Indian Ocean.

In addition to extreme wind speeds, the design of coastal infrastructure requires the quantification of the risk exposure to ocean response in the form of extreme waves, storm surge and currents. It is recommended that the present research be extended to include ocean

response modelling using a coupled spectral wave and hydrodynamic model. Such research would include an assessment of the ability of parametric wind field models to reproduce measurements of waves, storm surge and currents in the region of the South-West Indian Ocean. Coupling the ocean response model to the synthetic track model would allow for the calculation of waves, water levels and currents due to each synthetic track at any location of interest. Design parameters can then be calculated in an analogous way as carried out for the calculation of extreme wind speeds in this study. An example of the application of this methodology - to the Australian east coast - is provided by Harper et al. (2004). A similar application to the southern African east coast would be of value.

Although the effects of climate change on tropical cyclone activity in the South-West Indian Ocean has not been explicitly considered in this study, synthetic track models provide powerful tools for the quantification of these impacts (Hallegate, 2007). In this approach, synthetic track models can be adjusted according to the predicted impacts of climate change by editing relevant components of the model such as track genesis or maximum potential intensity. In so doing, various climate change scenarios can be directly translated into changes in the risk exposure to tropical cyclones in the form of extreme wind speeds, waves, storm surge and currents.

9. REFERENCES

- Atkinson, G., & Holliday, C. (1977). Tropical Cyclone Minimum Sea Level Pressure/Maximum Sustained Wind Relationship for the Western North Pacific. *Monthly Weather Review*, *105*, 421 - 427.
- Bister, M., & Emanuel, K. (n.d.). *Climatological Hurricane Potential Intensity Maps*. Retrieved October 20, 2013, from <http://wind.mit.edu/~emanuel/pcmin/climo.html>
- Chang-Seng, D., & Jury, M. (2010). Tropical Cyclones in the SW Indian Ocean. Part 1: Inter-Annual Variability and Statistical Prediction. *Meteorol Atmos Phys*, *106*, 149 - 162.
- Chu, P., & Wang, J. (1998). Modeling Return Periods of Tropical Cyclone Intensities in the Vicinity of Hawaii. *American Meteorological Society*, *37*, 951 - 960.
- Darling, R. (1991). Estimating Hurricane Wind Speed Probability using a Large-Scale Empirical Model. *American Meteorological Society*, *4*, 1035 - 1046.
- Depperman, C. (1947). Notes on the Origin and Structure of Philippine Typhoons. *Bulletin of the American Meteorological Society*, *28*, 399 - 404.
- DHI. (2012a). *DFS File User Guide*. Copenhagen, Denmark: Danish Hydraulics Institute.
- DHI. (2012b). *EVA, Extreme Value Analysis, User Guide*. Copenhagen, Denmark: Danish Hydraulics Institute.
- DHI. (2012c). *EVA, Extreme Value Analysis, Technical Reference and Documentation*. Copenhagen, Denmark: Danish Hydraulics Institute.
- Dima, I., & Desflots, M. (2010, July). *Wind Profiles in Parametric Hurricane Models*. Retrieved October 19, 2013, from <http://www.air-worldwide.com/Publications/AIR-Currents/2010/Wind-Profiles-in-Parametric-Hurricane-Models/>
- Dvorak, V. (1984). *Tropical Cyclone Intensity Analysis using Satellite Data*. Springfield: NOAA Technical Report NESDIS 11, NTIS.
- Emanuel, K. (1988). The Maximum Potential Intensity of Hurricanes. *Journal of Atmospheric Science*, *45*, 143 - 1155.
- Emanuel, K. (1995). Sensitivity of Tropical Cyclones to Surface Exchange Coefficients and a Revised Steady-State Model Incorporating Eye Dynamics. *Journal of Atmospheric Science*, *52*, 3969 - 3976.
- Emanuel, K., Vivant, S., & Risi, C. (2006). A Statistical Deterministic Approach to Hurricane Risk Assessment. *American Meteorological Society*, *87*, 299 - 314.
- Franklin, J., Black, M., & Valde, K. (2003). GPS Dropwindsonde Wind Profile in Hurricanes and their Operational Implications. *Weather Forecasting*, *18*, 32 - 44.

- Graf, M., & Nishijima, K. (2009). A Probabilistic Typhoon Model for the Northwest Pacific Region. Taipei, Taiwan: Paper Presented at the Seventh Asia-Pacific Conference on Wind Engineering.
- Gray. (1998). The Formation of Tropical Cyclones. *Meteorology and Atmospheric Physics*, 67, 37 - 69.
- Gray, W., Landsea, C., Mielke, P., & Berry, K. (1994). Predicting Atlantic Seasonal Tropical Cyclone Activity. *Weather and Forecasting*, 9, 103 - 115.
- Hall, T., & Jewson, S. (2007). Statistical Modeling of North Atlantic Tropical Cyclone Tracks. *Tellus*, 59A, 486 - 498.
- Hall, T., & Jewson, S. (2008). Comparison of Local and Basin-Wide Methods for Risk Assessment of Tropical Cyclone Landfall. *Journal of Applied Meteorology and Climatology*, 47, 361 - 367.
- Hallegate. (2007). The Use of Synthetic Hurricane Tracks in Risk Analysis and Climate Change Damage Assessment. *Journal of Applied Meteorology and Climatology*, 46, 1956 - 1966.
- Harper, B., Hardy, T., Mason, L., & Astorquia, A. (2004). Queensland Climate Change and Community Vulnerability to Tropical Cyclones, Ocean Hazards Assessment. Stage 2. Tropical Cyclone Induced Water Levels and Waves: Hervey Bay and Sunshine Coast. Queensland Government.
- Harper, B., Hardy, T., Mason, L., Bode, L., Young, I., & Nielsen, P. (2001). *Queensland Climate Change and Community Vulnerability to Tropical Cyclones, Ocean Hazards Assessment - Stage 1*. Brisbane, Queensland, Australia: Department of Natural Resources and Mines.
- Harper, B., Kepert, J., & Ginger, J. (2008). *Guidelines for Converting Between Various Wind Averaging Periods in Tropical Cyclone Conditions*. World Meteorological Organisation.
- Ho, C., Kim, J., Jeong, J., Kim, H., & Chen, D. (2006). Variation of Tropical Cyclone Activity in the South Indian Ocean: El Nino-Southern Oscillation and Madden-Julian Oscillation Effects. *Journal of Geophysical Research*.
- Holland, G. (1980). An Analytical Model of the Wind and Pressure Profiles in Hurricanes. *Monthly Weather Review*, 108, 1212 - 1218.
- Holland, G. (2008). A Revised Hurricane Pressure-Wind Model. *Monthly Weather Review*, 136, 3432 - 3445.
- Holland, G., & Emanuel, K. (2011, November 22). *Limits on Hurricane Intensity*. Retrieved October 20, 2013, from <http://wind.mit.edu/~emanuel/holem/holem.html>
- Holland, G., Bellanger, J., & Fritz, A. (2010). A Revised Model for Radial Profiles of Hurricane Winds. *American Meteorological Society*, 138, 4393 - 4401.
- Hughes, L. (1952). On the Low Level Wind Structure of Tropical Cyclones. *Journal of Meteorology*, 9, 422 - 428.
- IBTrACS. (2014). *International Best Track Archive for Climate Stewardship*. Retrieved March 10, 2014, from <http://www.ncdc.noaa.gov/oa/ibtracs/index.php?name=ibtracs-data-access>

- INGC. (2009). *Sea Level Rise and Cyclone Analysis, INGC Climate Change Report*. Mozambique: National Institute for Disaster Management.
- James, M., & Mason, L. (2005). Synthetic Tropical Cyclone Database. *Journal of Waterway, Port, Coastal, and Ocean Engineering*, 131, 181 - 192.
- Knaff, & Harper. (2010). *Tropical Cyclone Surface Wind Structure and Wind-Pressure Relationships*. Seventh International Workshop on Tropical Cyclones.
- Knaff, Brown, Courtney, Gallina, & Il, B. (2010). An Evaluation of Dvorak Technique–Based Tropical Cyclone Intensity Estimates. *Weather and Forecasting*, 25, 1362-1379.
- Knaff, J., & Zehr, R. (2007). Reexamination of Tropical Cyclone Wind-Pressure Relationships. *Weather and Forecasting*, 22, 71 - 88.
- Knaff, J., De Maria, M., Molenaar, A., Sampson, C., & Seybold, M. (2011). An Automated, Objective, Multiple-Satellite-Platform Tropical Cyclone Surface Wind Analysis. *Journal of Applied Meteorology and Climatology*, 50(10), 2149 - 2166.
- Knaff, J., DeMaria, M., Marchok, T., Gross, J., & McAdie, C. (2007). Statistical Tropical Cyclone Wind Radii Prediction Using Climatology and Persistence. *American Meteorological Society*, 22, 781-791.
- Knapp, K., Kruk, M., Levinson, D., Diamond, H., & Neumann, C. (2010). The International Best Track Archive for Climate Stewardship (IBTrACS): Unifying Tropical Cyclone Data. *American Meteorological Society*, March 2010, 364 - 376.
- Lange, K. (2003). *Applied Probability*. New York: Springer-Verlag.
- Lee, K., & Rosowsky, D. (2007). Synthetic Hurricane Wind Speed Records: Development of a Database for Hazard Analyses and Risk Studies. *Natural Hazards Review*, 8(2), 23 - 34.
- Levinson, D., Diamond, H., Knapp, K., Kruk, M., & Gibney, E. (2010). Toward a Homogenous Global Tropical Cyclone Best-Track Dataset. *Bulletin of the American Meteorological Society*, 91, 377 - 380.
- Mattocks, C., & Forbes, C. (2008). A Real-Time, Event-Triggered Storm Surge Forecasting System for the State of North Carolina. *Ocean Modelling*, 25, 95 - 119.
- Mavume, A., Rydberg, L., Rouault, M., & Lutjeharms, R. (2009). Climatology and Landfall of Tropical Cyclones in the South-West Indian Ocean. *Western Indian Ocean Journal of Marine Science*, 8(1), 15 - 36.
- MFR. (2013). *Meteo France, Toujours un Temps D'avance*. Retrieved November 22, 2013, from http://www.meteo.fr/temps/domtom/La_Reunion/meteoreunion2/
- Neumann, C. (1999). *The HURISK Model: An Adaption for the South Hemisphere (A User's Manual)*. Science Applications International Corporation.

- Neumann, C., McAdie, C., Jarvinen, B., & Hammer, G. (1999). *Tropical Cyclones of the North Atlantic Ocean, 1871 - 1998*. Asheville, NC: National Oceanic and Atmospheric Administration (NOAA).
- NOAA. (2014). *Frequently Asked Questions*. Retrieved from Hurricane Research Division, National Oceanic & Atmospheric Administration: <http://www.aoml.noaa.gov/hrd/tcfaq/F1.html>
- NOAA-NWS. (1979). *Meteorological Criteria for Standard Project Hurricane and Probable Maximum Hurricane Windfields, Gulf and East Coasts of the United States*. NOAA Technical Report NWS 23.
- NWS. (2012, June 8). *National Weather Service Instruction 10-604: Tropical Cyclone Definitions*. Retrieved November 13, 2012, from <http://www.nws.noaa.gov/directives/>
- Penn State. (2014). *Tromelin Island*. Retrieved 6 4, 2014, from College of Earth and Mineral Sciences: <http://www.ems.psu.edu/~williams/states/te.htm>
- Powell, M., & Black, G. (1990). The Relationship of Hurricane Reconnaissance Flight-Level Wind Measurements to Winds Measured by NOAA's Oceanic Platforms. *Journal of Wind Engineering and Industrial Aerodynamics*, 36, 381 - 392.
- Powell, M., Soukup, G., Cocke, S., Gulati, S., Morisseau-Leroy, N., Hamid, S., . . . Axe, L. (2005). State of Florida Hurricane Loss Projection Model: Atmospheric Science Component. *Journal of Wind Engineering and Industrial Aerodynamics*, 93, 651 - 674.
- Powell, M., Vickery, P., & Reinhold, T. (2003). Reduced Drag Coefficient for High Wind Speeds in Tropical Cyclones. *Nature*, 422, 279 - 283.
- R Core Team. (2013). *R: A Language and Environment for Statistical Computing*. Vienna, Austria: R Foundation for Statistical Computing. ISBN 3-900051-07-0, URL <http://www.R-project.org/>.
- Resio, D., Boc, S., Borgman, V., Cardone, A., Cox, W., Dally, R., . . . Vickery, P. (2007). *White Paper on Estimating Hurricane Inundation Probabilities*. U.S. Army Corps of Engineers, ERDC-CHL.
- Rhome, J., & Raman, S. (2006). Environmental Influences on Tropical Cyclone Structure and Intensity: A Review of Past and Present Literature. *Indian Journal of Marine Sciences*, 35(2), 61 - 74.
- Rossouw, C. (1999). *The Probability of Occurrence and the Intensity of Tropical Cyclones along the Southern African East Coast*. Stellenbosch, South Africa: Department of Civil Engineering. University of Stellenbosch.
- Rumpf, J., Weindl, H., Hoppe, P., Rauch, E., & Schmidt, V. (2007). Stochastic Modelling of Tropical Cyclone Tracks. *Mathematical Methods of Operations Research*, 66, 474 - 490.
- Russel, 1. (1971). Probability Distributions for Hurricane Effects. *Journal of Waterways Harbors Coastal Eng. Div. ASCE*, 97(1), 139 - 154.

- Schloemer, R. (1954). *Analysis and Synthesis of Hurricane Wind Patterns over Lake Okeechobee. Hydrometeorological Rep. 31*. Washington D.C.: Department of Commerce and U.S. Army Corps. of Engineers.
- Thompson, E., & Cardone, V. (1996). Practical Modelling of Hurricane Surface Wind Fields. *Journal of Waterway, Port Coastal and Ocean Engineering, July/August*, 195 - 205.
- Torn, R., & Snyder, C. (2012). Uncertainty of Tropical Cyclone Best-Track Information. *American Meteorological Society*, 715-729.
- USACE. (2008). *Coastal Engineering Manual, Part II, Chapter 2: Meteorology and Wave Climate*. Washington, USA: United States Army Corps of Engineers.
- USGS. (2013). *Coastal Change Hazards: Hurricanes and Extreme Storms*. Retrieved October 19, 2013, from <http://coastal.er.usgs.gov/hurricanes/extreme-storms/hurricanes.php>
- Velden, Harper, Wells, II, B., Zehr, Olander, & Mayfield. (2006). *The Dvorak Tropical Cyclone Intensity Estimation Technique, A Satellite-Based Method that has Endured for over 30 Years*. American Meteorological Society.
- Vickery, Masters, Powell, & Wadhera. (2009b). Hurricane Hazard Modeling: The Past, Present and Future. *Journal of Wind Engineering and Industrial Mechanics*, 97, 392 - 405.
- Vickery, P., & Twisdale, L. (1995). Prediction of Hurricane Wind Speeds in the United States. *Journal of Structural Engineering*, 121(11), 1691 - 1699.
- Vickery, P., & Wadhera, D. (2008). Statistical Models of Holland Pressure Profile Parameter and Radius to Maximum Winds of Hurricanes from Flight Level Pressure and H*Wind Data. *Journal of Applied Meteorology*, 47, 2417 - 2497.
- Vickery, P., Skerlj, P., & Twinsdale Jr., L. (2000b). Simulation of Hurricane Risk in the US using an Empirical Track Model. *Journal of Structural Engineering*, 126(10), 1222 - 1237.
- Vickery, P., Skerlj, P., Steckley, A., & Twinsdale Jr., L. (2000a). Hurricane Wind Field Model for use in Hurricane Simulations. *Journal of Structural Engineering*, 126(10), 1203 - 1221.
- Vickery, P., Wadhera, D., Powell, M., & Chen, Y. (2009a). A Hurricane Boundary Layer and Wind Field Model for used in Engineering Applications. *American Meteorological Society*, 48, 381 - 405.
- Vitart, F., Anderson, J., & Stockdale, T. (2003). Seasonal Forecasting of Tropical Cyclone Landfall over Mozambique. *Journal of Climate*, 16, 3932 - 3945.
- Wand, M., & Jones, M. (1995). *Kernel Smoothing*. London: Chapman and Hall.
- Wand, M., & Ripley, B. (2013). KernSmooth: Functions for Kernel Smoothing for Wand & Jones (1995). R package version 2.23-10.

- Willoughby, H. E., & Rahn, M. E. (2004). Parametric Representation of the Primary Hurricane Vortex. Part I: Observations and Evaluation of the Holland (1980) Model. *Monthly Weather Review*, 132, 3033-3048.
- Willoughby, H. E., Darling, R., & Rahn, M. E. (2006). Parametric Representation of the Primary Hurricane Vortex. Part II: A New Family of Sectionally Continuous Profiles. *Monthly Weather Review*, 134, 1102 - 1120.
- WMO. (1993). *Global Guide to Tropical Cyclone Forecasting*. Geneva: World Meteorological Organisation, Report No. TCP-31.
- Xie, L., Bao, S., Pietrafesa, L., Foley, K., & Fuentes, M. (2006). A Real-Time Hurricane Surface Wind Forecasting Model: Formulation and Verification. *American Meteorological Society*, 134, 1355 - 1370.
- Xu, L., & Brown, R. (2008). *A Hurricane Simulation Method for Florida Utility Damage and Risk Assessment*. IEEE.
- Yin, J., Welch, M., Yashiro, H., & Shinohara, M. (2009). Basinwide Typhoon Risk Modelling and Simulation for Western North Pacific Basin. Taipei, Taiwan: Paper Presented at The Seventh Asia-Pacific Conference on Wind Engineering (APCWE7).
- Zhang, S., & Nishijima, K. (2012). *Statistics-Based Investigation on Typhoon Transition Modeling*. Shanghai, China: The Seventh International Colloquium on Bluff Body Aerodynamics and Applications.

APPENDIX A: TIME-SERIES OF MODELLED AND MEASURED WIND SPEEDS

This appendix presents time-series of modelled and measured 10-min average wind speeds at a number of measurement stations in the South-West Indian Ocean, forming part of the validation of the parametric wind field models described in Section 5.2. Measured wind data for this study has been kindly provided by Mr Francois Bonnardot of Météo France (personal communication). The location of each measurement station is shown in Figure 5-3. Each time-series plot provides the name of the corresponding tropical cyclone which generated the considered extreme wind event.

Figure A-1: Time-series of modelled vs measured 10-min average wind speeds at Europa.

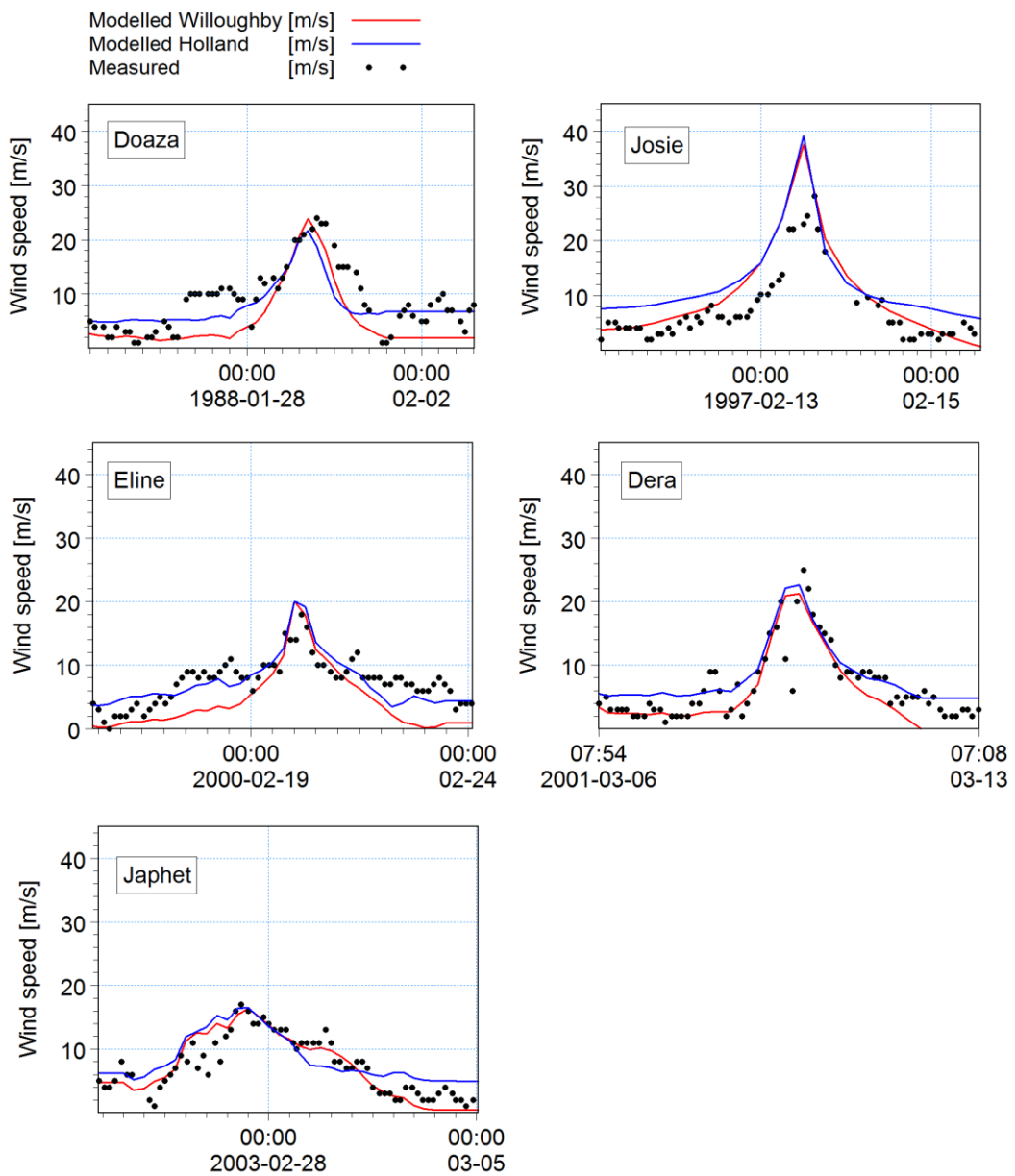


Figure A-2: Time-series of modelled vs measured 10-min average wind speeds at Tromelin.

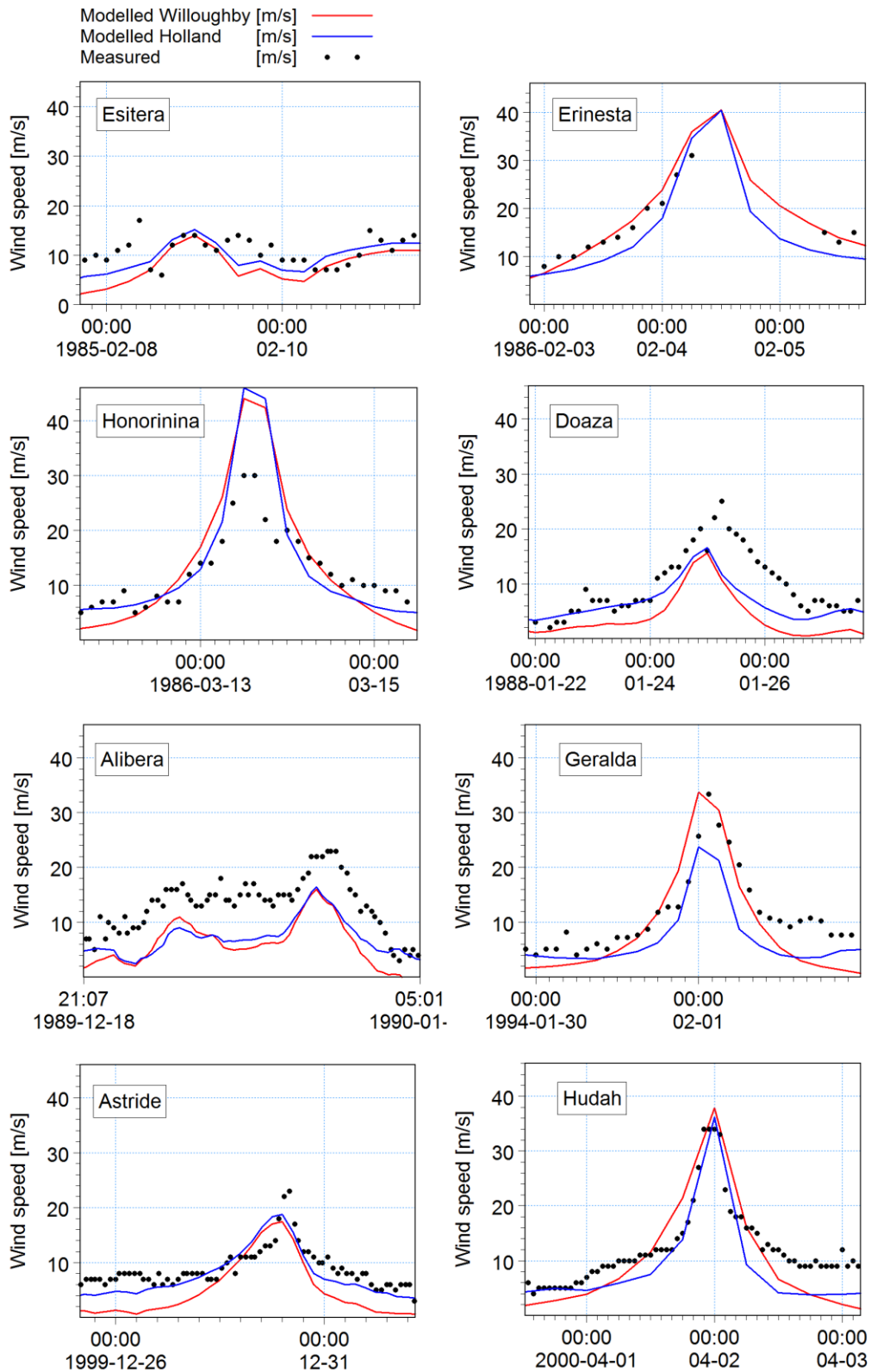


Figure A-2 (continued): Time-series of modelled vs measured 10-min average wind speeds at Tromelin.

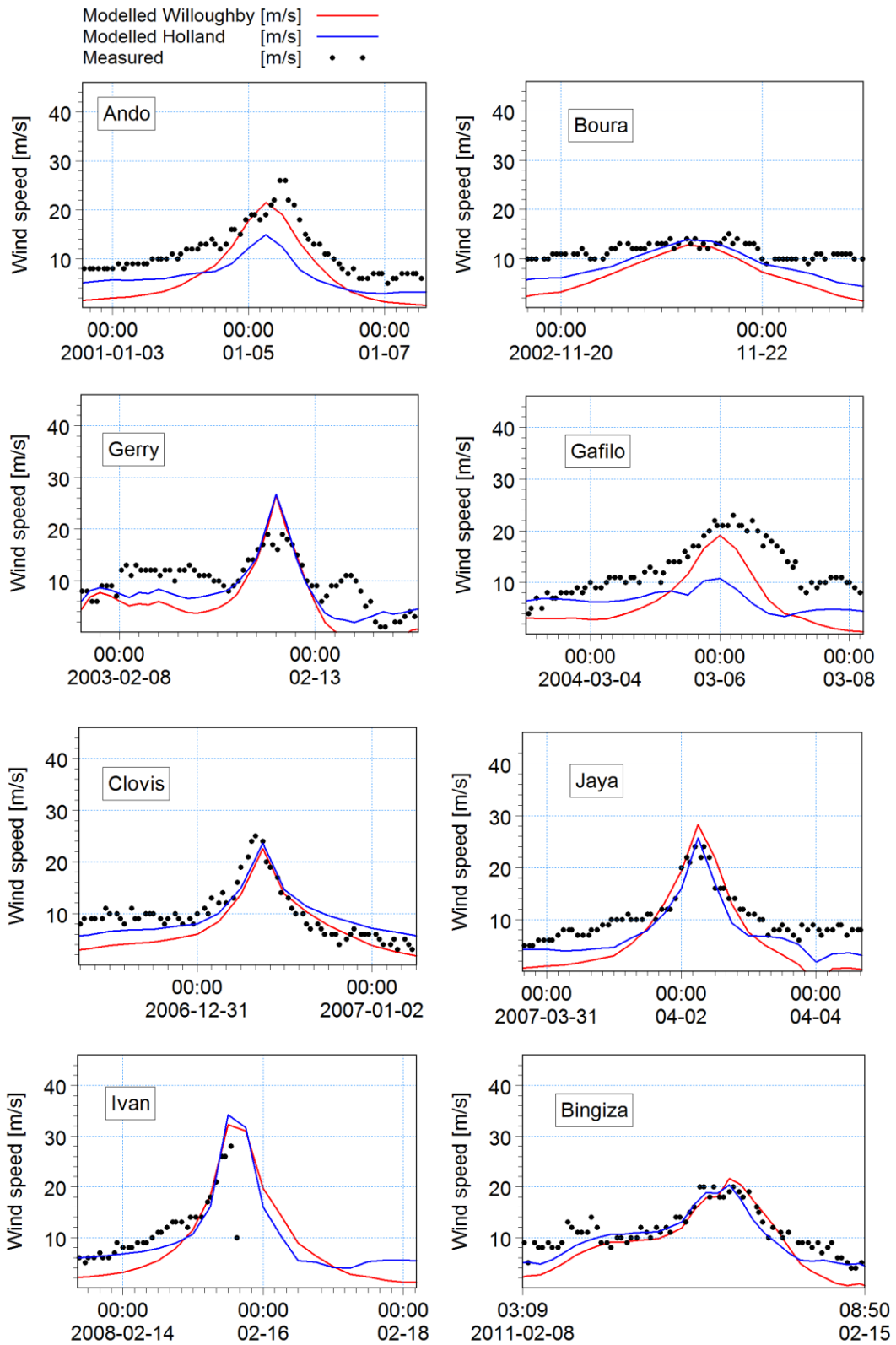


Figure A-3: Time-series of modelled vs measured 10-min average wind speeds at Juan de

Nova

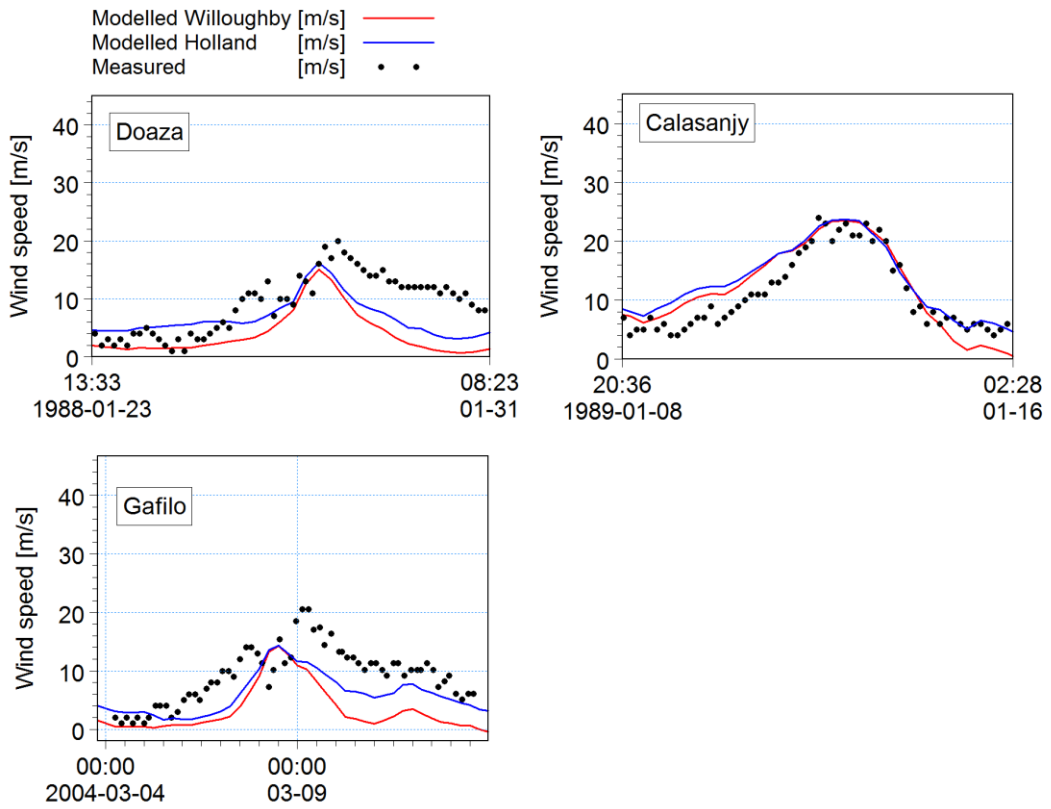


Figure A-4: Time-series of modelled vs measured 10-min average wind speeds at Pierrefonds Airport

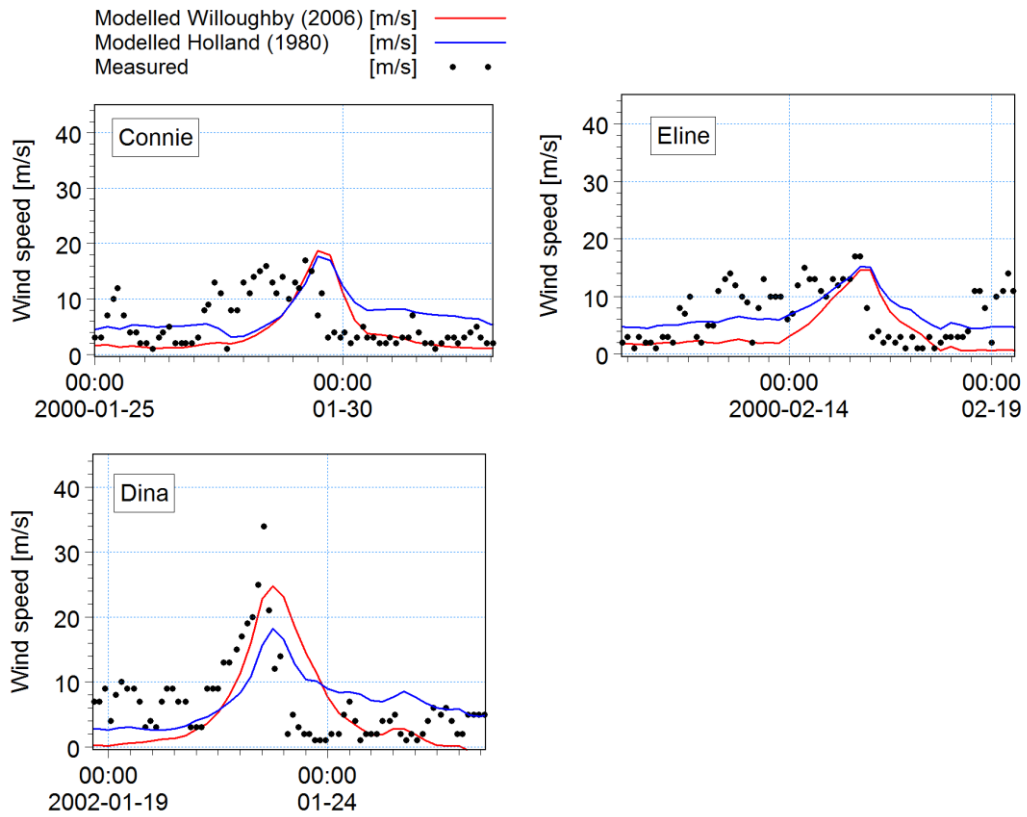


Figure A-5: Time-series of modelled vs measured 10-min average wind speeds at Pamandzi (Mayotte)

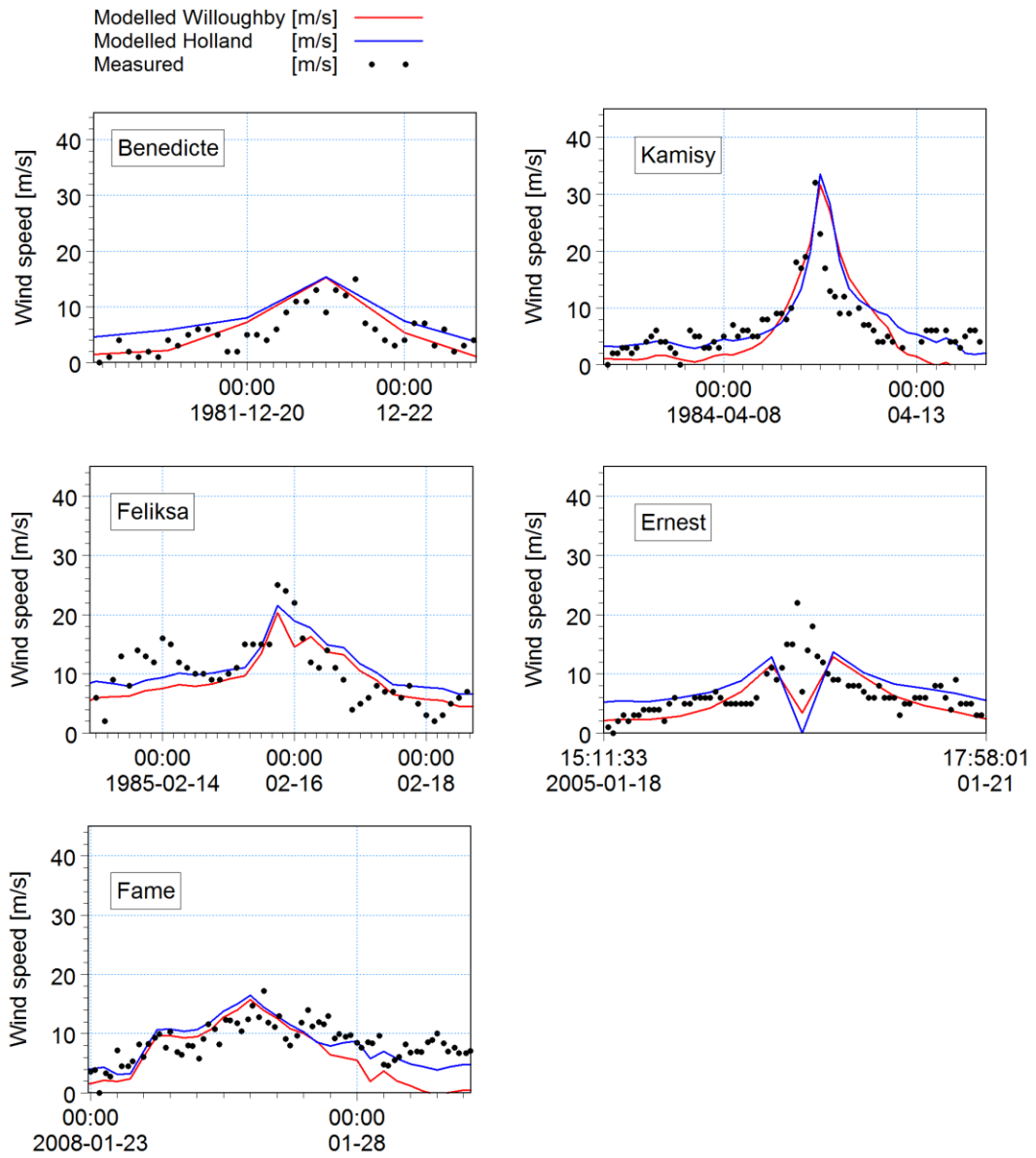


Figure A-6: Time-series of modelled vs measured 10-min average wind speeds at Saint-Pierre

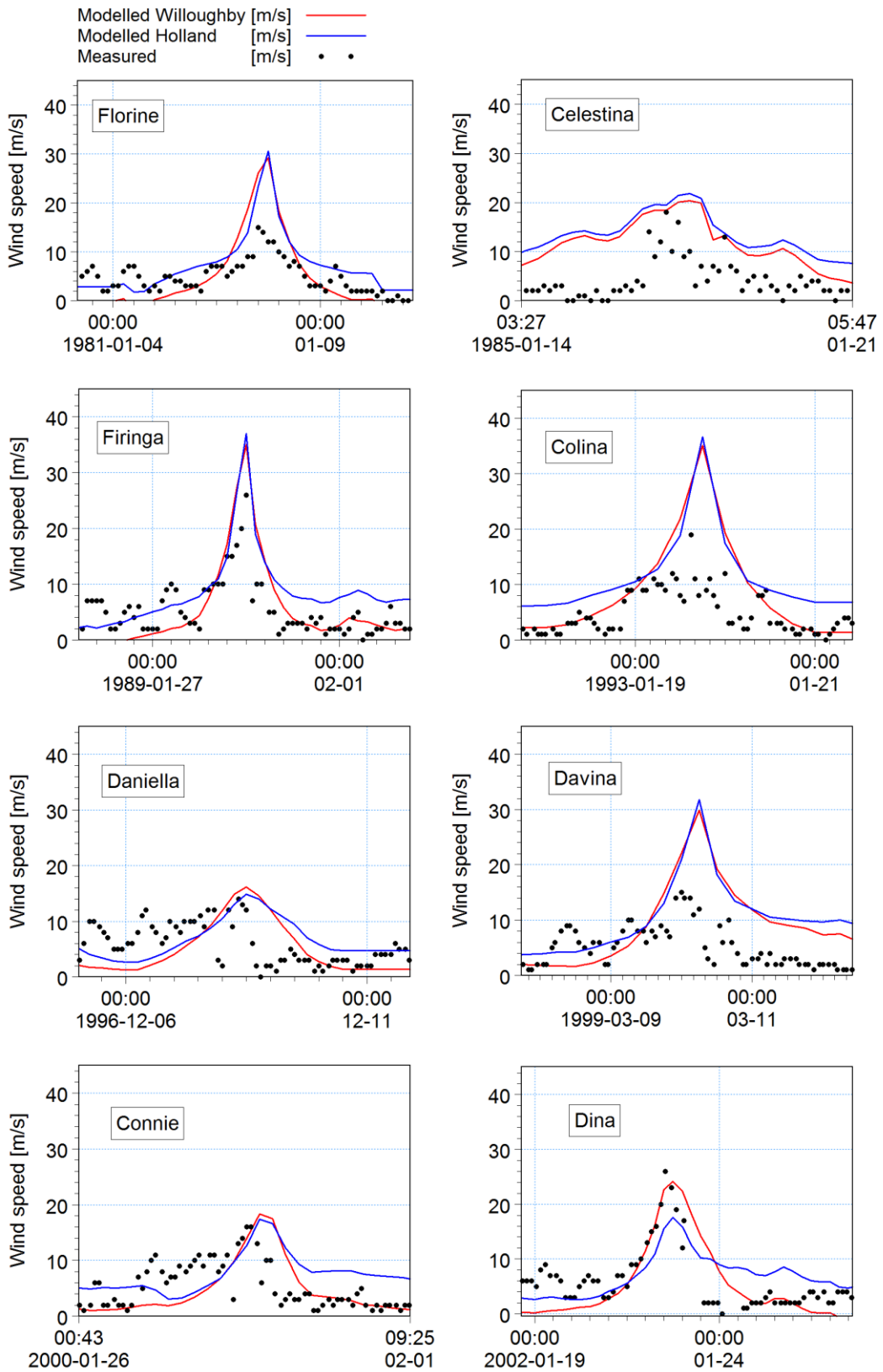


Figure A-7: Time-series of modelled vs measured 10-min average wind speeds at Gillot

Airport.

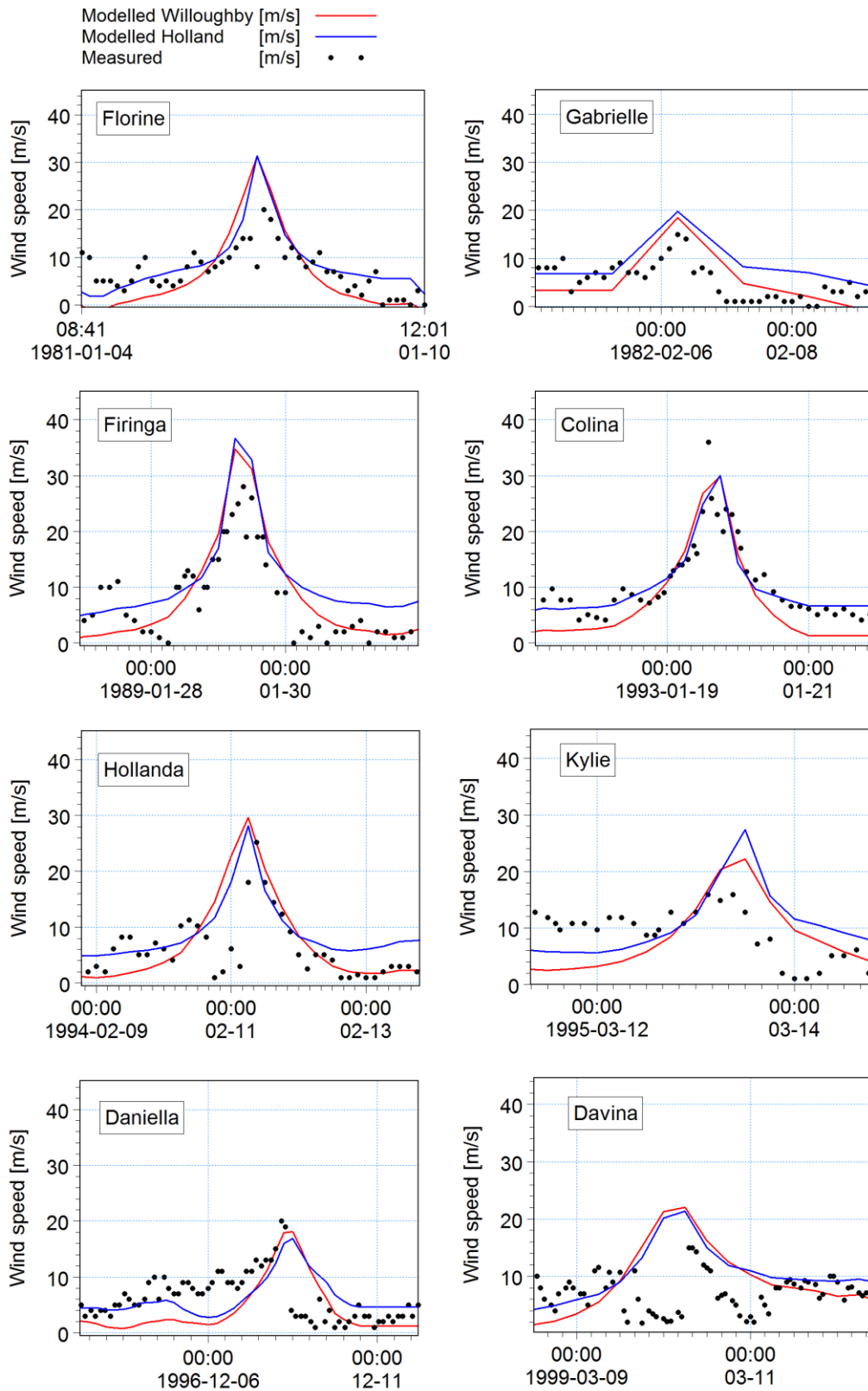


Figure A-7 (continued): Time-series of modelled vs measured 10-min average wind speeds at Gillot Airport.

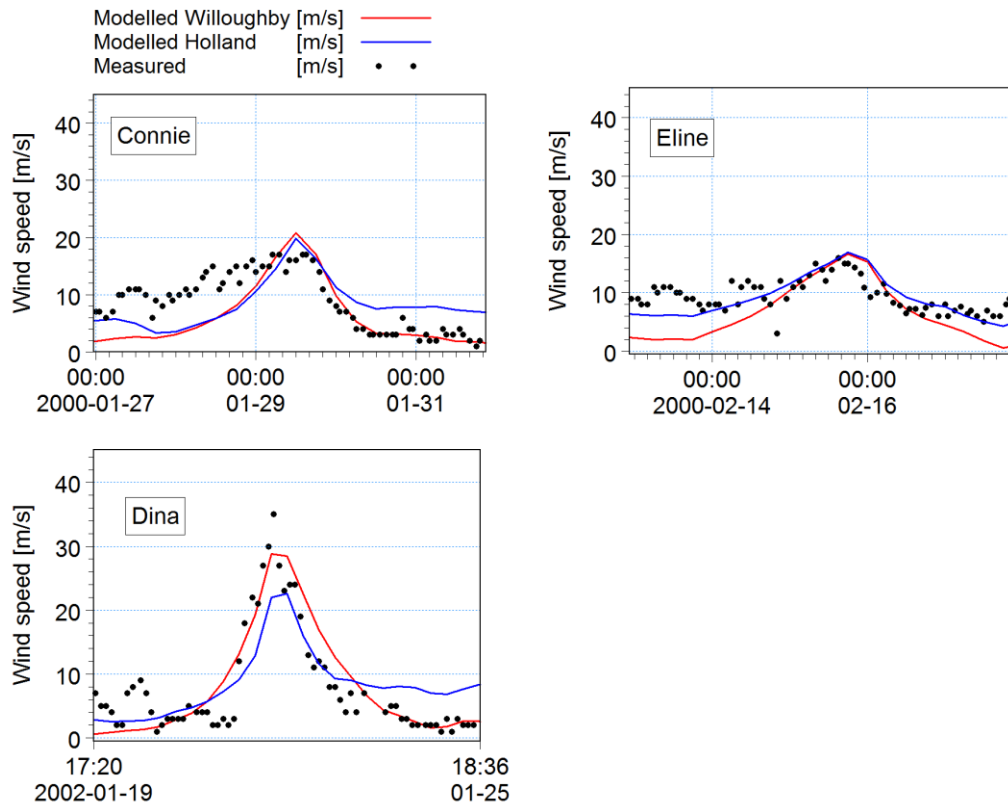
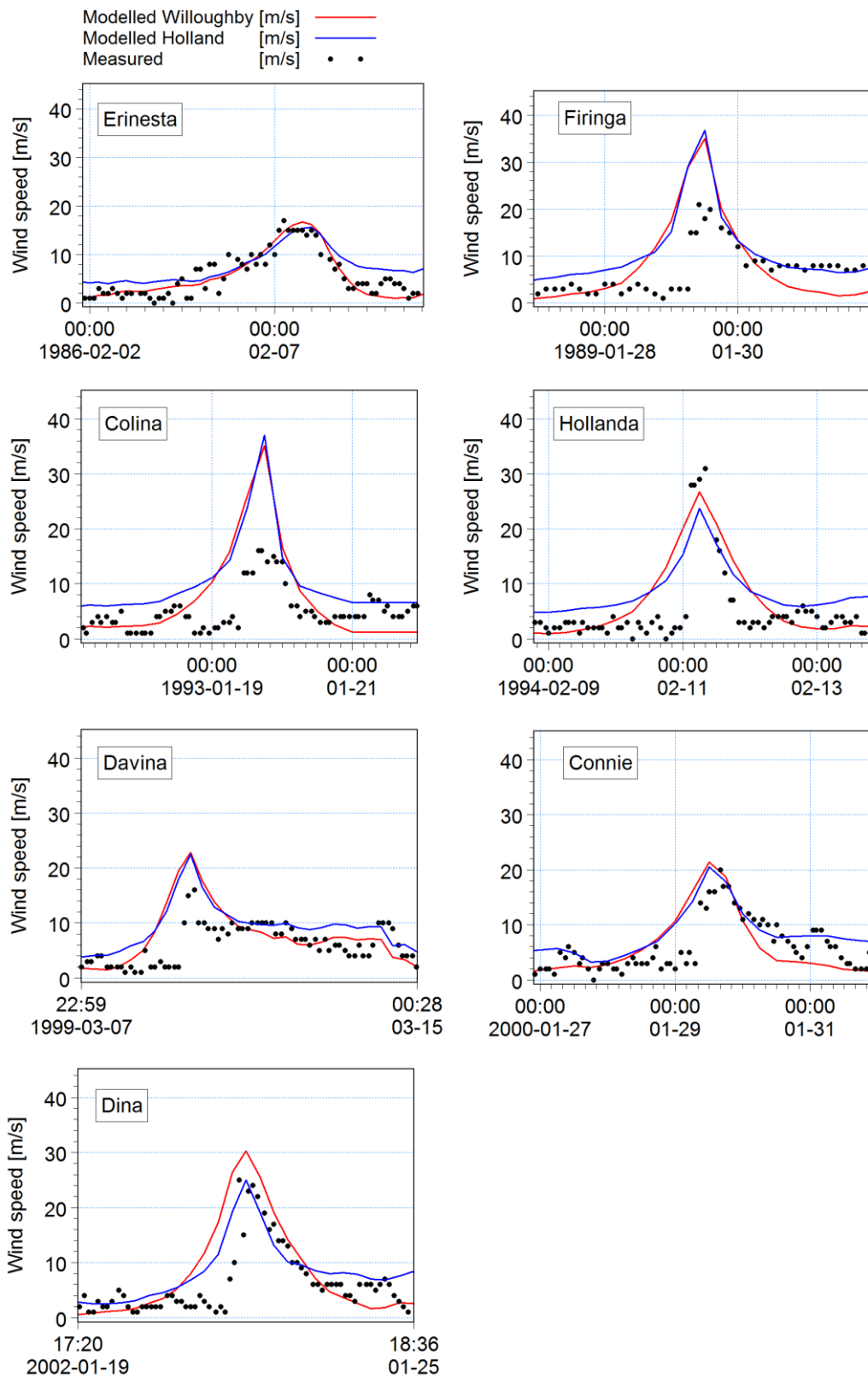


Figure A-8: Time-series of modelled vs measured 10-min average wind speeds at Le Port.



APPENDIX B: NON-PARAMETRIC PROBABILITY DENSITY FUNCTIONS**B.1 Introduction**

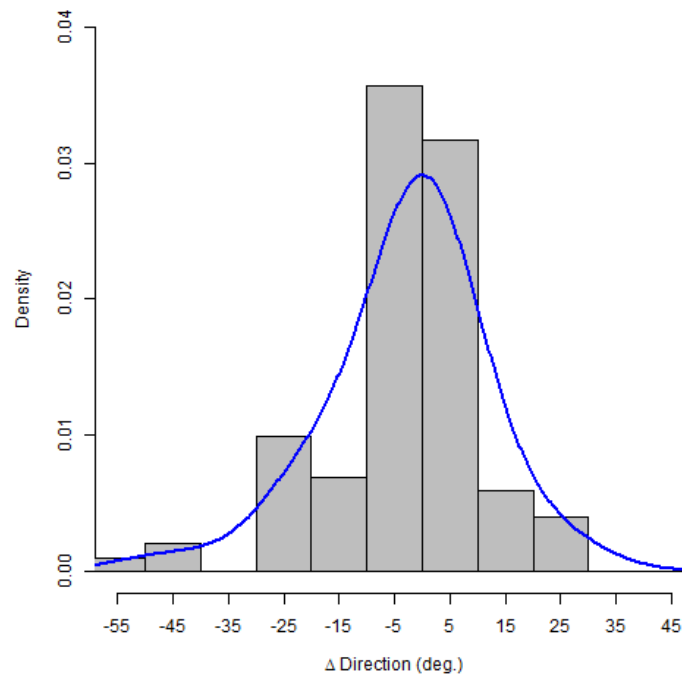
Non-parametric probability density functions (PDFs) are an important component of the synthetic track model described in Section 6. This appendix provides some background into the methods employed in this study to both generate and sample non-parametric PDFs.

B.2 Generation of Non-Parametric Probability Density Functions

Statistical modelling for this study was carried out using the programming language R, a widely used software environment for statistical computing and graphics (R Core Team, 2013). The generation of non-parametric PDFs was carried out using the 'KernSmooth' package (Wand & Ripley, 2013) which provides functions for kernel smoothing according to Wand & Jones (1995).

The shape of the output PDF is highly dependent on the adopted kernel bandwidth smoothing parameter. Larger values of bandwidth make smoother estimates, while smaller values of bandwidth make less smooth estimates. The default bandwidth is computed from the variance of the data, specifically the 'oversmoothed bandwidth selector' of Wand and Jones (1995). The default bandwidth was found to produce visually pleasing density estimates of the data, and was used throughout this study, unless otherwise specified.

Figure B - 1 provides an example of a probability density function fitted to data for change in track direction. The data for the presented example are taken from tracks with their directions ranging between 225° and 270°, falling within 2 geographical degrees (approximately 200 km) of the location 51° E, 19° S. The density estimates are automatically normalised so that the integration of the density function is equal to one.

Figure B - 1: Example of a non-parametric PDF fitted to data for change in track direction.

B.3 Sampling of Non-Parametric Probability Density Functions

Non-parametric PDFs have been sampled using the ‘acceptance and rejection’, or ‘hit and miss’ algorithm. The algorithm is summarised as follows:

- Generate a random number x between x_{\min} and x_{\max} (e.g. x_1 or x_2 in Figure B - 2)
- Compute the density of the PDF (y_{PDF}) at x
- Generate a random number y between 0 and y_{\max} (e.g. y_1 or y_2 in Figure B - 2)
- If $y > y_{\text{PDF}}$, then x is rejected (‘miss’)
- If $y \leq y_{\text{PDF}}$, then x is accepted (‘hit’)

The ‘hit and miss’ algorithm is graphically displayed in Figure B - 2. In this example, the combination of random numbers x_1 and y_1 would result in x_1 being rejected, while the combination of random numbers x_2 and y_2 would result in x_2 being accepted. The repeated sampling of the PDF in this manner yields data conforming to the desired distribution. Figure B - 3 compares histograms of the raw data with data generated from 10 000 repeated samples of the PDF shown in Figure B - 2. The figure serves to highlight the sound execution of the ‘hit and miss’ algorithm adopted for this study.

Figure B - 2: Example of the 'hit and miss' method for sampling PDFs.

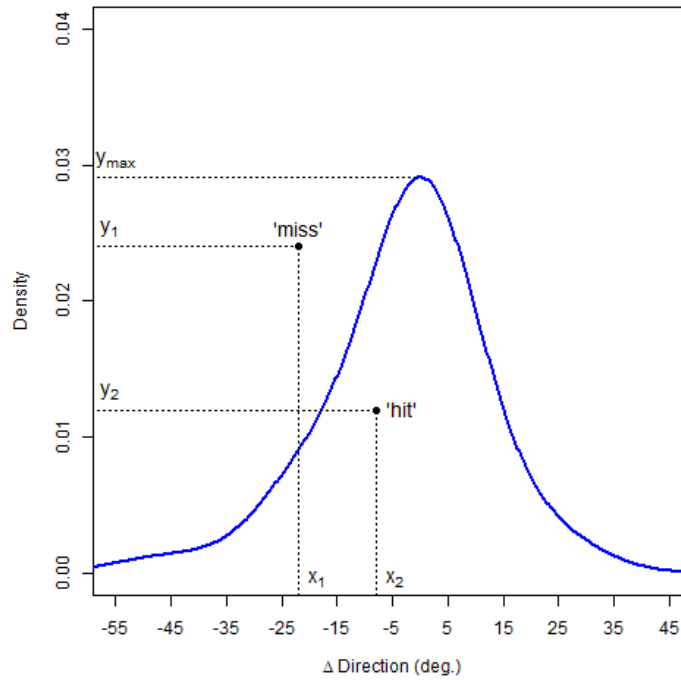
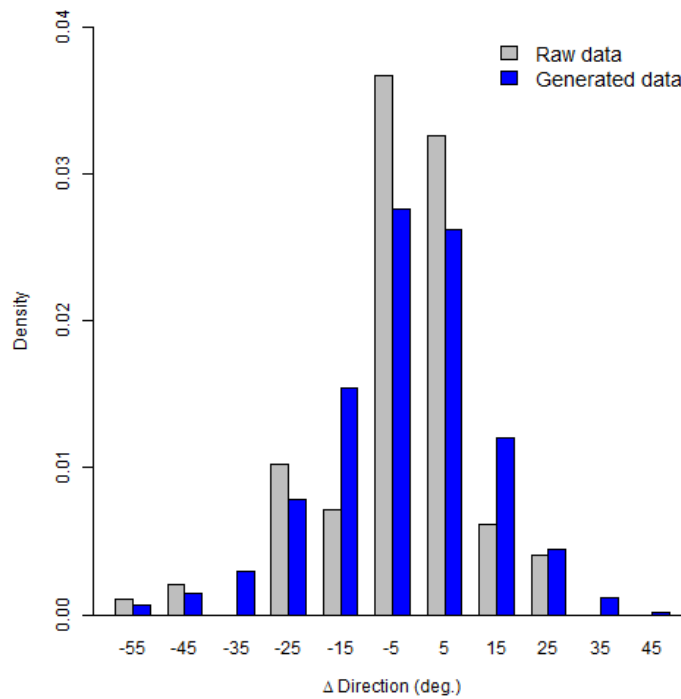


Figure B - 3: Comparison of raw data and data generated from repeated sampling of non-parametric PDF.



APPENDIX C: MAXIMUM POTENTIAL INTENSITY ESTIMATES

The monthly mean maximum potential intensity (MPI) estimates presented in this appendix have been kindly provided by Professor Kerry Emanuel of the Massachusetts Institute of Technology (personal communication). These data have been used to define upper limits for the modelling of intensity of synthetic tracks (Section 6.3.4.1). Details of the calculation procedure of the MPI estimates follows Emanuel (1988, 1995), and is summarised online by Bister & Emmanuel (n.d.).

Figure C -1: Mean monthly MPI estimates for the South-West Indian Ocean.

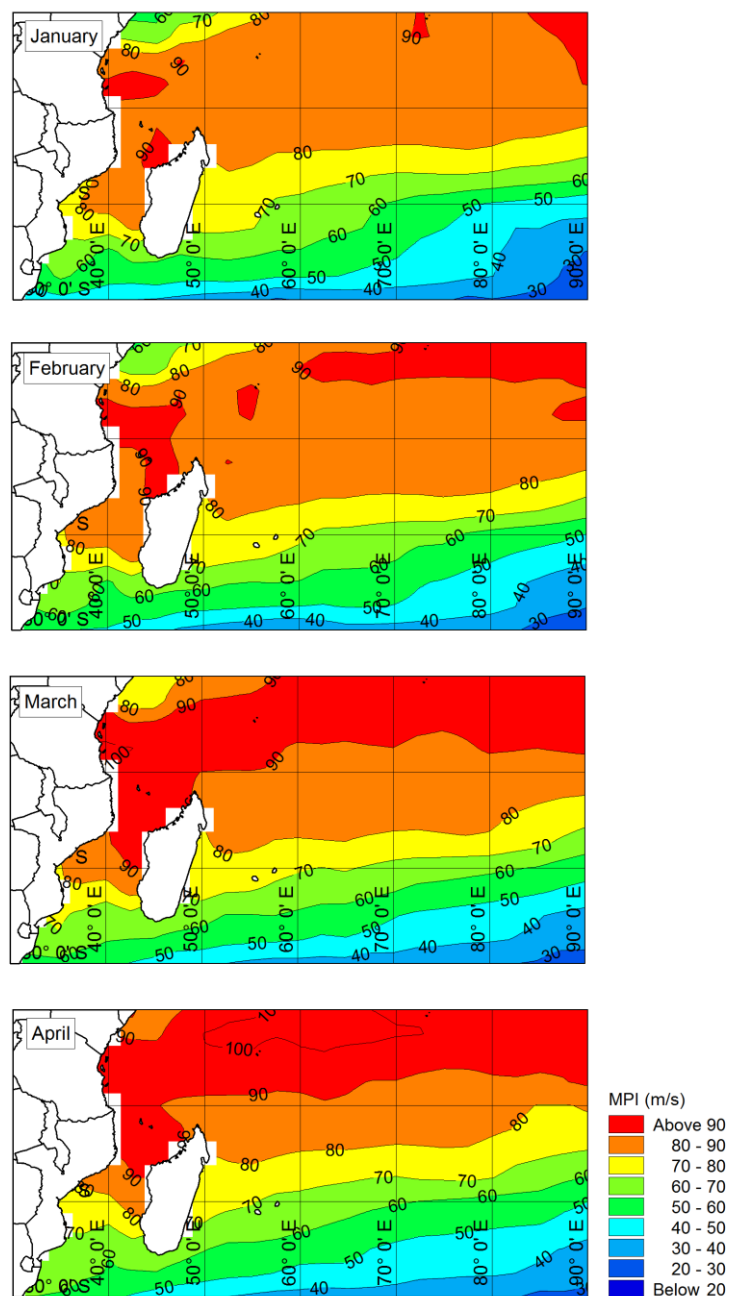


Figure C -1 (continued): Mean monthly MPI estimates for the South-West Indian Ocean.

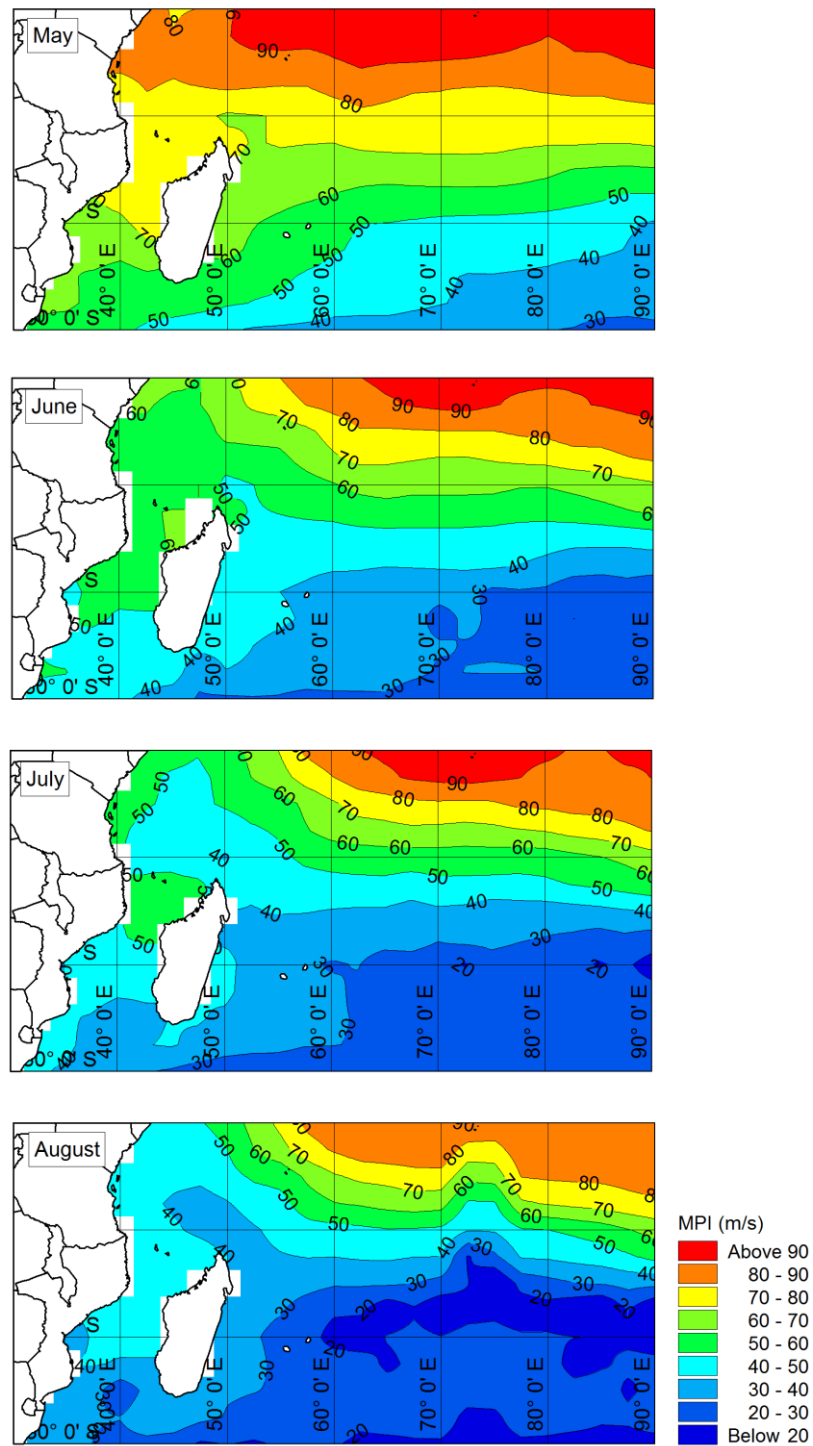


Figure C -1 (continued): Mean monthly MPI estimates for the South-West Indian Ocean.

